Physics Department. Annual progress report 1 January - 31 December 1980

Risø National Laboratory, Roskilde

Publication date:
1980

Document Version
Publisher's PDF, also known as Version of record

Risø-R-441

RISØ

Risø-R-441

Physics Department Annual Progress Report

1 January – 31 December 1980

Risø National Laboratory, DK-4000 Roskilde Denmark
December 1980

RISØ-R-441

PHYSICS DEPARTMENT ANNUAL PROGRESS REPORT
1 January - 31 December 1980

edited by H. Bjerrum Møller and B. Lebech

UDC 53

December 1980
Risø National Laboratory, DK 4000 Roskilde, Denmark

This report contains unpublished results and should not be quoted without permission from the authors.

ISBN 87-550-0761-9
ISSN 0106-2840

Risø Repro 1981

PREFACE

Research in the Physics Department at Risø covers three main fields:

Solid-state physics
Plasma physics
Meteorology

The principal activities in these fields are presented in this report, which covers the period from 1 January to 31 December 1980. Introductions to the work in each of the main fields are given in the respective sections of the report.

CONTENTS

Page

Page

Page

1. SOLID STATE PHYSICS

The purpose of the work in solid state physics is to contribute to the fundamental understanding of the physical properties of condensed matter. Neutron beams have properties that make them a unique tool for studies of solids and liquids on the microscopic level, and the largest experimental facility at Risø, the 10 MW DR3 reactor, is excellently suited to this type of research. Hence, the experimental work in the solid state physics section is primarily concerned with the use of the DR3 reactor for a wide variety of neutron scattering experiments, and most of the section's theoretical efforts are also related to neutron scattering experiments. In the last few years, however, intense x-ray sources have become available for condensed matter physics research, and although neutron scattering is the dominant experimental technique used, a portion of the section's efforts has been directed towards the use of these new sources.

The instruments at the horizontal neutron beams of the DR3 reactor are five triple-axis spectrometers, one double-axis spectrometer and a four-circle diffractometer. A small angle scattering facility is under design and construction.

In three of the four tangential through-tubes of the reactor, water scatterers placed close to the reactor core scatter beams of thermal neutrons out through the tube to the spectrometers. The thermal flux in the centre of the beam tube is about $2 \cdot 10^{14}$ neutrons/cm^2/s. A liquid hydrogen cold source was installed in the fourth tangential tube in the spring of 1975. This cold source provides two of the spectrometers in the reactor hall with beams of cold neutrons. At these spectrometers the cold neutron flux peaks at 15 meV and the cross-over between the cold neutron flux and thermal flux is at about 20 meV. A curved neutron-conducting tube leading from the cold neutron beam in the reactor hall to an experimental hall supplies cold neutrons to an additional triple-axis spectrometer placed in the experimental hall at the end of the neutron conducting tube. Here the flux peaks at about 10 meV and the useful range is 2.5-15 meV. The low extrin-

sic background of less than one count per ten minutes makes this instrument an excellent tool for studies requiring high resolution and sensitivity. Amongst the plans for instruments to be installed in the experimental hall is a small-angle neutron scattering facility (1.30) to be used, for instance, for problems of metallurgical interest of for studies of biological molecules. This project is supported by grants from both the Danish and the Swedish Natural Sciences Research Councils.

All the neutron spectrometers are fully automatized and may be operated from remote terminals via a modem and telephone line. At present, most of the neutron spectrometers are controlled by PDP-8 computers, which in the coming years will be replaced by PDP-11 computers. Apart from controlling all the necessary spectrometer angles, the PDP programs allow setting and changing of sample temperature and/or ambient magnetic field. The data from the PDP-8 controlled spectrometers are stored in an 18-K memory buffer or on a DEC-cassette. From the buffers or the cassettes the data may either be transferred via (i) a direct line to an HP-9830 desk calculator and plotter system placed in the reactor hall, or (ii) via the modem and telephone line to the main computer at Risø, a Burroughs 6700. The data from the PDP-11 controlled spectrometers are stored on floppy disks and can be processed directly by the PDP-11 computer or after transfer to a larger computer. With the exception of the oldest triple-axis spectrometer and the double-axis spectrometer, all the spectrometers move on air-cushions. The double-axis spectrometer is equipped with a tilting detector arm, which allows studies of reflection out of the horizontal scattering plane.

The four-circle neutron diffractometer is a paper-tape-controlled Ferranti four-circle instrument, which has been operated since 1967 by the Chemical Institute of the University of Århus on behalf of the Danish National Committee for Crystallography and serves all Danish crystallographers. A grant from the Danish Natural Sciences Research Council has made it possible to replace this instrument by a more up-to-date diffractometer based on a Huber goniostate and a PDP-11 computer, which will become operational during 1981.

The x-ray facility is a joint project between Risø National Laboratory and the University of Copenhagen, supported by the Danish Natural Sciences Research Council. The x-ray source, at Risø, is a 12 kW x-ray generator with a rotating anode of Cu or Mo. The source has two exit ports. Installed at one of the ports is a general-purpose triple-axis spectrometer (1.31). Placed at the other port is a mechanically simple diffractometer consisting of a position-sensitive x-ray detector in conjunction with a multichannel analyzer. This diffractometer has proved to be an efficient instrument for studying the two-dimensional structures of adsorbed monolayers (1.23, 1.24). During a four week period in 1980 the triple-axis spectrometer was installed at a preliminary version of the permanent beam line D4 at HASYLAB, Hamburg, F.R.G. The three experiments (1.21, 1.22 and 1.25) carried out during this period demonstrated the experimental possibilities opened by the use of synchrotron radiation for studies of condensed matter. It was found that the monochromatic beam from the storage ring is more than a hundred times more intense than that from a 10 kW rotating anode tube, and at the same time the vertical resolution is typically 25 times better! Another x-ray instrument, a white-beam energy-dispersive diffractometer for work at a synchrotron radiation source, was built and installed at a temporary beam line at the electron storage ring DORIS at HASYLAB (1.32). The diffractometer is mainly funded by DESY and its construction is a joint project of the University of Copenhagen, the Technical University of Denmark, and HASYLAB in collaboration with Risø. It was tested and used for high pressure structural studies of, for instance, YbH_2 (1.13).

The experimental and theoretical work of the solid state physics section falls into four major categories, namely: studies of magnetic materials (1.1 - 1.16), phase transitions (1.17 - 1.22), surfaces (1.23 - 1.25) and studies of non-magnetic materials (1.26 - 1.29). An increasing portion of the section's work is carried out in collaboration with Danish universities and research centres and universities in other countries.

Neutron scattering is well suited for studies of magnetic materials, and a majority of experiments fall into this category. The magnetic ordering and the excitations were studied experimentally in several compounds. In a study of the magnetic ordering and the excitations in a Pr-2.5% Nd alloy (1.2) it was found that the Nd levels are observed more readily when a magnetic field is applied. The study of the magnetic ordering of pure Pr and Nd was continued in collaboration between several laboratories (1.5-1.7). Amongst these studies was an investigation of the effects of uniaxial pressure applied to a single crystal of Nd, which revealed that even a small pressure (~150 bar) modifies the complex magnetic structure of Nd. The study of the magnetic excitations in rare-earth transition metal compounds R_2T_{17} (1.8) was brought to an end and the data could be interpreted in terms of a linear spin wave model. The analysis showed that the rare earth and the transition metal sublattices form two very different subsystems and the excitation spectra of these two systems are basically observed in two well-separated ranges of energy transfer. The magnetic field dependence of the magnetic excitation energies of the mixed valence system TmSe was investigated (1.12) and the results could be interpreted in terms of a two level model where the degenerate ground-state is split by the magnetic field. The crystal field and exchange interactions were studied in dilute Y-Er alloys (1.10) and the influence of the onset of superconductivity on the crystal field transition was initiated (1.11). In dilute alloys of $La_{1-x}Tb_xAl_2$ it was found that the onset of superconductivity leads to an abrupt change in the line width of the crystal field transition.

Theoretical studies were aimed at developing a generalization of the random phase (RPA) approximation by including correlation effects in order to be able to describe accurately the static and dynamic properties of general multi-level systems, e.g. crystal field systems. Illustrative calculations for the Heisenberg magnet in the paramagnetic phase (1.1) show a change in the line-shape between a double peak to a lorentzian line-shape as the wave vector varies from the zone boundary to the zone centre. A RPA-theory (1.2) describing the damped spin waves in a sinusoidally modulated structure was developed. In addition, self-consistent

calculations of the atomic volume through the actinide series (1.15) confirmed the experimental observation that the 5f-electrons in the actinides, up to and including Pu, are itinerant and form band states. First principles calculations of the equation of state of La (1.16) show that both the termination of the 6s-5d transition and the onset of a significant pressure contribution from the overlap of the Xe cores do occur in the vicinity of the experimentally observed stiffening of the shock data for La.

A considerable part of the section's research has always been the study of magnetic and structural phase transitions. This work was continued by both neutron (1.17 - 1.20) and x-ray (1.21 - 1.22) scattering techniques. A search for a bi-critical point in CeAs (1.17) revealed that, in contrast to theoretical predictions, the Néel temperature is unchanged by the application of a magnetic field up to 0.5 T. An investigation of the critical fluctuations in the dipolar coupled ferromagnets $LiTb_x Y_{1-x}F_4$ (1.18) indicates that the extreme anisotropy of the fluctuations observed for $x = 0$ is retained in the diluted compound having $x = 0.3$. A phase transition study of a more applied nature was initiated in collaboration with the Metallurgy Department at Risø, that is, a study of recrystallization kinetics (1.20). In the initial experiment, the effect of temperature on the texture of heavily rolled copper was studied using neutron diffraction techniques, and the results indicate that the recrystallization kinetics of those texture components which were monitored are determined by nucleation and not by growth.
The phase transitions of the smectic-A phase of the liquid crystal 4.08 (1.21), and the critical fluctuations in the nematic to smectic-A re-entrant nematic phase transitions in liquid crystal mixtures (1.22) were studied extensively by x-ray scattering at HASYLAB, Hamburg, F.R.G. In the former experiment, the previously observed quasi-long-range order was studied in more detail, and the use of synchrotron radiation allowed the quasi-long-range order peak to be traced over four decades in intensity and much further out in reciprocal space than in the original experiment using a 10 kW rotating anode x-ray source. In the study of liquid crystal mixtures, the aim was to study the critical behaviour of the fundamental quantity driving the phase transition in both the

nematic and the re-entrant nematic phase of liquid crystal mixtures. In this experiment, the advantage of synchrotron radiation is primarily the fast data accummulation rate, which allowed the study of a large number of mixtures.

The research in surfaces (1.23 - 1.25) consists of studies by neutron and x-ray scattering of phase transitions and the structures of CD_4, Kr and Ar physisorbed on graphite. Two types of phase transitions in the two-dimensional adsorbate system, namely melting and the commensurate to incommensurate transition, were studied in monolayers of CD_4 (1.23). In an x-ray study of the commensurate to incommensurate phase transition of monolayers of Kr, it was found that the transition is of first order, a result that disagrees with the LEED results. A study of the structures of physisorbed Kr and Ar revealed that Kr may, at certain temperatures and densities, be in registry (commensurate) with the underlying graphite honeycomb lattice. For Ar the structure is incommensurate with the substrate lattice at all temperatures and densities.

The dynamic and static properties were studied in some non-magnetic systems. The study of the phonon dispersion relations in the zero-gap semiconductor HgTe (1.26) showed that the optical branches are degenerate at the Γ point, an effect which may be explained by screening by holes of the long-range Coulomb interaction. Another example is a study of the phonon dispersion relations in the organic conductor $TEA(TCNQ)_2$ (1.27), revealing a Kohn anomaly which magnitude showed that the on-site Coulomb interaction is comparable or smaller than the electron hopping integral. In addition, elastic and inelastic neutron scattering studies of the solid electrolyte $LiI \cdot D_2O$ (1.28) were performed in collaboration with the Metallurgy Department at Risø. The results indicate that the unexplained behaviour of the ionic conductivity may be due to the influence of "antiferroelectric" dipolar forces between the D_2O-molecules on the Li-diffusion.

1.1 Correlation theory of static and dynamic properties of multilevel systems

(P.A. Lindgård and D. Yang (University of West Virginia, Morgantown, West Virginia, U.S.A.))

The basic goal of this theory is to develop a simple generalization of the random phase approximation (RPA) by including correlation effects. Using calculated damped and renormalized excitation modes, the static properties can be calculated quite accurately (and self-consistently) although the dynamics are described rather crudely. We use a two-pole approximation for the line shape of a single excitation and find in general an asymmetric line shape. For the Heisenberg ferromagnet in the ordered phase, the two poles have the physical meaning of being spin waves created in predominantly spin-up and spin-down regions. For temperatures decreasing from the ordering temperature, T_c, one of these regions will be dominant and the corresponding modes increase in frequency and sharpness. The modes in the minority regions on the other hand decrease in frequency and become broader. In the paramagnetic phase, a self-consistent theory for

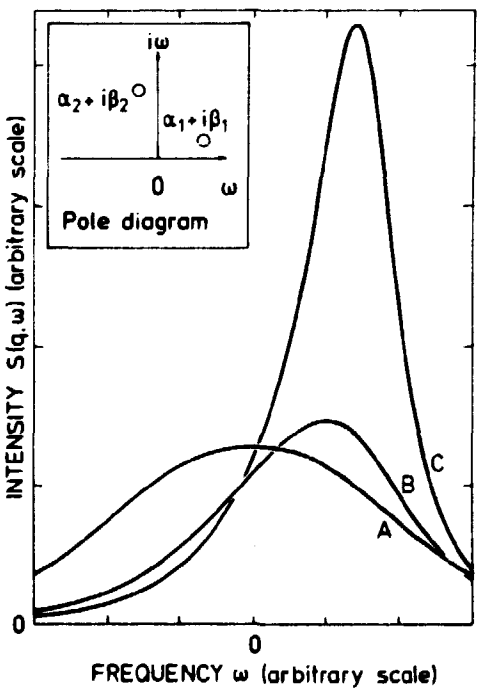

Fig. 1 Examples of the skew line shapes found in the two pole approximation for the Heisenberg ferromagnet. The damping is increased from C to A, and A corresponds to $T > T_c$. The insert shows the corresponding pole diagram. The real part, α_1, of the pole $\omega_1 = \alpha_1 + i\beta_1$ is kept fixed and β_1 is varied; the position of the other pole $\omega_2 = \alpha_2 + i\beta_2$ then follows.

the line shape is set up which shows that (Fig. 1) the line shape becomes basically lorentzian (two imaginary poles) as $q \to 0$ or $T \to T_c$, whereas for higher q and T the line shape is broader, consisting of two complex poles with a finite real part. In order to calculate the self-consistent equations accurately, computer programs have been developed which calculate the Watson sums in terms of elliptic integrals (Morita and Horiguchi (1971)) with 24 digits accuracy. The accuracy is of particular importance for calculating the properties near the critical temperature T_c.

1.2 Theory of spin waves in sinusoidially modulated structures

(P.A. Lindgård)

A sinusoidial structure is the mean field ground state for a system described by the following hamiltonian

$$H = - \sum_{\vec{q}} J(\vec{q}) \vec{S}_{\vec{q}} \cdot \vec{S}_{-\vec{q}} - D \sum_i (S_i^z)^2 ,$$

where the exchange interaction $(\vec{q})$ has a maximum for q = Q, the ordering wave vector. In the simplest case, $J(\vec{q})$ may be composed of two plane exchange constants, J_1 and J_2.
is then determined from $\cos Q = -J_1/4J_2$ for $|J_1| < 4|J_2|$. It is an incommensurate structure if $Q \neq \pi N/M$, where N and M are integers. The axial anisotropy constant D must be sufficiently large to prevent the simpler spiral structure in which the magnetic moment is the same for all sites in the crystal, but of different direction. For large D, the anisotropy gives rise to crystal field quenching of the moments such that only the component along the z-direction is finite, but varying from site to site. The theory of the excitations in such a structure is very complicated because all spin-wave modes generated by $S^+_{\vec{q}}$ couple to all others generated by $S^+_{\vec{q}+n\vec{Q}}$. The problem is solved by constructing a second order differential equation of the Sturm Liouville type for the Green function $G_{\vec{q}}(\omega) = \langle\langle S^+_{\vec{q}}; S^-_{-\vec{q}} \rangle\rangle_\omega$ near a commensurate wave vector Q_o. The resulting excitation spectrum consists of a continuous distribution of frequencies for any

wave vector q. For example, for small Q, $G_{\vec{q}}(\omega)$ assumes the form

$$G_{\vec{q}}(\omega) = \frac{S}{\omega - \omega_{\vec{q}} + Q^2\Sigma_{\vec{q}}(\omega)}$$

where $\omega_{\vec{q}}$ is the ferromagnetic spectrum, and the self-energy $\Sigma_{\vec{q}}(\omega)$ is expressed in terms of D, J_1 and J_2. For $0<<q<<\pi$, the result is an asymmetric broadening of the mode at $\omega_{\vec{q}}$. The model is of relevance for describing the excitations in Nd and in Pr under pressure, and can be used for $Nd_{1-c}Pr_c$ alloys with modifications allowing for the alloy effect.

1.3 Magnetic ordering and excitations in Pr-2.5% Nd alloy

(M. Wulff*, A.R. Mackintosh* (*University of Copenhagen), H. Bjerrum Møller, O.D. McMasters† and K.A. Gschneider, Jr.† (†Ames Laboratory-DOE, Iowa State University, U.S.A.))

The mechanism of magnetic ordering and its relation to the magnetic excitation is being studied in a single crystal of Pr doped with 2.5% Nd. Neutron diffraction measurements reveal that this alloy orders at $T_N \simeq 6$ K with an incommensurable antiferromagnetic structure similar to that of pure Nd. At higher tempera-

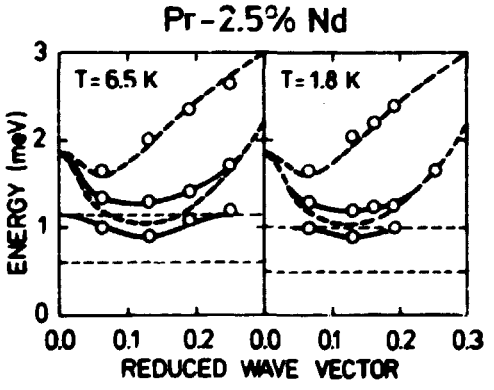

Fig. 2 Dispersion relations in the b-direction on the hexagonal sites in Pr-2.5% Nd, above and below T_N. The higher Nd-level falls with increasing magnetic ordering, causing a pronounced change in the interaction with the Pr-excitations.

tures, a significant amount of static short-range order is observed. Inelastic neutron scattering experiments have been performed both above and below T_N in fields up to 4 T. In addition

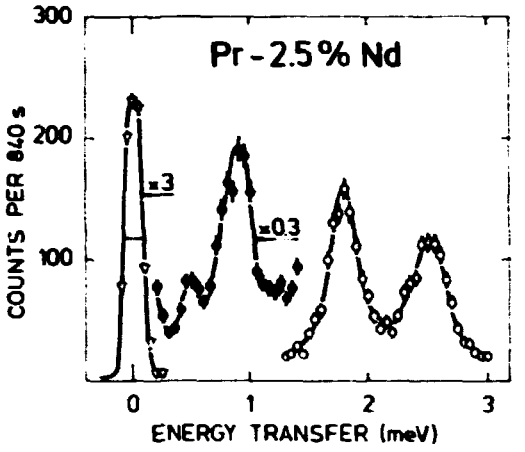

Fig. 3 A typical inelastic scattering spectrum observed in a Pr-2.5% Nd alloy in a magnetic field (T = 6.5 K, H = 1.96 T and q = 0.13). Both the weaker predominantly Nd-excitations at low energies and the predominantly Pr-excitations are strongly field dependent.

to the excitation observed in pure Pr, extra peaks due to the Nd appear. As illustrated in Fig. 2, above T_N a Nd level intersects this dispersion relation for the Pr hexagonal sites, resulting in a mixing and splitting of the modes. When the temperature is reduced, this Nd level falls in energy or the modes repel each other. As illustrated in Fig. 3, the predominantly Nd excitations can be observed very clearly in a magnetic field and have a pronounced field dependence. These modes and their field dependence may be interpreted in terms of a single-ion crystal-field model, while the excitations of the whole system and their relation to the magnetic ordering process are being analyzed by means of a CPA calculation.

1.4 Bifurcation phenomena in modulated structures: theory of concentration-dependent structures of PdH_c

(P.A. Lindgård)

The behaviour of H in Pd can be represented by an Ising model in a magnetic field. The uniform magnetization M_o corresponds to the concentration c. At low temperatures (below approximately 50 K) H forms ordered structures or concentration waves with wave vectors Q; these vary with concentration and temperature, and show lock-in-phenomena. In the Ising model, the concentration waves are represented by a sinusoidial magnetization wave with

amplitude M_Q. Using the Landau expression for the free energy in terms of M and M_Q, the field (i.e. the concentration) dependence is considered. The nonlinear equations allow for the bifurcation phenomena, by which a single Q-mode splits into two with different Q-vectors. This is observed experimentally (Bond et al. 1981). The model can also be applied to magnetic systems such as Nd, for example.

1.5 Magnetic structure of Nd metal

(B. Lebech, R.M. Moon* and W.C. Koehler* (*Oak Ridge National Laboratory, Oak Ridge, Tennessee, U.S.A.))

The magnetic phase diagram of Nd metal is rather complex and has been studied intensively by neutron diffraction and other techniques (Lebech 1981 and references therein). The magnetic ordering takes place via a continuous transition at T_N = 19.9 K, where the moments on both symmetry sites of the dhcp structure, cubic (C) and hexagonal (H) order in an incommensurably modulated structure with the modulation vectors ($\vec{q}$) along equivalent crystallographic b-directions (<100> directions). Near T_N, the moments on the hexagonal sites are parallel to the corresponding modulation directions, while the moments on the cubic sites have a large component along the crystallographic c-direction ([001] direction) and much smaller basal plane components parallel to the corresponding modulation directions. These latter components may be considered as induced by the order in the basal plane of the moments on the hexagonal sites.

At T_2 = (19.3 ± 0.2) K, there is another transition (Figs. 4 and 5) to a phase which persists down to 8.3 K. Here the basal plane components of the moments on the two sites and $\vec{q}$ turn away from the crystallographic b-direction. In this phase the basal plane moment components and $\vec{q}$ are in general not parallel, that is, the basal plane moment components on the two sites and $\vec{q}$ both have components which are parallel (μ_{ix},q_x (i = H,C)) and perpendicular (μ_{iy},q_y) to the crystallographic b-directions. Raw data illustrating the appearance of this second phase is shown in Fig. 4, which display the results of crystal rock scans

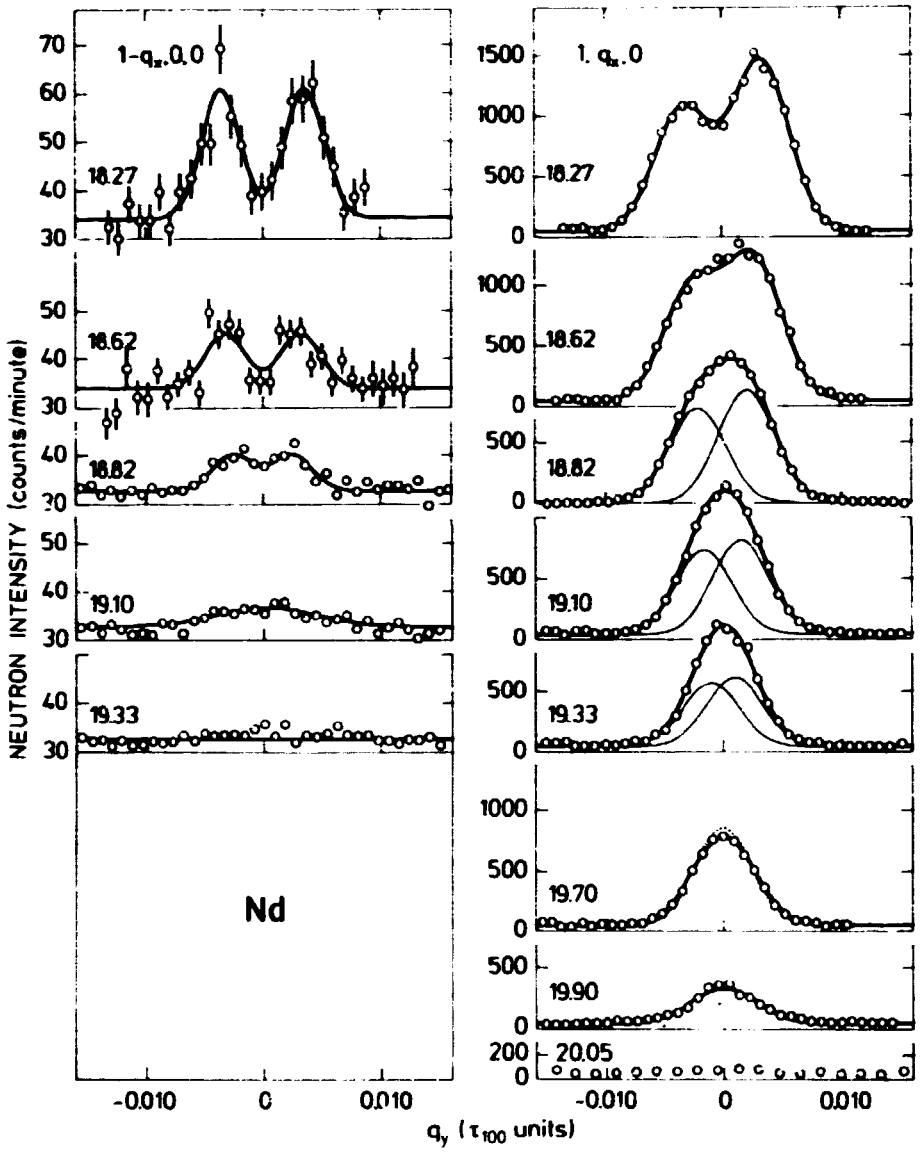

Fig. 4 Temperature dependence of the $(1-q_x,0,0)$ and $(1,q_x,0)$ magnetic satellite pairs in Nd near the transition T_2 = (19.3 ± 0.2) K. The solid lines are fits to two gaussians of resolution width separated by $2q_y$.

through $(1-q_x,0,0)$ and $(1,q_x,0)$ (q_x = 0.143) at different temperatures close to 19.3 K in Nd. The solid lines show fits to two gaussians of resolution width separated by $2q_y$, where q_y = 0.0035 at 18.3 K and $q_y \simeq 0$ at 19.3 K (Fig. 5b). The $(1-q_x,0,0)$ satellite intensities are caused alone by μ_{Hy}, and,

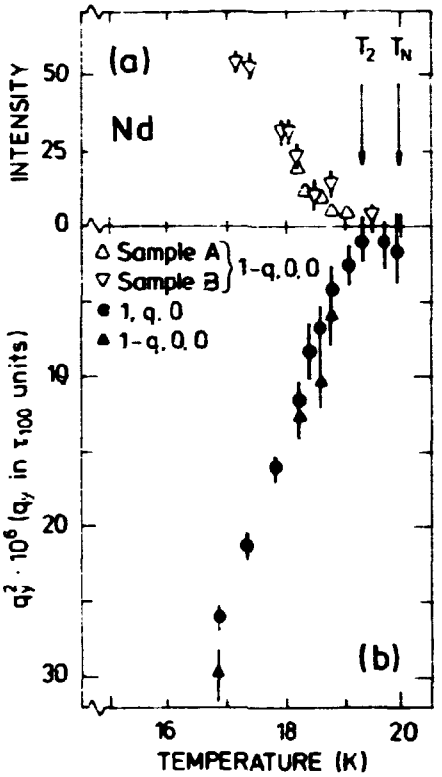

Fig. 5 Temperature dependence of the $(1-q_x,0,0)$ magnetic satellite intensity (a) and the q_y^2 (b), (see section 1.5) near the transition T_2 = (19.3 ± 0.2) K in Nd.

as seen by the disappearance and simultaneous coalescence of the $(1-q_x,0,0)$ satellites at 19.3 K both μ_{Hy} and q_y vanish at 19.3 K. (Figs. 4 and 5). The $(1,q_x,0)$ satellite intensities are caused by both μ_{Hx} and μ_{Hy}. Above 19.3 K the satellite pair which was observed below 19.3 K has coalesced to a single peak of resolution width at $(1,q_x,0)$. This peak persists to T_N and the intensity in it is caused alone by μ_{Hx}. In Fig. 5 we show the temperature dependence of the $(1-q_x,0,0)$ satellite intensity (Fig. 5a) and of q_y^2 (Fig. 5b). The variation of q_y^2 is deduced from the positions of the $(1-q_x,0,0)$ and the $(1,q_x,0)$ satellite pairs and agrees with the q_y^2 dependence deduced from another set of data using the $(q_x,0,1)$ satellite pairs. The finite value of q_y^2 above 19.3 K is an artifact of the analysis, in that we used the resolution width to fit the $(1-q_x,0,0)$ and $(1,q_x,0)$ peak(s) to double gaussians even close to T_N. This approach is incorrect because (Lebech 1981) the peaks broaden considerably near T_N due to critical scattering.

From the above description, it is clear that the magnetic structure of Nd is complex. However, when combining unpolarized neutron diffraction data with the results of polarized neutron diffraction data, the magnetic ordering of the relatively small basal plane moment components parallel to the crystallographic a-directions (μ_{Hy} and μ_{Cy}) can be separated from the ordering of the moment components perpendicular to the a-directions (μ_{Hx}, μ_{Cx} and μ_{Cz}). We have made a structure refinement of a set of polarization analysis data from Oak Ridge National Laboratory and a set of unpolarized data from Risø, obtained for a particular set of magnetic satellites ((h ± q,0,ℓ) type) and find that at 10 K,

$$\mu_{Hx} = 2.5\ \mu_B,\ \mu_{Hy} = 0.6\ \mu_B \quad \text{and}$$

$$\mu_{Cx} = 0.2\ \mu_B,\ \mu_{Cy} = 0.05\ \mu_B,\ \mu_{Cz} = 0.6\ \mu_B.$$

The above estimates of the amplitudes of the moment components neglect the effects of $q_y \neq 0$ and assume either three equally populated "single-$\vec{q}$" domains or a "triple-$\vec{q}$" structure. The phases between the different components are undetermined in the above analysis.

1.6 Effects of uniaxial pressure on the magnetic structure of Nd metal

(K.A. McEwen (University of Salford, Salford, U.K.), B. Lebech and C. Vettier (ILL, Grenoble, France))

The effects of uniaxial pressure on the magnetic structure of Nd metal were studied at the D10 neutron spectrometer at the Institute Laue-Langevin, Grenoble, France. A 4.20×4.27×5.23 mm^3 single crystal of Nd was mounted in the same uniaxial pressure assembly that was recently used in a similar study of $CeAl_2$ (Barbara et al. 1980). The uniaxial pressure was applied along the crystallographic a-direction [$\bar{1}$20] and we studied the influence of pressure at 10 K on the magnetic satellites around several (h,0,ℓ) reflections. At 10 K, even small stress (~150 bar) severely modifies the relative intensities of the satellites (Fig. 6). At

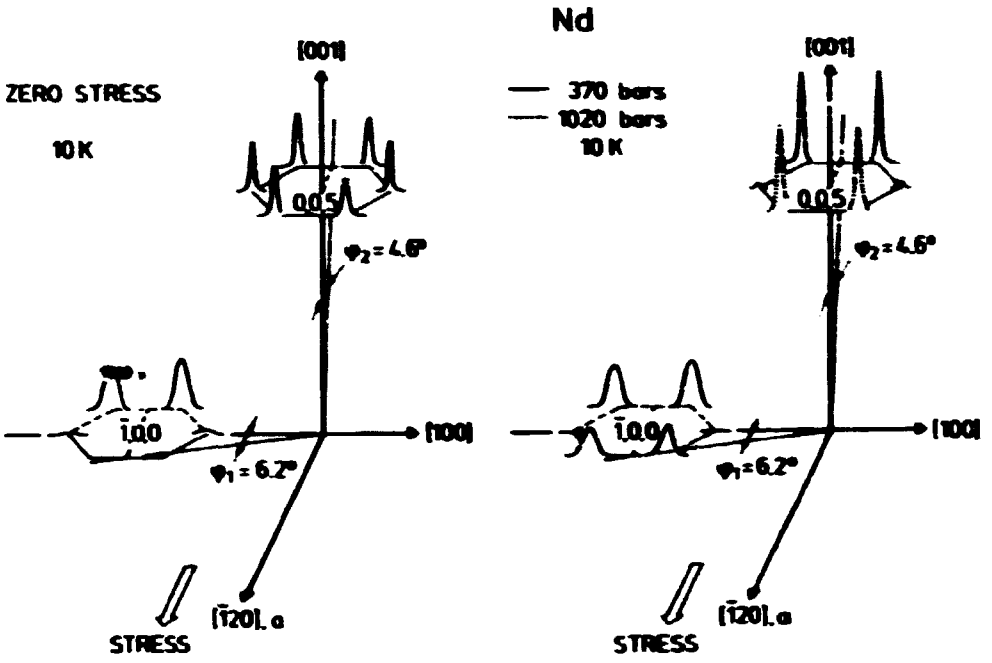

Fig. 6 The effect of uniaxial pressure along a [1̄20] direction in Nd illustrated by the change of the magnetic satellites observed around the (1̄,0,0) and (0,0,5) reciprocal lattice points.

1020 bar, the satellites corresponding to modulation vectors, $\vec{q}$, perpendicular to the stress direction ((h±q,0,l) types) are almost suppressed while some of the ones corresponding to modulation vectors parallel to the stress direction are enhanced. This is illustrated in Fig. 6, where the (±q,0,5) and the (1̄±q,0,0) satellite intensities diminish with increasing pressure, the (0,±q,5) and the (±q,∓q,5) intensities increase with pressure, and the (1̄±q,∓q,0) and the (1̄,±q,0) intensities remain unchanged with increasing pressure. The effects of uniaxial pressure applied to Nd are opposite to those observed in Pr (McEwen et al. 1978) and similar to those observed in $CeAl_2$.

1.7 Magnetic form factor of Pr metal

(S.A. Burke (ILL, Grenoble, France), B. Lebech, B.D. Rainford (University of Southampton, Southampton, U.K.) and K.A. McEwen (University of Salford, Salford, U.K.))

In a neutron diffraction study, the dhcp crystal structure of Pr metal in principle allows a separate determination of the induced magnetic form factors on the two different symmetry sites (hexagonal and cubic) of the structure. Furthermore, the hexagonal site form factor can be determined independently by an appropriate selection of reflections.

Measurements using conventional polarized neutron diffraction (Lebech et al. 1979) showed that for a magnetic field applied along a $[\bar{1}20]$ direction, there is very little anisotropy in the form factors deduced for the hexagonal sites only, and that to a very good approximation $\mu_h f_h = 2\mu_c f_c$. Here μ_h, f_h and μ_c, f_c refer to the moments and the form factors on the hexagonal and the cubic sites, respectively, and the $[h,k,\ell]$ to a reciprocal lattice vector direction. Earlier measurements (Lebech and Rainford 1972) showed that at 4.2 K a field applied along the [001] direction in Pr induces an almost negligible moment on the hexagonal sites and a measurable moment on the cubic sites. Hence, the induced magnetic form factors determined for a field applied along the [001] at 4.2 K will predominantly give information about the cubic site form factor. Using the D3 polarized neutron spectrometer at the Institute Laue-Langevin, Grenoble, France, the induced magnetic form factor for a field applied along the [001] direction was determined. A preliminary analysis shows that within the experimental uncertainties the induced form factor for a field along [001] is consistent with the form factor determined for a field along $[\bar{1}20]$. This indicates that the induced magnetic form factors on the two sites are nearly identical. An analysis of the data using the previously determined f_h (Lebech et al. 1979) showed that at 4.2 K and for a field of 4.6 T applied along [001] $\mu_c = 0.32\ \mu_B$, in good agreement with the earlier results (Lebech and Rainford 1972).

1.8 Localized magnetic excitations in Ho_2Co_{17} and Ho_2Fe_{17}

(K. Clausen and B. Lebech)

The low-energy part (<20 meV) of the magnetic excitation spectrum of the uniaxial ferrimagnets Ho_2Co_{17} and Ho_2Fe_{17} (Clausen 1981) contains three branches: a highly dispersive mode of parabolic shape, a non-dispersive mode, and a dispersive mode that is degenerate with the q-independent mode at the zone boundary.

For the non-dispersive mode it is a good approximation to regard the rare earth spins as independent from the transition metal spins, situated in a molecular field within a crystal field originating from the surrounding ions. The single ion mean field hamiltonian describing this situation is given by

$$H_{MF} = H_{CF} - \vec{\mu}\cdot\vec{B} = H_{CF} + g\,\mu_B\,\vec{B}\cdot\vec{J}_R$$

where $\vec{J}_R$ is the total angular momentum on the rare earth sites. $H_{CF} \simeq B_2^0\,O_2^0 + B_6^6\,O_6^6$ is the crystal field hamiltonian in the c-axis representation (B_4^0 and B_6^0 are assumed to be negligible). The molecular field $\vec{B}$ is given by the magnetic moment of the transition metal ions and the rare earth-transition metal exchange constant.

In the independent dipole approximation, the intensity of the scattering from this mode at a given temperature T - including instrumental resolution - can be calculated as (de Gennes 1963),

$$I(\omega,T) = \sum_{if} \{\rho_i |\langle f|\hat{J}_\perp|i\rangle|^2\, k_i/k_f \times$$

$$C \exp(-(\hbar\omega - E_j + E_i)^2/\sigma_{if}^2)\} + B$$

where

- C is a normalizing constant,
- $\hat{J}_\perp$ is the component of the momentum operator perpendicular to the scattering vector $\vec{\kappa} = \vec{k}_i - \vec{k}_f$,
- $\vec{k}_i, \vec{k}_f$ are the initial and final wave vectors,

σ_{if} is the energy resolution width of the spectrometer for an energy transfer of $E_i - E_f$,

ρ_i is the Boltzmann population factor for the initial state,

B is a constant background.

The initial and final energies, E_i and E_f, and wave functions, $\langle i|$ and $\langle f|$, are determined by diagonalization of the mean field hamiltonian,

$$H_{MF} |n\rangle = E_n |n\rangle$$

where n = i or f.

From an analysis of the observed magnon dispersion relations, the crystal field parameters B_2^0 and B_6^6 and the molecular field $\vec{B}$ on the rare earth sites are known in terms of a linear spin-wave picture (Clausen 1981). Using these results, the level schemes and transition probabilities $|\langle f|\tilde{J}_\perp|i\rangle|^2$ between adjacent states were calculated, together with the component of the total angular momentum of the Ho ions along the quantization axis for Ho_2Co_{17} and Ho_2Fe_{17}. As shown on the right-hand sides of Figs. 7 and 8, almost pure J_z states were found in both cases. The calculations also show that the transition probabilities between non-adjacent states are about two orders of magnitude lower than for adjacent state transitions, and the former type of transitions has therefore been neglected in the analysis. The solid lines on the left-hand sides of Figs. 7 and 8 are the calculated scattering from the non-dispersive mode at different temperatures, and the open circles are the observed scattering. In the calculations, the background B was taken from the experiment as the observed scattering outside the regions of the peaks. The normalization constant was estimated by inspection, and kept temperature invariant. The rest of the parameters in the calculations are given by the parameters deduced from the spin-wave fits (Clausen 1981) and the known resolution of the spectrometer.

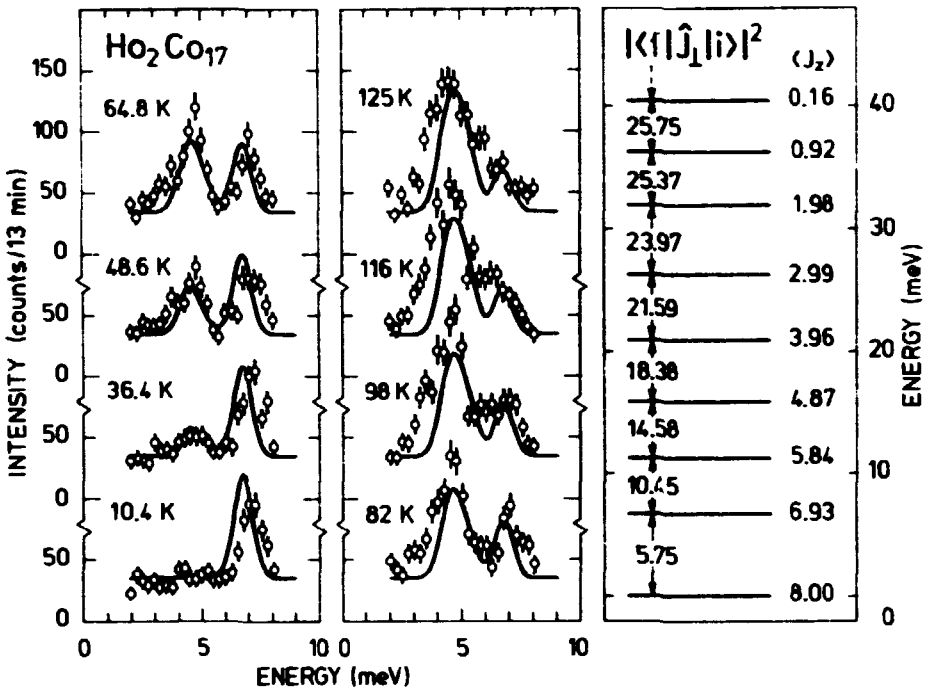

Fig. 7 The scattering from the localized (non-dispersive) mode in Ho_2Co_{17} at different temperatures. The solid curves are calculated from a mean field model using the parameters deduced from the fit to the linear spin-wave model. The energy levels, the z-component of the total angular momentum J_z, and the transition probabilities within the mean field model are given in the right-hand part of the figure. The line shape of the scattered intensity is calculated using the known energy resolution of the spectrometer (Clausen 1981).

For Ho_2Co_{17}, the agreement between the observed and calculated scattering is remarkably good (see Fig. 7). For Ho_2Fe_{17}, the peak at approximately 5 meV starts developing at too low a temperature, and the peak at ~8 meV dies out too slowly. This discrepancy is due to the neglect of B_4^0, which according to magnetization data (field slong the hard direction) is not negligible for Ho_2Fe_{17} (Clausen and Nielsen 1981).

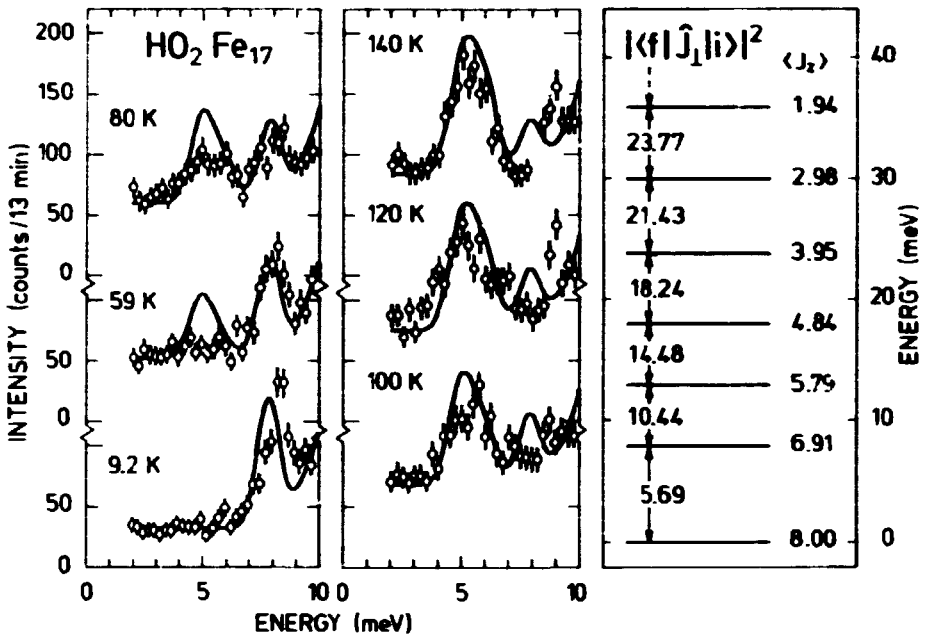

Fig. 8 The temperature dependence of the scattering from the localized (non-dispersive) mode in Ho_2Fe_{17}. The solid curves are the result of a mean field calculation (see caption for Fig. 7).

1.9 Crystal field splittings of dilute rare earth ions in Mg-crystals

(J.K. Kjems and M. de Jong (University of Amsterdam, The Netherlands))

Inelastic neutron scattering has been used to study the crystal field excitations of dilute Tb, Ho, Dy, Er and Tm in single crystals of Mg (x = 0.003 to 0.008). Well resolved spectra are observed and most of the observed features can be readily assigned on the basis of their temperature dependence and their dependence on crystal orientation. In each case the crystal field parameters have been determined by least squares fitting and the results are compared with the parameters derived from susceptibility data. A fair agreement is found in most cases except for Dy, where the susceptibility results have large errors.

1.10 Crystal field effects and exchange interactions in dilute Y-Er alloys

(D. Justesen and J.K. Kjems)

The spectra of the crystalline electrical field excitations were measured in the dilute rare earth alloys Y_{1-x} Er_x (x = 0.02 and 0.003) by means of inelastic neutron scattering using a high resolution triple-axis spectrometer. The sample temperature was 4.2 K, so only elastic scattering or scattering from the crystal-field ground level with energy loss could occur. For Y_{1-x} Er_x, (x = 0.003) the neutron spectra contained four well-defined peaks, which can be fully reproduced by theoretical calculations (Rathmann et al. 1974) using the following crystal-field parameters in the single-ion crystal-field hamiltonian,

$$B_2^0/\alpha = (-\ 125.9 \pm 0.2)\ K$$

$$B_4^0/\beta = \quad (8.59 \pm 0.1)\ K$$

$$B_6^0/\gamma = (10.15 \pm 0.05)\ K$$

$$B_6^6/B_6^0 = \pm\ 77/8$$

These results are within the uncertainties in accordance with those obtained by magnetization measurements (Rathmann et al. 1974). Measurements at 42 K indicate that the crystal-field parameters derived in this manner are temperature-dependent, i.e. B_4^0/β (42 K) = (0.85 ± 0.1) K for Y_{1-x} Er_x (x = 0.2).

In the Y_{1-x} Er_x, (x = 0.2) spectra, there was a significant line broadening of the excited levels. This can be explained by indirect exchange coupling to the nearby Er-ions; a simple Ising-model with nearest neighbour interactions can reproduce the experimental results.

1.11 The influence of superconductivity on the crystal field transitions in La(Tb)Al_2

(J.K. Kjems, R. Feile (Joh. Gutenberg University, Mainz, F.R.G.) and M. Loewenhaupt (KFA, Jülich, F.R.G.))

Dilute crystals of $La_{1-x}Tb_xAl_2$ (x = 0.001 to 0.010) have been studied by inelastic neutron scattering. $LaAl_2$ is superconducting below T_c = 3.15 K and the addition of Tb lowers T_c (T_c = 2.5 K for x = 0.003). The crystal field splitting of the Tb J = 6 ground multiplet leads to a Γ_1 singlet ground state and a Γ_4 triplet excited state at 0.66 meV. The onset of superconductivity leads to an abrupt change in the line width of Γ_1-Γ_4 transition, which can be used to study the details of the interaction between the localized 4f electrons and the conduction electrons. The temperature dependence of the line width is shown in Fig. 9 and is in good agreement with a model calculation by Keller and Halzer (1975). A small increase in the observed intensity at the lowest temperatures has so far not been explained satisfactorily.

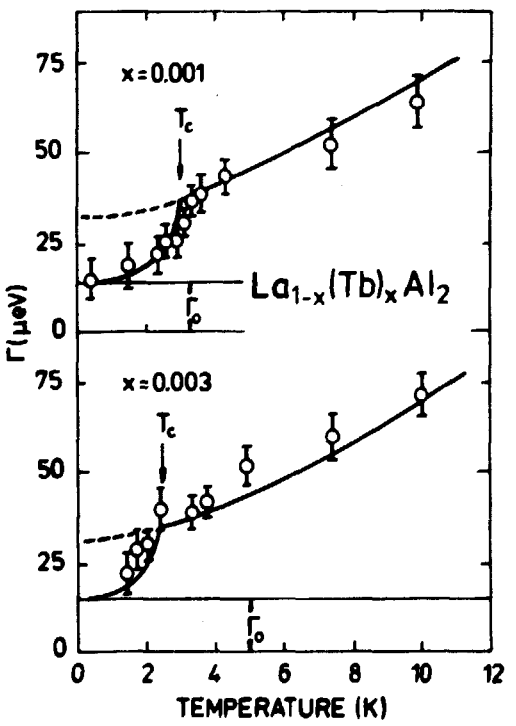

Fig. 9 Temperature dependence of the line width of the Γ_1-Γ_4 crystal field transition in $La_{1-x}Tb_xAl_2$. The abrupt change of width signifies the onset of superconductivity.

1.12 Magnetic field dependence of the excitation energies in the mixed valence system TmSe

(M. Loewenhaupt (KFA, Jülich, F.R.G.) and H. Bjerrum Møller)

Inelastic neutron scattering measurements have been performed on a polycrystalline sample of TmSe in applied magnetic fields up to 9 T. The measurements in zero field show an inelastic line at ~1 meV below the ordering temperature T_N = 3.2 K, and a line at 10 meV both below and above T_N, in agreement with previous measurements (Loewenhaupt and Holland-Moritz 1979). The low energy line exhibits a very strong linear field dependence below T_N, as shown in Fig. 10. Above T_N the same linear field dependence is observed once the magnetic field is sufficiently strong to create ferromagnetic order. The extrapolation of the

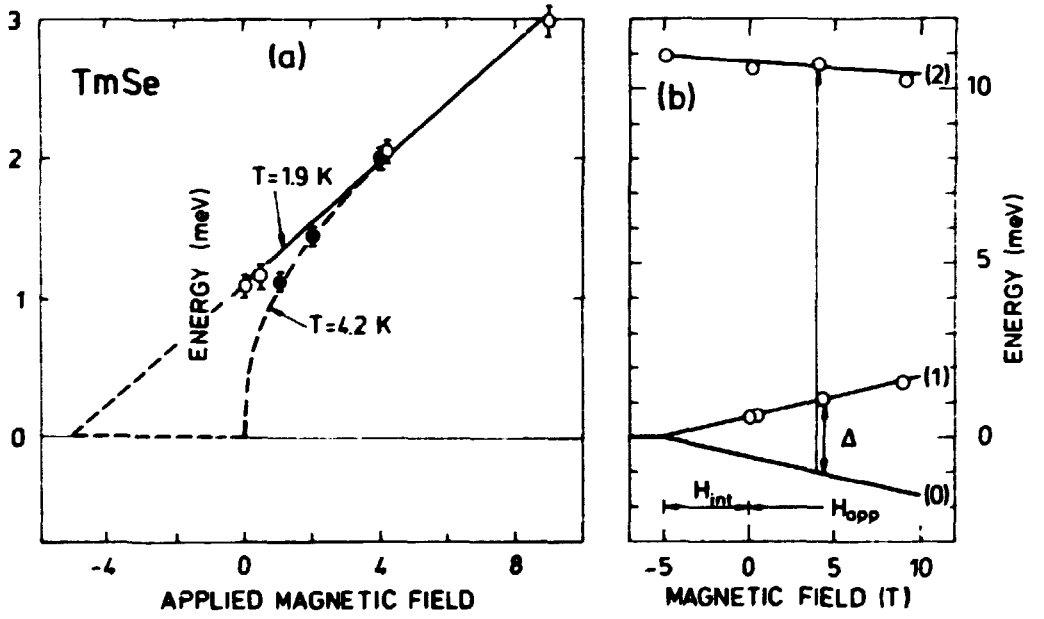

Fig. 10 (a) Magnetic field dependence of the low energy excitation in TmSe at 1.9 K (below T_N) and 4.2 K (above T_N). The extrapolation of the excitation energy to zero (below T_N) gives the internal molecular field in the ordered sample. (b) Two-level model in which the results can be interpreted. The degenerate ground-state split in the magnetic field (internal + applied). Only the lowest level |0> is populated at low temperatures and the transitions observed are therefore from the lowest level |0> to levels |1> and |2>.

excitation energy to zero (below T_N) gives the internal molecular field of the ordered sample. The high energy line (at ~10 meV) shows only a very weak dependence on the applied magnetic field.

These results can be interpreted in terms of the model shown in Fig. 10, where a degenerate ground level of a two-level system is split in the magnetic field. Only the lowest level $|0\rangle$ is populated at low temperatures and the transitions observed are therefore from this level to levels $|1\rangle$ and $|2\rangle$. The magnitude of the splitting of the ground level in a field of $H_{int} + H_{appl}$ = 5 T + 9 T = 14 T is Δ = 3.05 meV, giving a magnetic moment of 1.9 μ_B of the ground-state in agreement with previous neutron diffraction results (Bjerrum Møller et al. 1977). The ground-state may thus be described by S_{eff} = 1/2 and g_{eff} = 3.8.

1.13 Possible valence transition in YbH_2

(B. Buras, L. Gerward (Technical University of Denmark), B. Johansson (University of Aarhus, Denmark), B. Lebech, J. Staun Olsen*, H. Skriver and S. Steenstrup* (*University of Copenhagen, Denmark))

At normal pressures and temperatures the rare earth elements as a general rule form trivalent dihydrides, the only two exceptions being EuH_2 and YbH_2, which are divalent. This behaviour is typically reflected in the variation of the crystal structure as a function of atomic number. Thus, EuH_2 and YbH_2 form orthorhombic crystals while the other rare earth dihydrides crystallize in the fluorite structure. At atmospheric pressure, the energy difference between the divalent and the trivalent state in metallic Yb is ~0.5 eV, and one expects Yb metal to undergo a transition to the trivalent state at a pressure of 150 kbar. Heat of formation data indicates that this energy difference between the two valence states is lowered considerably when Yb forms the dihydride. As a result, one would expect YbH_2 to undergo a first-order transition from the divalent to the trivalent state at not too high a pressure. Furthermore, the valence transition might be followed by a change in crystal structure to the fluorite structure characteristic of the trivalent dihydrides.

In view of the above, we undertook a structural study of YbH_2 at high pressures, using both neutron and x-ray diffraction techniques[†]. The neutron study was performed using the fixed scattering angle high pressure cell described by Buras et al. (1977). Up to ~40 kbar only shifts of diffraction peaks were observed. The x-ray study was performed using a diamond squeezer and the white-beam energy-dispersive diffractometer (Staun Olsen et al. 1981) at the synchrotron radiation source DORIS (DESY-HASYLAB, Hamburg). Up to ~70 kbar, again only shifts of diffraction peaks were observed. The data are being analyzed and the study will be continued by application of higher pressures.

1.14 Intra- and intermolecular interactions in $[Ni_2(ND_2C_2H_4ND_2)_4Br_2]Br_2$ studied by neutron scattering

(J.K. Kjems, A. Stebler*, H.U. Gudel* (*University of Bern, Switzerland) and A. Furrer (ETHZ, Würenlingen, Switzerland))

Complexes of the type $[Ni_2(en)_4X_2]^{2+}$, where X stands for Cl^-, Br^- or SCN^-, are well known dimers with ferromagnetic interactions. The excitation spectrum of the bromine compound has been studied by inelastic neutron scattering using the TAS 7 cold source spectrometer. Only two inelastic peaks were observed at 0.6 and 2.8 meV, respectively. The analysis of the intensities and the dependence on momentum transfer and temperature leads to an energy level scheme for this compound as shown in Fig. 11. The corresponding hamiltonian has a intra dimer exchange constant of $J = 0.45 \pm 0.04$ meV and an unexpectedly large axial anisotropy constant $D = -0.8 \pm 0.1$ meV.

[†]The sample was kindly provided by the Institute of Low Temperature and Structural Studies, Wroclaw, Poland.

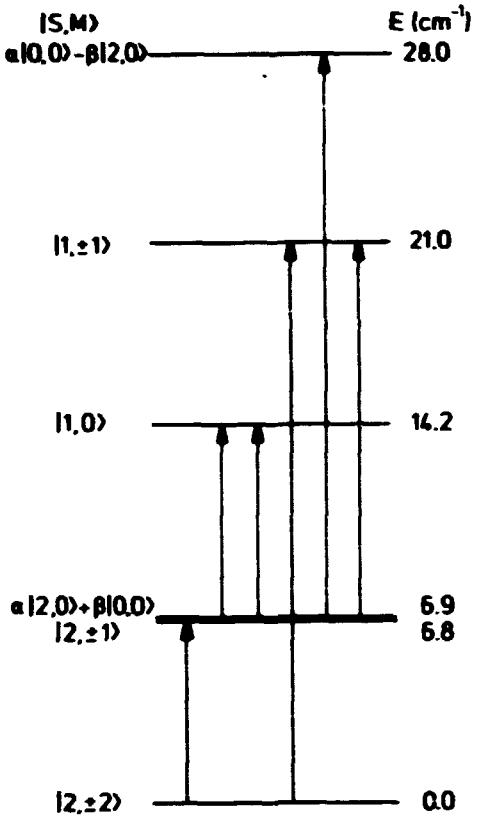

Fig. 11 Energy level scheme for $[Ni_2(ND_2C_2H_4ND_2)_4Br_2]Br_2$ deduced from inelastic neutron scattering data.

1.15 Delocalization of 5f-electrons in Am

(H.L. Skriver, O.K. Andersen (Max Planck Institute, Stuttgart, F.R.G.) and B. Johansson (University of Aarhus, Denmark))

The variation of cohesive, structural, magnetic and superconducting properties through the series of the actinide metals indicates that up to and including Pu, the 5f-electrons are itinerant and form band states similar to that of the d-electrons in the 3d, 4d and 5d transition metals. In contrast, Am behaves like a rare earth metal, indicating that the 5f-electrons are localized and occupy a non-magnetic (J=0) $5f^6$ configuration. This abrupt change in properties is thought to originate from the contraction of the 5f orbital through the series, and one expects Am to undergo a transition to a dense phase with itinerant 5f electrons when pressure is applied.

The above view of the nature of the 5f-electrons has been substantiated by self-consistent calculations of the atomic volume

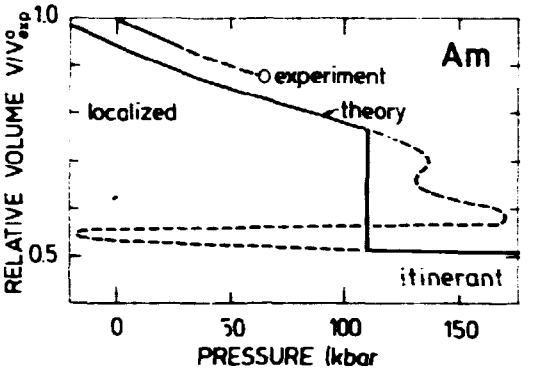

Fig. 12 Theoretical and experimental pressure-volume relations for Am. The experimental curve is that of Stephens et al. (1968) and the point that of Akella et al. (1979). The volume is normalized by the experimental volume V^{o}_{exp} at zero pressure.

through the actinide series (Skriver et al. 1978) giving quantitative agreement with experiments. Recently, we calculated (Skriver et al. 1980) a pressure-volume relation (Fig. 12) for Am which shows a first-order phase transition from a localized to an itinerant 5f-electron behaviour. We propose to identify this change in properties with the phase transition observed by Akella et al. (1979) at 110 kbar.

1.16 The s-d transition in compressed La

(A.K. McMahan (Lawrence Livermore Laboratory, California, U.S.A.), H.L. Skriver and B. Johansson (University of Aarhus, Denmark))

The shock compression data for most of the rare earths display an anomaly at about 40% compression. Explanations have focused on three interrelated issues: 1) termination of the 6s-5d electronic transition, 2) overlap of the Xe cores, and 3) melting. The f-electrons do not appear to play a crucial role as the shock anomaly is also exhibited by Sc and Y, for which there are no nearby f-levels at all.

In order to resolve some of the ambiguities in understanding the high pressure behaviour of the rare earths, we performed a first principles calculation of the equation of state of La, both at zero and at finite temperatures. Our results (Fig. 13) show that both the termination of the 6s-5d transition and the onset of a significant pressure contribution from the overlap of the Xe

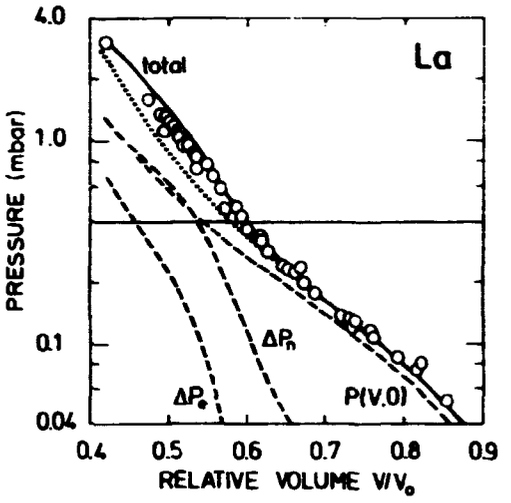

Fig. 13 Theoretical and experimental results for the La Hugoniot; pressure versus relative volume. Present calculation with temperature-dependent Slater γ (solid curve) and with a temperature-independent linear γ (dotted curve). The total pressure (solid curve) is resolved into zero temperature P(v,0), electron thermal ΔP_e, and nuclear motion thermal ΔP_n contributions (dashed curves). The open circles are the experimental values.

cores do occur in the vicinity of the observed stiffening in the shock data. However, the core contribution is found to be a much more gradual effect, and the abrupt nature of the anomaly evident in the data is due primarily to the termination of the s-d transition.

1.17 Search for a bi-critical point in CeAs

(J.K. Kjems and H.R. Ott (ETH, Zürich, Switzerland))

The evolution of the antiferromagnetic order parameter as a function of temperature and an applied magnetic field along <100> and <110> has been studied by neutron diffraction from a small single crystal of CeAs, which is a type I antiferromagnet with the moment parallel to the ordering wave vector (1/2,0,0) and cyclic permutations. A theoretical analysis by Knak Jensen et al. (1979) has suggested that T_N represents a bicritical point in zero field and that the application of an uniaxial stress or a magnetic field would initially increase T_N. The measurements on CeAs showed that T_N is unchanged to within ±2 mK up to 0.5 T and then shows a slight decrease with increasing field. The critical exponent β was found to be 0.37 ± 0.02 with no systematic trend for increasing field.

1.18 Magnetization and critical fluctuations of the random ferromagnet $LiTb_{0.3}Y_{0.7}F_4$

(K. Kjær, J. Als-Nielsen and I. Laursen (Technical University of Denmark))

As a good approximation, $LiTbF_4$ may be regarded as a dipole coupled Ising ferromagnet (Holmes et al. 1973, 1975). The splitting of 1.3 K (Laursen and Holmes 1974) of the ground state of the Tb ions may safely be ignored when compared with the couplings of the spins, yielding a transition temperature of 2.87 K. Because of the dipole coupling, the critical fluctuations become extremely anisotropic (Als-Nielsen 1976), reducing the marginal dimensionality to $d^* = 3$, so that the critical phenomena are described by mean field theory with only logarithmic corrections (Aharony 1973). Upon dilution of the magnetic ions with Y, the susceptibility of $LiTb_{0.3}Y_{0.7}F_4$ is reported (Beauvillain et al. 1980) to display a marked departure from the behaviour characteristic of marginal dimensionality.

Using double-axis neutron diffraction, we investigated the magnetization and the critical fluctuations of $LiTb_{0.3}Y_{0.7}F_4$. Preliminary results indicate that the extreme anisotropy of the

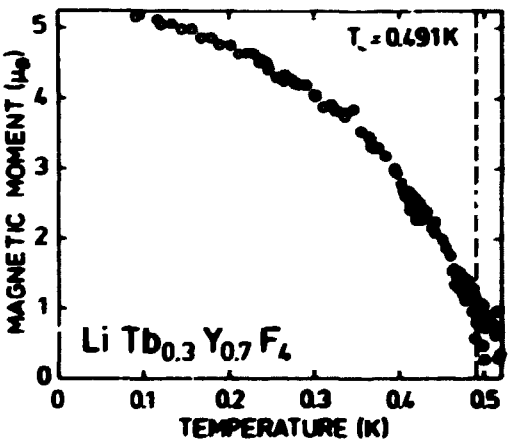

Fig. 14 Temperature dependence of the magnetization in $LiTb_{0.3}Y_{0.7}F_4$ below the transition temperature $T_c = 0.491$ K. As the precise atomic positions in the diluted compound is unknown at present, the scale of the magnetization is only tentative.

fluctuations is retained. In the temperature range from T_c = 493 mK to 90 mK, the magnetization exhibits a remarkably slow increase (Fig. 14). A possible explanation for this is that the ground state splitting, which is comparable to the reduced, effective spin couplings in the diluted compound, gives the system essentially a Van Vleck character.

1.19 Tetragonal phase transition and other structural aspects of $Cs_2NaLnCl_6$

(G.P. Knudsen*, F.W. Voss*, R. Nevald* (*The Technical University of Denmark), H.D. Amberger (Institute for Inorganic and Applied Chemistry, University of Hamburg, F.R.G.), H. Bjerrum Møller and J.K. Kjems)

Some of the $M_2M'LnHa_6$, where M and M' are monovalent metals, Ln is an element of the lanthanide series, and Ha is a halogen, crystallize in the cubic elpasolite structure, which is related to the even simpler perovskite structure.

This group of materials constitutes an ideal model system for studying and testing many basic magneto-physical effects, and they are thus attacked by many experimental means by us and others (Dunlap and Shennoy 1974, Schwartz et al. 1976, Anistratov et al. 1978, Amberger 1978). As a part of this investigation, structural details were studied by neutron diffraction, using triple-axis spectrometry. So far the work has been concentrated on the subgroup $Cs_2NaLnCl_6$ of which single crystals with Ln = Nd and Yb and powders with Ln = Pr, Tm and Yb were used. The neutron diffraction data confirmed our earlier qualitative observations that crystals containing light lanthanides undergo a phase transition to tetragonal symmetry, whereas those containing heavy lanthanides stay cubic to low temperatures. The earlier qualitative observations stem from single crystal macroscopic magnetization measurements and ^{23}Na- and ^{133}Cs - NMR spectroscopy (Nevald et al. 1979). The structural features seem to be reasonable, taking into account the more ideal packing in the crystals with the smaller, heavier lanthanides, than in those with the larger, lighter ones. These considerations, however, fail if one attempts

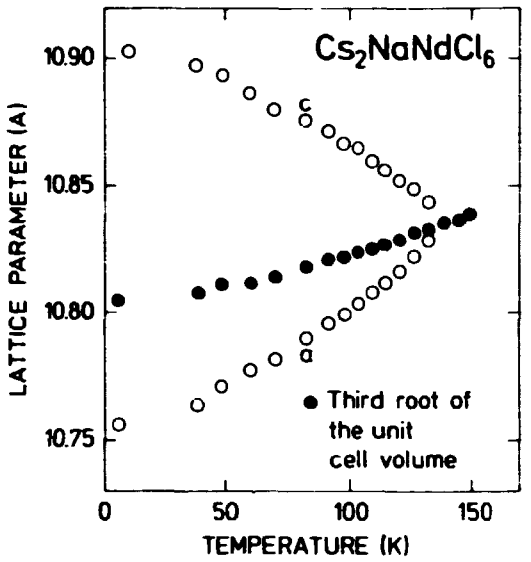

Fig. 15 The temperature dependence of the cell dimensions, c and a, in $Cs_2NaNdCl_6$-elpasolite, having a tetragonal/cubic phase transition around 135 K. Also included is the third root of the volume of the unit cell.

to make an extension to all the observed and missing phase transitions investigated in elpasolites.

In the cubic phases, the only free parameter (besides the size of the unit cell) is the Cl position on the line connecting Na and Ln. It is close to 48% from the Ln-end of that line for all the systems. This agrees well with the expectation from ionic radii. Of the materials involving the phase transition, the Nd-compound has been studied in greatest detail. The temperature dependence of the cell dimensions, a and c, has been established (Fig. 15). Furthermore, the tetragonal to cubic phase transition temperature has been determined by analyzing the merging of two diffraction peaks when the transition is approached from below (Fig. 16). The determination of the more complicated Cl movements awaits further measurements.

Our results so far may be summarized as follows:

(i) The third root of the volume of the unit cell increases smoothly from 4.2 K to 300 K by ~1%, independent of whether a phase transition takes place or not.

(ii) The Cl positions in the cubic phases are nearly the same in all the compounds and those expected from ionic radii considerations.

(iii) In the tetragonal phase of $Cs_2NaNdCl_6$, the c/a-ratio is about 1.014 at low temperature and decreases continuously to about 1.002 around 135 K.

(iv) The phase transition occurs at (136±1) K in $Cs_2NaNdCl_6$.

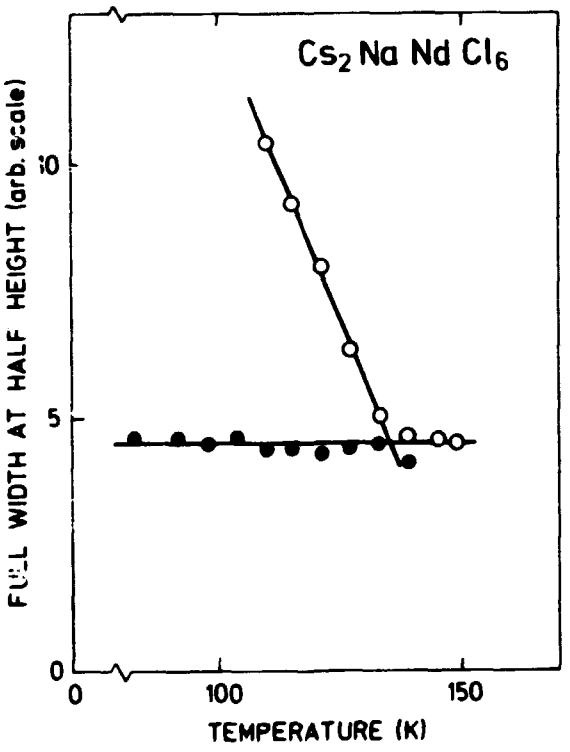

Fig. 16 Determination of the transition temperature from the merging of two unresolved diffraction peaks. The line widths resulting from fits to one or two gaussians are shown as • and o, respectively. The crossing of curves through the two types of circles is taken as the transition temperature.

It has not been possible to determine experimentally whether the transition is of first order or continuous, but it is evident from the data shown in Fig. 15 that at least 80% of the structural changes take place continuously.

1.20 A study of recrystallization kinetics using neutron diffraction

(N. Hansen*, D. Justesen, J.K. Kjems and T. Leffers* (*Department of Metallurgy, Risø))

In textured materials, recrystallization is normally accompanied by a change in texture. Such a change is an ideal measure of the degree of recrystallization, since the intensity of the diffraction signal from a given texture component is proportional to the amount of material with this specific texture. A large number of detailed investigations of the structural evolution during recrystallization have been made, but data on the kinetics are scarce. The present experiments were conceived with the aim of demonstrating the potential of neutron diffraction texture measurements as a tool for the investigation of recrystallization kinetics.

The principles of texture studies by neutron diffraction are similar to those of x-ray diffraction (Szpunar 1976), but because of the lower absorption factor, neutron diffraction seems to be more amenable. The first experiments were carried out on a conventional neutron spectrometer and the intensity of the (2,0,0) reflection of heavily rolled copper (99.98% purity) was measured as a function of temperature. It was possible to rotate the specimen under automatic control around a vertical axis. Consequently, pole-densities (or the texture) could be measured automatically along a large circle in the (2,0,0) pole-figure. The orientation of the specimen determined the position of the large circle in the pole-figure. The results, when interpreted in terms of an Avrami equation (Avrami 1940), indicate that the recrystallization kinetics for the texture components monitored are determined by nucleation and not by growth.

These very promising initial results suggested that specially designed equipment should be constructed for texture studies. Such an apparatus is now being developed. The improvements incorporated in the new design are: (i) An Euler-goniometer crate, which enables automatic setting of the sample in any orientation

and with which it is possible to measure a complete pole-figure without changing the experimental set-up. (ii) A position-sensitive neutron detector which scans 40° of the Debye-Sherrer ring simultaneously. The goniometer crate and the detector are connected, via electronics, to the JUPITER (Canberra) systems multichannel-analyzer, motor drive units and PDP-11 computer. PDP-11-software for the motor controls and data collection have been developed.

Calculations based on the first measurements indicate that a complete pole-figure for Cu with a resolution of 5° may be obtained in approximately 15 minutes. With the traditional x-ray reflection technique more than one hour is needed to measure 70% of the pole-figure. Hence one can expect to be able to follow the temporal evolution of the full three-dimensional orientation distribution during a recrystallization process within a few hours. Finally, it should be emphasized that the method is not limited to heat treatment processes. One could equally well envisage the study of textural changes during deformation as well as during thermo-mechanical processing.

1.21 Phase transitions of the smectic-A phase of the liquid crystal 4.08

(D.E. Moncton (Bell Laboratories, Murray Hill, New Jersey, U.S.A.), P.S. Pershan (Harvard University, Massachusetts, U.S.A.) and J. Als-Nielsen)

Liquid crystals consist of long rod-like molecules, typically containing two benzene-rings in the centre and aliphatic hydrocarbon chains in each end. In the present case one hydrocarbon chain has 4 members, the other 8, and the linkage between the former tail and the benzene rings is via an oxygen atom, hence the name 4.08.

In the smectic-A phase (de Gennes 1974) the molecules are arranged in layers with the molecular axis normal to the layers. There is a well-defined layer repetition distance, but liquid-like order within each layer. The order parameter for this phase

is a one-dimensional density wave characterized by an amplitude and a phase. In some materials the order parameter vanishes almost continuously as the temperature is raised towards the transition temperature T_c to the nematic phase where the layer ordering is destroyed, but an overall orientation of the molecules is maintained. Smectic-A-like fluctuations occur of course in the nematic matrix within a correlation range ξ (or rather $\xi_{\parallel}$ along the axis and $\xi_{\perp}$ perpendicular to the axis) and ξ diverges as $T \to T_c$. A phenomenological Landau analysis shows readily that the transition is isomorphous to that of superconductivity in metals (de Gennes 1972, McMillan 1972).

In lowering the temperature through the smectic-A phase 4.08 undergoes a phase transition to the B-phase, which has been interpreted to be another smectic phase with short range order within the planes. Recently, however, Moncton and Pindak (private communications 1980) and Pershan, Aeppli, Litster and Birgeneau (private communications 1980) showed independently by high resolution x-ray diffraction techniques that the B-phase was nothing more than a genuine three-dimensional crystalline phase.

The smectic-A phase itself does not have <u>true</u> long range order. This peculiarity comes about for very much the same reason that thermal fluctuations inhibit true positional long range order in a two-dimensional crystal (Landau 1965, Peierls 1934). Consequently, the Bragg scattering from the stack of layers, the (0,0,1) reflection, is not a delta-function (Caille 1972) but is rather to be described by a divergence $q^{-2+\eta}$, where q is the difference between the wave vector transfer and the (0,0,1) point, and η is a small parameter depending on two elastic constants describing longitudinal and transverse fluctuations of the layer arrangement.

This phenomenon of quasi-long-range order was recently observed by Als-Nielsen et al. (1980) in a so-called bi-layer smectic-A material. Here the molecule does not have aliphatic chains in both ends but rather a polar head and tail, and a molecular pair by sticking their polar heads together. There is no fundamental reason for the quasi-long-range order to be associated with bi-

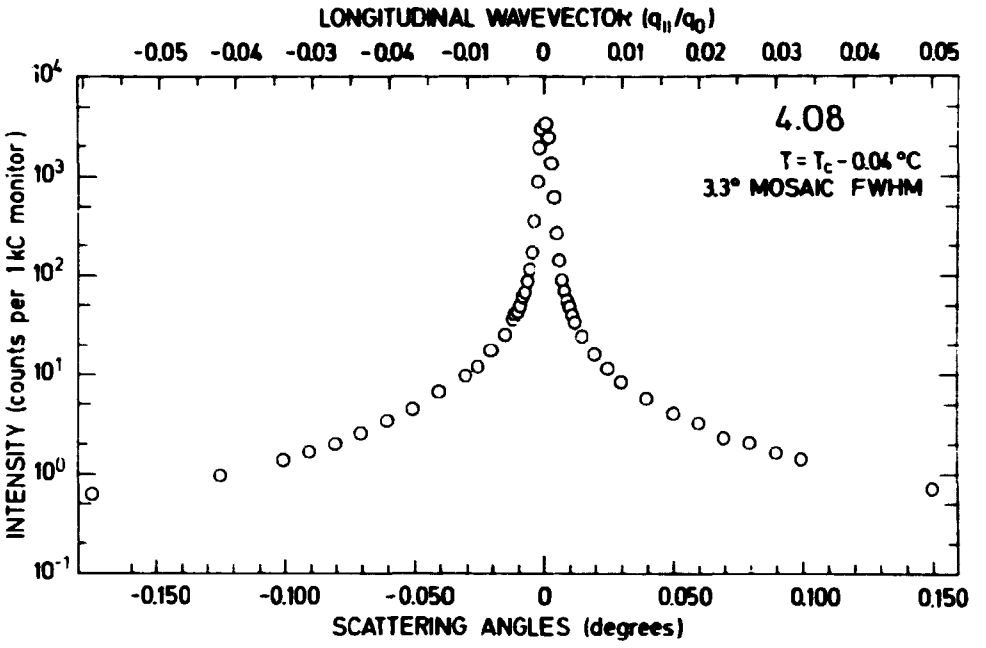

Fig. 17 Line shape of the (0,0,1) "Bragg" reflection in the smectic-A phase of the liquid crystal 4.08. The data extending over 4 orders of magnitude in intensity are consistent with a cross section diverging as $q_{\parallel}^{-2+\eta}$ rather than a delta function at $q_{\parallel} = 0$ superimposed on some thermal diffuse background. This divergence corresponds to algebraic decay of the layer stacking order, a phenomenon to be expected also in two-dimensional crystals due to thermal fluctuations.

layer type materials, so we felt it was of some importance to observe it also in single-layer materials. Furthermore, in 4.08 the $q^{-2+\eta}$ divergence should change in the B-phase to a true Bragg peak plus thermal diffuse scattering.

After this exposition of the motivations for the experiment, let us give an example of experimental results on the quasi-long-range order obtained with synchrotron radiation. A sharp, narrow resolution was obtained by using channel-cut crystals as both monochromator and analyzer. The profile of the (0,0,1) reflection is indicated in Fig. 17 showing the logarithm of the intensity versus wave vector deviation q. With the synchrotron source the quasi-long-range order peak can be traced over 4 decades in intensity and much further out in reciprocal space than in the

original experiment (Als-Nielsen 1980) at a 10 kW rotating anode. We have also measured the profile in the B-phase, as well as the critical fluctuations in the nematic to smectic-A transition.

1.22 Critical fluctuations in the nematic-smectic A re-entrant nematic phase transitions in liquid crystal mixtures

(F. Christensen and J. Als-Nielsen)

In section 1.21 we discussed the phase transition from the high temperature nematic phase to the low temperature smectic-A phase. In lowering the temperature further, one may obtain the nematic phase again, the re-entrant nematic phase. This striking phenomenon occurs in some bi-layer compounds at elevated pressures (Cladis et al. 1977), in mixtures of different molecules (Cladis 1975) and even in pure substances at ambient pressure (Hardouni 1979).

In a recent study by Bhattacharya and Letcher (1980) of the viscosity in the ternary mixture of heptylcyanobiphenyl (7CB), octyloxycanobiphenyl (80CB), and pentylcyanoterphenyl (5CT) in the ratio 73:18:9 by weight, it was noted that the re-entrant phase was not metastable as found in many other mixtures, and the phase diagram versus relative concentration of 80CB and 7CB shown in the lower part of Fig. 18 indicates an interesting point at 76.8% 7CB, where the material barely becomes smectic-A at any temperature. (Preliminary data on the phase diagram were kindly reported to us by E.P. Raynes, RSRE, Malvern Laboratory, U.K.)

Our aim was to study the critical behaviour of the fundamental quantity driving the phase transition, the correlation range ξ, in both the nematic and the re-entrant nematic phase, and for a number of concentrations encompassing the critical concentration of 76.8% 7CB. In order to measure the critical divergence of ξ up to several hundred times the molecular length, high-resolution x-ray diffraction experiment must be used. We established the technique for such measurements a couple of years ago using perfect crystal techniques and a rotating anode as the x-ray source (Als-Nielsen et al. 1977). In the present case, the ad-

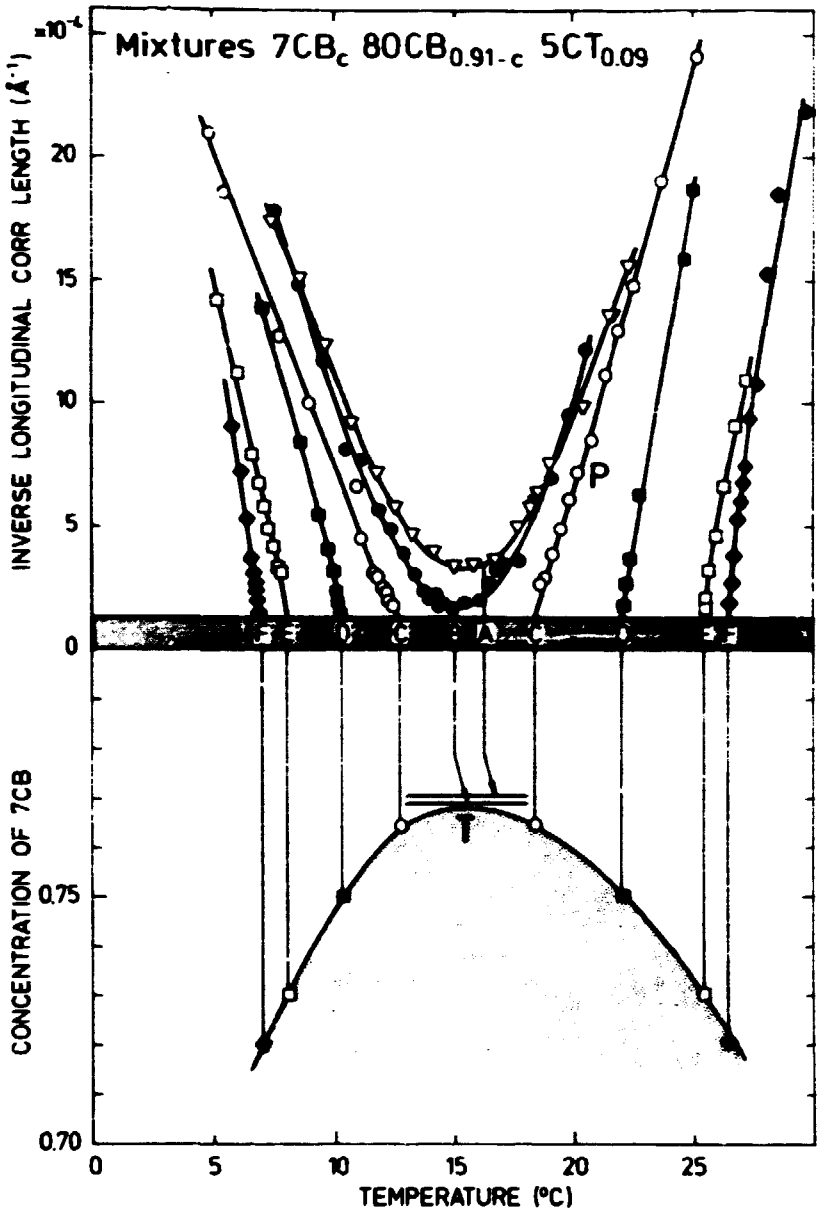

Fig. 18 Top: Correlation range of smectic-A fluctuations in the nematic phase in liquid crystal mixtures versus temperature. The grey area indicates the resolution limit of the correlation range. Bottom: Phase diagram of liquid crystal mixtures. The grey area denotes the smectic-A phase.

vantage of synchrotron radiation is primarily the fast data accumulation rate. Within one week we were able to obtain high quality data for 6 mixtures at both phase transitions corresponding to 12 experiments of the kind described by Prost (1981).

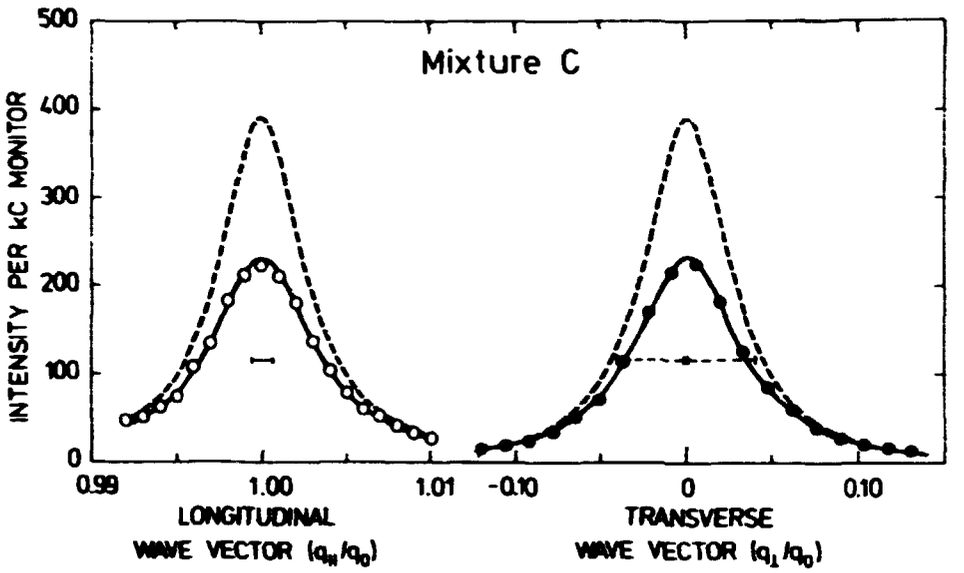

Fig. 19 Longitudinal and transverse scans through the (0,0,1) reciprocal lattice point show the smectic-A fluctuations in the nematic phase of liquid crystal mixtures at 20.17°C. Full lines are least squares fit of the cross section (dashed curve) folded with the resolution.

A summary of our results is given in Fig. 18. Let us first discuss one temperature point on the curve labelled C corresponding to a certain concentration. A longitudinal scan and a transverse scan through the (0,0,1) point of reciprocal space at 20.17°C are shown in Fig. 19. Both peaks become more intense and narrow as the temperature is lowered towards the transition temperature T_c. The width of the transverse peak exhibits a distinct kink at $T = T_c$, the limiting width being the mosaic width of the smectic-A phase. The kink determines the critical temperature within a few milli-degrees. The full line profile of the longitudinal scan is a best fit of a lorentzian cross section (dashed line) of full width $2/\xi$ at half maximum folded with the experimental resolution. All of the data in Fig. 19 are thus recorded to a single point, $\xi^{-1}(c)$, plotted on curve C in Fig. 18.

The data at a concentration slightly larger than the limiting one of 76.8% for obtaining the smectic-A phase (curve B) are particularly amusing. Smectic-A fluctuations clearly occur in the high

temperature nematic phase with a correlation range growing with decreasing temperature. But the growth never makes it to a divergence and when the temperature is lowered below T = 15.5°C, the correlation range starts to decrease with decreasing temperatures. In summary, the critical behaviour of ξ versus $|T-T_c|$ depends on the path in the phase diagram: the more tangential to the phase boundary the path is, the more gentle is the temperature dependence of ξ. A phenomenological Landau theory for this behaviour has already been outlined by Prost (1981), and we plan to analyze our data along these lines.

1.23 Monolayers of CD_4 physisorbed on graphite

(M. Nielsen, S.K. Sinha*, P. Dutta* (*Argonne National Laboratory, Illinois, U.S.A.) and M. Bretz (University of Michigan, Ann Arbor, Michigan, U.S.A.))

Neutron diffraction measurements have been performed on monolayers of CD_4 with the purpose of studying two types of phase transitions in the two-dimensional adsorbate system, namely melting and the commensurate to incommensurate transition. Melting of incommensurate physisorbed monolayers may be model systems for Kosterlitz-Thouless (1973) theory of melting. The experimentmental data for the commensurate to incommensurate transition are compared with recent theories of Villain (1980).

The phase diagram of adsorbed CD_4 monolayers is known from neutron measurements (Vora et al. 1979, Dutta et al. 1980). In the measurements described here, the high quality substrate UCAR-ZYX† is used. Figure 20 shows examples of Bragg scattering groups where the temperature or the layer density is changed so that we pass through either the melting or the commensurate to incommensurate transitions.

†UCAR-ZYX is the trade name of an exfoliated graphite product from Union Carbide, U.S.A.

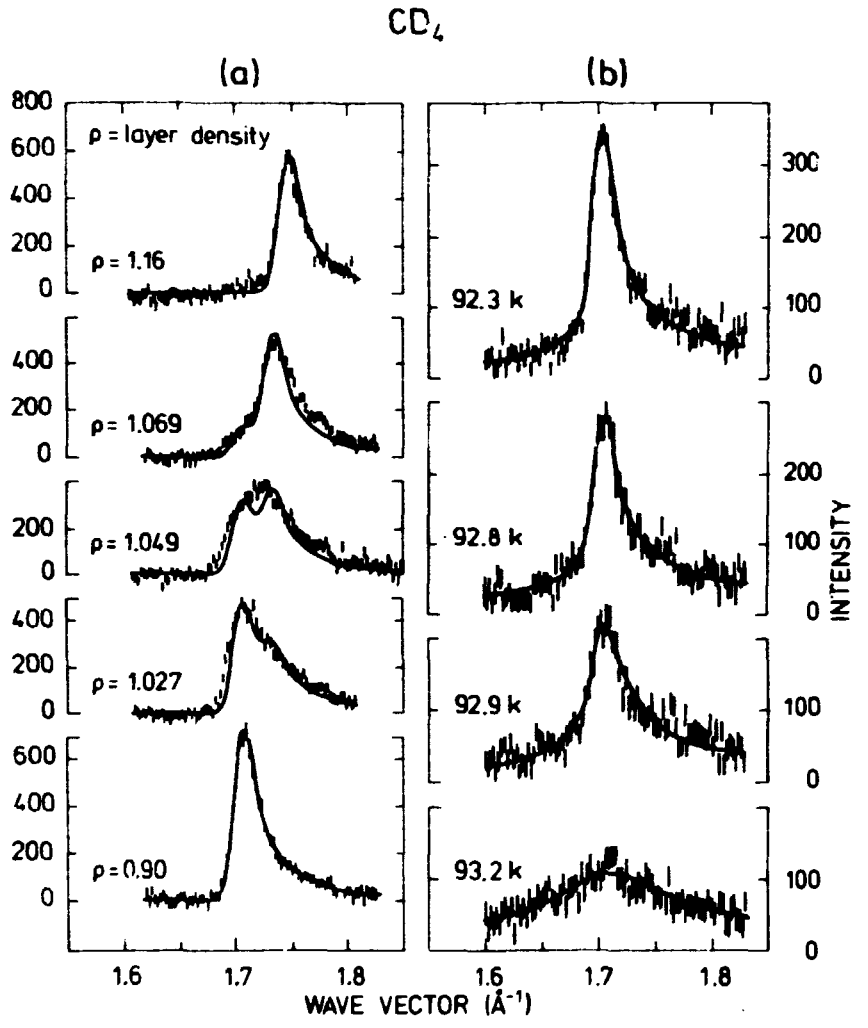

Fig. 20 Neutron scattering groups measured near the (1,0) Bragg point of the two-dimensional adsorbate structure of CD_4 on graphite. (a) and (b) illustrate the behaviour through the commensurate to incommensurate transition and through the melting transition, respectively.

It is concluded from the measurements near the melting transition that the quasi-long-range order, which is special for two-dimensional crystals and described by the scattering function

$$S(\vec{q}) = \frac{\text{constant}}{|\vec{q}|^{2-\eta}} ,$$

can be identified below the melting point. Above this temperature

the scattering is described by a lorentzian function for $S(\vec{q})$ as for a liquid. However, due to the powder nature of the exfoliated substrate it is impossible to conclude unambiguously what the nature of the melting transition is itself.

In the commensurate to incommensurate transition, the two phases involved have different and, for each, distinctive diffraction patterns. This is illustrated in Fig. 20, which shows that in a rather narrow interval of mean layer density, ρ, the two phases co-exist and this means that the transition is of first order.

1.24 The commensurate to incommensurate phase transition in monolayers of Kr adsorbed on (002) surfaces of graphite studied by x-ray diffraction

(J. Bohr, M. Nielsen and J. Als-Nielsen)

Monolayers of Kr physisorbed on (002) surfaces of graphite have been studied by x-ray diffraction in a set-up where a rotating x-ray source in conjunction with a position-sensitive detector gave a very efficient data acquisition. Using UCAR-ZYX exfoliated graphite as a substrate, we studied the commensurate to incommensurate phase transition down to low temperatures. At high temperatures, the transitions have been shown, in LEED (Chin and Fain 1977) and x-ray studies (Stephens et al. 1979, Birgeneau et al. 1980), to be continuous. Our data show at low temperatures a first order transition. This is illustrated in the example of the measured diffraction groups shown in Fig. 21. The group at 80 K is the (0,1) Bragg profile from a $\sqrt{3}$-commensurate monolayer. As the temperature is lowered, the commensurate to incommensurate phase transition sets in, but instead of a continuous displacement of the Bragg peak, we observe double groups indicating that two phases with slightly different lattice parameters co-exist. This is tantamount to a first order transition.

Kr on graphite is the system studied in most detail of the physisorbed monolayers and its phase transitions are model systems for recent theories (Villain 1980). Our conclusion that the commensurate to incommensurate transition is of first order at low

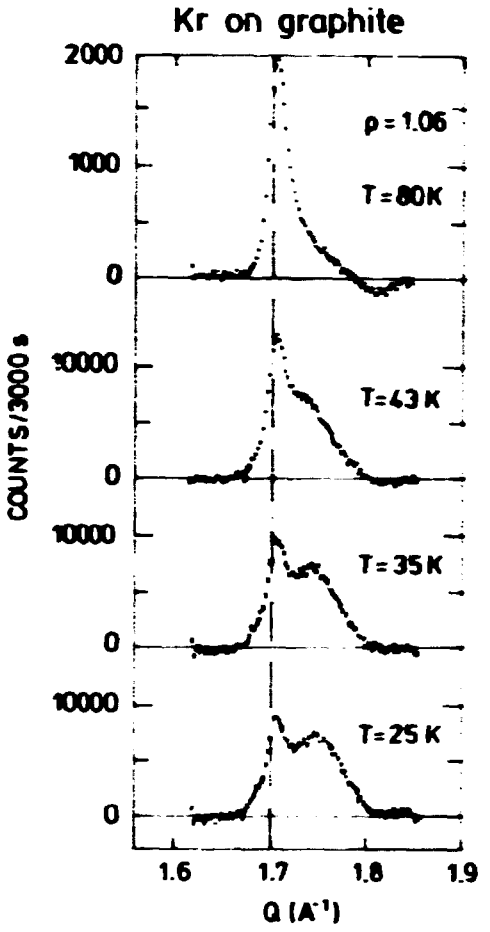

Fig. 21 The (0,1) Bragg profile observed at various temperatures by x-ray scattering from Kr physisorbed on graphite. At 80 K the observed monolayer has a $\sqrt{3}$-commensurate structure. The scattering from those regions of the monolayer that are not parallel to the scattering plane gives rise to scattering vectors that are larger than the $\sqrt{3}$-commensurate structure, i.e. the tail observed above $\tau_{01} = 1.703\ A^{-1}$ at 80 K. At lower temperatures, we observe a double peak which signifies a co-existence of phases.

temperature does not disagree with the earlier x-ray measurements (Stephens et al. 1979) which are at T = 85-89 K, but they do disagree with the LEED (Chin and Pain 1977) results. It is important to stress, however, that the effect of final size of the monolayer and of finite equilibrium times are vital and may influence the data. These effects must be studied systematically before final conclusions can be drawn.

1.25 Synchrotron x-ray diffraction on two-dimensional structures of Kr and Ar physisorbed on graphite

(M. Nielsen, J. Als-Nielsen, J. Bohr and J.P. McTague (University of California, Los Angeles, California, U.S.A.))

Synchrotron x-ray diffraction measurements on physisorbed monolayers on graphite have been initiated. Such measurements became of particular interest when it was recently discovered that the graphite substrate UCAR-ZYX can have ideally smooth surfaces over much larger areas than thought earlier. Our first aim was the determination of the coherence length in our ZYX substrate cell. A monolayer of Kr atoms was physisorbed in the cell. For a complete monolayer the Kr lattice is in registry with the graphite surface honeycomb lattice (the so-called $\sqrt{3}$ structure) and the sharpness of the Bragg peak from the Kr lattice gives the coherence length. The left part of Fig. 22 shows the (1,0) diffraction peak of the $\sqrt{3}$-Kr structure (full circles). The full line is a least-squares fit of the Bragg line profile with the coherence length L as an adjustable parameter. The best fit value is L = 2000 Å.

The open circles show the intensity profile for the same Kr filling, but now cooled down to 82 K. At this temperature there are slightly more physisorbed Kr atoms than available sites in a registered structure, and the adsorbate is commensurate with density modulations imposed by the graphite potential but not with the graphite surface.

Our results for Kr are identical with those obtained by Moncton, Birgeneau, Stephens, Brown and Horn (private communications 1980) at the Stanford storage ring, both as far as the quality of substrate, resolution and intensities are concerned. We utilized the technique to study a fundamentally different system, that is Ar, which is incommensurate with the graphite honeycomb lattice at all fillings and temperatures. The signal is somewhat diminished from that of Kr, as can be seen in the right-hand part of Fig. 22, simply due to the lower atomic number of Ar. Also the background from inevitable flakes of graphite in the (0,0,2)

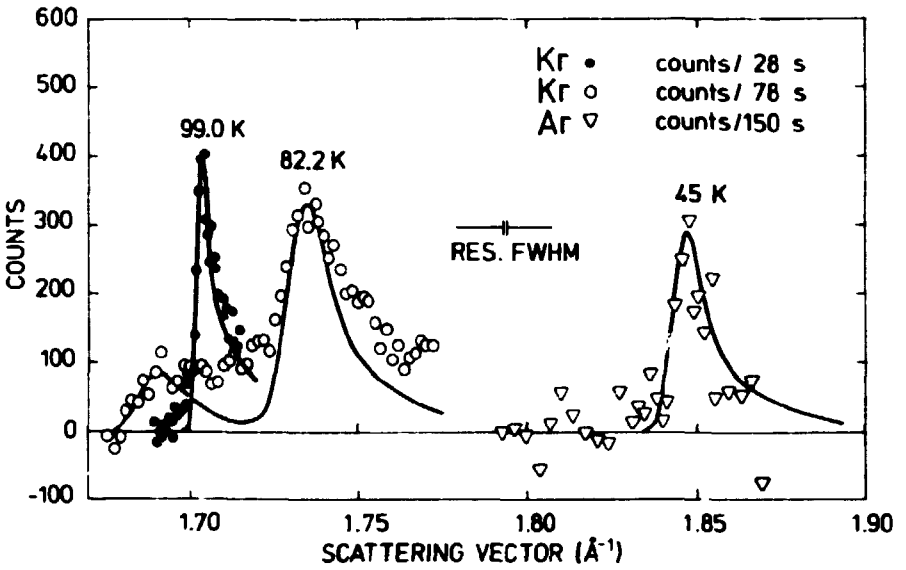

Fig. 22 Diffraction from the (1,0) peak of a two-dimensional "powder" of noble gas physisorbed on a graphite substrate, ZYX. For Kr the structure may be in registry with the graphite honeycomb lattice (●) and the sharpness of the low wave vector part of the peak gives the coherence length (2000 Å) of the substrate. At lower temperatures there are more Kr atoms than honeycomb sites and the incommensurate diffraction peak is broadened significantly (○). For Ar the structure is incommensurate at all fillings and temperatures. Nevertheless the diffraction part is relatively sharp corresponding to a coherence length of 750 Å.

orientation at 1.89 $Å^{-1}$ is considerably higher, but the incommensurate Ar peak can nevertheless clearly be measured with high resolution. The full line is the calculated profile corresponding to L = 750 Å.

1.26 Neutron scattering studies of phonon dispersion relations in HgTe and HgSe

(H. Kepa*, T. Giebultowicz* (*University of Warsaw, Poland), B. Buras, K. Clausen and B. Lebech)

HgTe and HgSe have the zincblende structure. Both are zero-gap semiconductors and the lattice dynamics of these substances are

essential for understanding their optical and electronic properties. The main difficulty in neutron scattering experiments on these compounds is the high absorption cross-section of naturally occurring Hg (210 barns for 1.08 Å neutrons). However, the previously reported studies (Kepa et al. 1979, 1980) of the acoustic phonon dispersion relations in HgTe showed that the high absorption of Hg did not prohibit a study of the lattice dynamics of Hg compounds. The previous study of the phonons in HgTe has been extended to include the optical phonons in HgTe. In addition, a study of the lattice dynamics of HgSe was initiated. As in the previous study, the measurements were made at the DR3 reactor using a triple-axis spectrometer at the cold source.

For the measurements on HgTe in the <110> and <100> directions we used the same sample as previously. For the measurements in the <111> direction, a similar but slightly smaller differently oriented sample was used. Because the cross-section for coherent inelastic scattering of neutrons decreases with increasing phonon energy, the measurements of the optical phonons were more difficult and required longer counting times (about 24 hours per phonon) than in the case of acoustical phonons (about 5 hours per phonon).

Three versions of the deformable bond approximation (DBA) model of lattice dynamics (Kunc et al. 1975a, 1975b), which includes short-range interactions up to the second nearest neighbour and long-range Coulomb interactions among polarizable and deformable ions, were fitted to the neutron data shown in Fig. 23. The three versions of the DBA model are characterized by the following simplifications concerning the short-range interactions:

(i) The non-central DBA model, where both first- and second-neighbour interactions are described by tensor coupling parameters in their most general form;

(ii) the central DBA model, where first-neighbour interactions are described by tensor parameters and second-neighbour interactions are supposed to be central, and

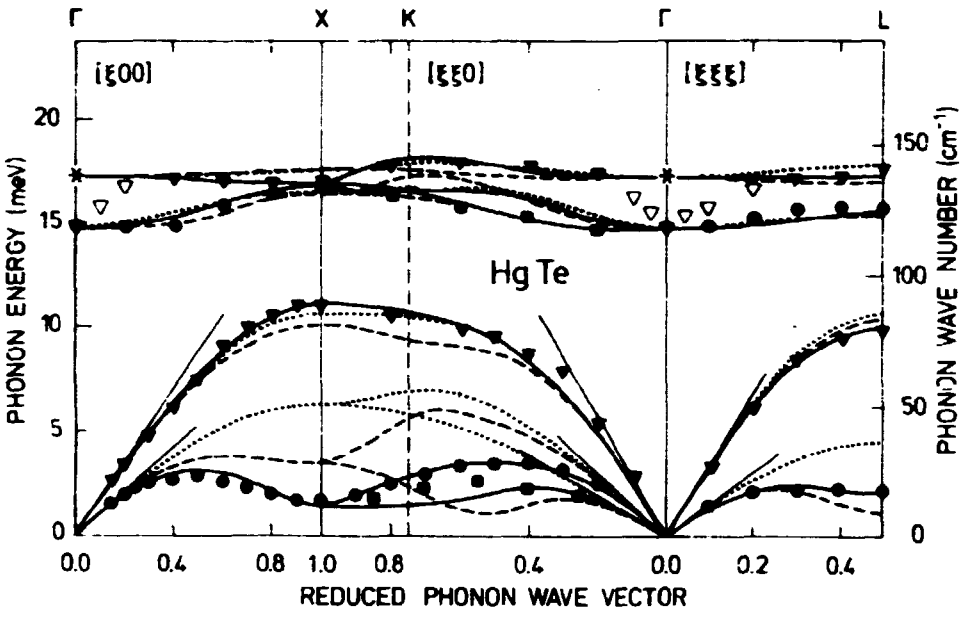

Fig. 23 Phonon dispersion relations in HgTe. The solid, dashed, and dotted curves are the results of fits to the three versions of the deformable bond approximation (DBA) model of lattice dynamics by Kunc (1975a, 1975b) described in section 1.26.

(iii) the AB μν model, where first-neighbour interactions are described by tensor parameters and second-neighbour interactions are described by spring-like potentials between the atoms.

In the fits, the experimental points marked by open triangles were omitted for reasons discussed below. As can be seen from Fig. 23, the best (and rather good) fit is obtained for only the non-central DBA model (solid curve). The crosses at the zone-centre represent the LO frequencies measured by Mooradian and Harman (1970) using Raman scattering ($\omega_{LO}(\Gamma) = 137\ cm^{-1}$). The measured neutron data for the LO branch close to the Γ point (open triangles in Fig. 23) indicate a degeneracy of LO and TO at Γ. This can be explained both qualitatively and quantitatively by free-carrier screening (in the present case - holes) of the long-range electric field of LO phonons (Mycielski et al. 1974 and references therein).

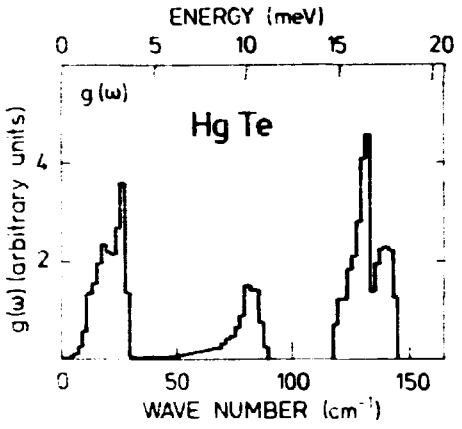

Fig. 24 Frequency distribution of phonons in HgTe derived from the phonon dispersion relations measured by neutron scattering.

On the basis of the non-central DBA model, the frequency distribution shown in Fig. 24 was calculated using the Gilat and Raubenheimer (1966) procedure.

For HgSe, so far we have measured only the acoustical phonons in the main symmetry directions <100>, <110> and <111> except for one of the transverse branches in the <110> direction. The dispersion relations for HgSe so far measured are very similar to those of HgTe.

1.27 Phonons in the organic conductor TEA(TCNQ)$_2$

(K. Carneiro, M. Almeida* and L. Alcacer* (*Instituto Superior Technico, Lisbon, Portugal))

The organic, quasi-one-dimensional conductor triethylamarium-di (tetracyanoquinodimethane), TEA(TCNQ)$_2$ consists of tetraedric stacks of $TCNQ^-$. It crystallizes in a triclinic cell (P1). The room temperature conductivity in the stacking direction is 7 $(\Omega cm)^{-1}$, which is intermediate for organic conductors. The compound is remarkable because crystals can be grown large enough for inelastic neutron scattering, whereas for most other organic conductors many crystals must be aligned to obtain an acceptable sample size.

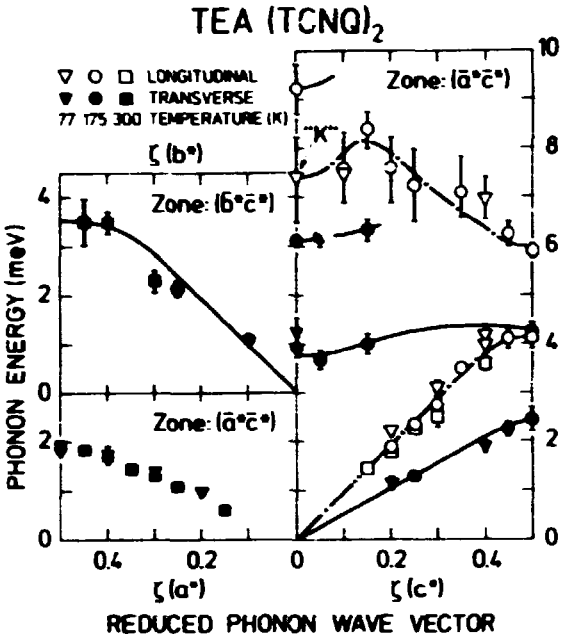

Fig. 25 Phonon dispersion relations of TEA(TCNQ)$_2$ in the a*, b* and c* directions. "K" indicates the pronounced Kohn-anomaly of the longitudinal acoustic branch.

The phonon spectrum $\omega(q)$ was studied along high-symmetry directions, particularly along c^*, which is close to being parallel to the stacking axis c. The results are shown in Fig. 25, and the following aspects should be noticed: Owing to the tetraedic structure as well as the electron-phonon coupling, gaps occur along c^*, both at the zone centre and at the boundary, but the dip at $q = 0$ can be ascribed only to the Kohn anomaly, stemming from the strong electron-phonon coupling at $q \sim 2k_F$, where k_F is the Fermi vector of the electrons. The magnitude of this Kohn-anomaly shows that the on-site Coulomb interaction is not very large compared with the electron hopping integral, a point which has been debated in the literature.

1.28 Neutron scattering study of the Li-conductor LiI·D_2O

(N. Hessel Andersen, J.K. Kjems and F.W. Poulsen (Metallurgy Department, Risø))

LiI·D_2O has a conductivity of 10^{-3} $(\Omega\ cm)^{-1}$ at 100°C, which is within the conductivity range of technological interest. The room temperature phase is cubic Pm3m with an excess of Li sites

on the face centre positions. Neutron scattering has been used to study the single crystals of this material in order to elucidate the role of the water molecule in the Li-diffusion. Diffraction shows that the preferred deuterium sites lie along the body diagonals. Anisotropic diffuse elastic scattering, which grows with decreasing temperature, is also observed. This can be explained by a model which assumed the existence of short range "antiferroelectric" correlations between the water molecules propagating in the <110> directions. At -66°C a transition to an orthorhombic phase, $P2_1am$, is observed. Here both the water molecules and the Li atoms appear to be ordered.

Inelastic scattering from powder of $LiI \cdot H_2O$ shows that the room temperature reorientation rate of the water molecules is less than 10^{10} s^{-1}. The acoustic phonon modes in $LiI \cdot D_2O$ have also been measured and appear without anomalies, whereas the optic phonon modes are strongly damped and could not be resolved.

1.29 Neutron scattering study of the ionic disorder in PbF_2 at elevated temperatures

(J.K. Kjems, K. Clausen (Clarendon Laboratory, Oxford, U.K.), M.T. Hutchings* and P. Schnabel* (*AERE Harwell, U.K.))

The collaboration with the Clarendon Laboratory, Oxford and AERE Harwell on neutron scattering studies of the fluorites was continued. PbF_2 was studied using the new high temperature furnace, and a pronounced quasielastic diffuse scattering was found in the F^--conducting phase similar to the earlier findings for CaF_2 (Kjems et al. 1978). However, the anisotropy in $\vec{q}$ was less pronounced and only small variations of the energy width with $\vec{q}$ were observed. A defect model has been developed to describe the distribution of the diffuse scattering integrated over energy transfer. Good agreement with the experiments is obtained with a model that resembles the well-known 222 defect in the fluorites. The defect cluster is centered on the cube edge of the fluorine lattice and it involves two interstitials, two displaced atoms and four vacancies.

1.30 A small angle neutron scattering facility, SANS

(J.K. Kjems, H. Bjerrum Møller and I.U. Heilmann)

The design and construction of a small angle scattering facility which will be situated at the end of the neutron guide behind TAS 7 and TAS 8 in the neutron house. The project is supported by grants from both the Danish and the Swedish Natural Sciences Research Councils. The main components of the instrument are:

(i) A mechanical velocity selector with 20' collimation and 6000 rpm, which can give $\Delta\lambda/\lambda = 0.1$ at 4 Å.

(ii) A 2.5 m evacuated collimation before the sample.

(iii) An evacuated sample chamber connected to a turbomolecular pump which can assure a cryogenic vacuum in the whole system.

(iv) A 3.5 m evacuated conical shielded tube to the detector.

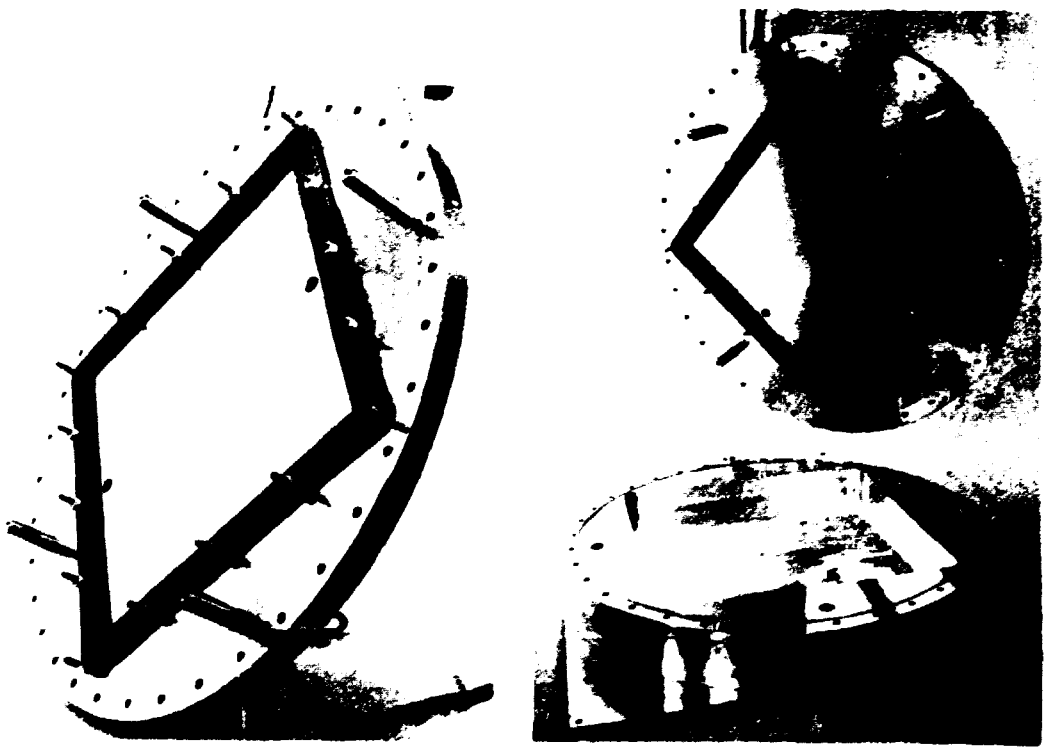

Fig. 26 Photographs showing details of the area detector to be used at the Small Angle Neutron Scattering facility, SANS. The detector specifications are described in section 1.30.

(v) A 40 cm×40 cm area detector (Fig. 26) with 64×64 pixel. The gas filling is 1.8 atm ^{3}He and 3 atm Xe + 5% CO_2 with an expected resolution of ~0.6 cm.

(vi) PDP-11/23 based data handling system with hard disc and floppy discs, and several terminals. The detector signals are processed by a Canberra 80 two parameter system which allows on-line display of the results in various projections.

The facility will be in operation by the end of 1981, and it will be available to users in many different fields of research such as molecular biology, metallurgy and solid state physics.

1.31 Synchrotron x-ray diffraction using triple-axis spectrometry

(J. Als-Nielsen, J. Linderholm, S. Jørgensen, P. Skaarup, E. Dahl Petersen* (*Department of Electronics, Risø) and B. Buras)

The broad wavelength band of intense electromagnetic radiation associated with the centripetal acceleration of electrons in a storage ring extends well into the x-ray region for typical storage rings like DORIS at the DESY laboratory in Hamburg. The superrelativistic electron energy E infers that the radiation be confined to the plane of the electron orbit within an angle of $m_o c^2/E$. A monochromatic beam obtained by Bragg reflection from a perfect Si (1,1,1) crystal face placed in the white beam after a 1 mm wide slit at a distance of 20 m from the electron orbit will have approximately the same band width as the natural width of the $CuK_{\alpha 1}$ line from a conventional x-ray tube. However, for identical monochromators at a storage ring (E = 4.3 GeV, I = 50 mA) and at an x-ray tube, the monochromatic beam from the former is more than a hundred times more intense than that from a 10 kW rotating anode tube, and at the same time the vertical resolution is typically 25 times better! These numbers have been derived by experimental comparison between our set-up at DORIS Hasylab and at the 12 kW rotating anode tube at Risø. Furthermore, the wavelength as well as the monochromatic band width can be varied at will at the synchrotron by changing Bragg angles,

apertures and monochromator crystals. With the accessibility of storage ring x-ray sources - so-called synchrotron radiation - the limits of x-ray diffraction methods have suddenly been extended by several orders of magnitude and new perspectives in experimental condensed matter physics are appearing.

In realizing the potential possibilities of synchrotron radiation, two of us (BB and JAN) started negotiations a couple of years ago with the synchrotron radiation group at DESY in Hamburg about building instruments for x-ray diffraction, to be placed at the beam lines of the then planned synchrotron radiation laboratory, HASYLAB. The instrument described below is a very flexible triple-axis x-ray spectrometer, the other (see section 1.32) is an energy-dispersive x-ray diffractometer.

The triple-axis spectrometer project was generously accepted by the German scientists, and the instrument was funded by the Danish Natural Sciences Research Council (Grant No. 511-8546) and Risø National Laboratory. Some parts of the instrument were produced in Physics Laboratory II, University of Copenhagen. We also realized the necessity of carrying out initial studies at the home base laboratory at Risø before taking the experiment to the synchrotron source, a conjecture that turned out to be very practical indeed: A rotating anode source (Grant No. 511-8546) was then funded, together with auxiliary x-ray diffraction equipment (Grant No. 511-15398).

Before actual experiments can be carried out successfully, the new technique requires experience in a whole set of unconventional problems. These include monitoring of the position and intensity of the incident white beam, suppression of higher-order contaminations in the monochromatic beam, and establishing an acceptably low background count rate. Furthermore, the relatively short periods of beam time available for synchrotron radiation in a foreign laboratory requires that the time spent in lining up the precision instrument should be minimized and the actual accumulation of data should be as effective as possible.

It was therefore a great help in addressing these problems that we had access to synchrotron radiation in the European Molecular Biology Laboratory (EMBL) outstation at DESY during the construction period of HASYLAB in 1979. Drawing on the experience gained here we were ready to set up a preliminary version of the permanent beam line D4 in HASYLAB, install the instrument and carry out several experiments during a four-week period in October-November 1980 (Als-Nielsen 1980). Below we give a description of the present set-up in HASYLAB. Three experiments completed in the above-mentioned period are described in sections 1.21, 1.22 and 1.25. The work was carried out in collaboration with a number of scientists from Denmark and the U.S.A., as well as members of the technical staff at Risø.

Our experience from a three-week period, during which the storage ring operated 12 hours a day in a mode dedicated to synchrotron radiation, is very encouraging. Once the dedicated mode had been established the beam was very stable within each run, one or two extra fillings of the storage ring during a twelve-hour period were sufficient, and the beam position was quite reproducible from one shift to the next.

A schematic top view of the set-up is given in Fig. 27. The synchrotron beam travels in a 20 m long, high vacuum tube terminated by a Be window, which has He gas at atmospheric pressure on the other side in order to avoid corrosion from radicals formed in air by the intense beam. The beam is limited to 1 mrad in the horizontal direction by a water-cooled Cu aperture at approximately 14 m from the source point. The beam is cut down to 0.1 from 0.2 mrad by a Pb beam definer in front of the monochromator and a Pb shield around the monochromator serves as an effective stop and trap for the powerful white beam.

The monochromatic beam is trimmed by a set of horizontal and vertical slits and monitored by an ionization chamber filled with 0.1 atm of an argon and methan mixture giving a transmission of approximately 95% at 1.5 Å. The current from the ionization chamber is converted to voltage by a Keithly amplifier (10^3 to 10^{11} V/A) and converted to a count rate by a CAMAC voltage to

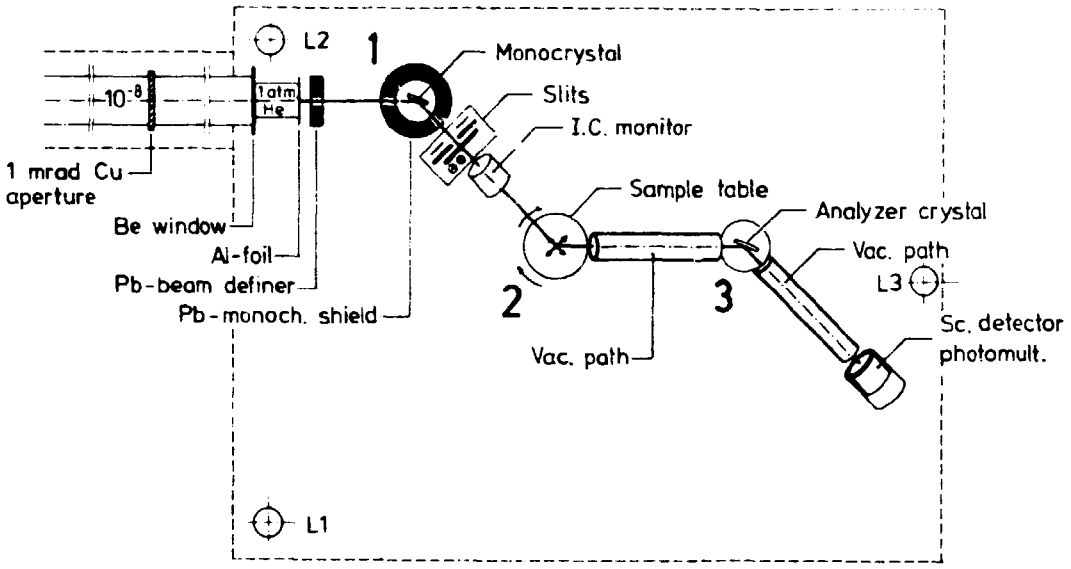

Fig. 27 Top view of the triple-axis spectrometer. The three axes marked 1, 2 and 3 are the monochromator, sample and analyzer axes. The dashed line indicates the Al-Pb-Al walls of the hutch necessary for radiation protection.

frequency converter. The wavelength of the monochromatic beam can be changed by scanning the Bragg angle θ_M of the monochromator. A convenient wavelength calibration is furnished by scanning θ_M while monitoring the fluorescent yield from a piece of Fe in the monochromatic beam. The yield increases discontinuously as one passes through the K-edge of Fe at 1.74334 Å.

The sample table mounted on the monochromator arm is centered in the beam by scanning the arm and watching the TV picture of the shadow of a pin on the table on a fluorescent screen behind the pin. The sample table is equipped with two horizontal translation stages and two perpendicular goniometer arcs (-20° to $+20^\circ$).

The analyzer table is identical to that of the monochromator. Evacuated Al tubes with Pb lining on the inside and Be windows in the ends are inserted between the sample and analyzer and between the analyzer and detector in order to minimize intensity losses by air absorption. The latter beam path has another very

important feature: it limits the detector solid angle to a few millisteradians aimed right at the analyzer crystal, so the background count rate can be kept as low as 0.5 c/sec even at E = 4.3 GeV in the rather high general radiation level present around the spectrometer when the beam is on. The entire spectrometer is situated in an enclosed hutch with Al-Pb-Al sandwich walls for radiation protection. The spectrometer can be viewed through a Pb-glass window with the beam on.

A photograph of the spectrometer is given in Fig. 28. The spectrometer arms are supported by air cushions supplied only by compressed air while the corresponding motor is running. The distances between axes can easily be varied as the arms are made of convenient Al profiles.

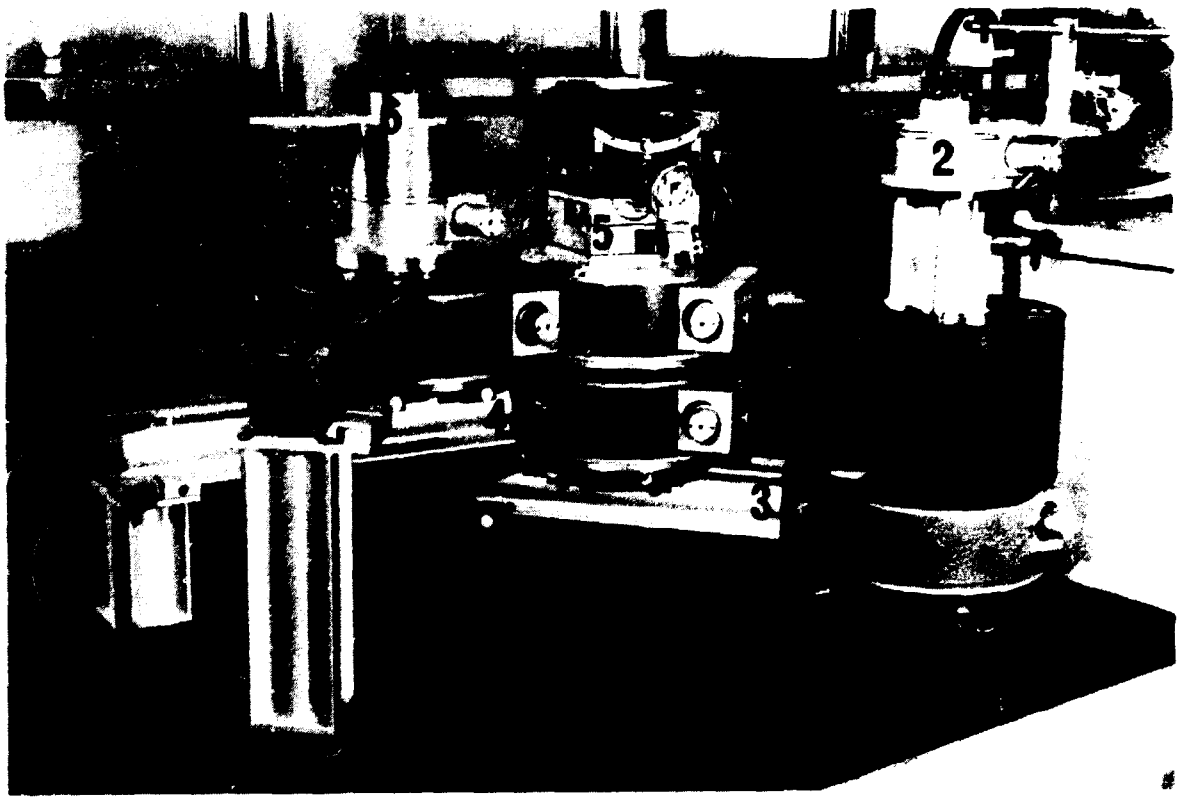

Fig. 28 Photograph of the x-ray triple-axis spectrometer. Monochromator, sample and analyzer axes are marked 2, 5 and 6, respectively. Note the possibility of sliding the axes on the arms (3, 4 and 7) and the air cushion (8).

For certain experiments the analyzer is unnecessary and the whole analyzer system can readily be detached from the spectrometer. The entire floor supporting the spectrometer can be adjusted to beam height by turning the three spindle legs L1, L2 and L3. All turntables (Huber) are driven by Slo-Syn stepping motors with 1 step = 0.001^{o} (except for the monochromator and analyzer tables, where 1 step = 0.0005^{o}) so a 1:2 ratio between the table and an arm is readily obtainable. The system is operated from a Decwriter terminal connected to a PDP11/34 computer with dual floppy discs. The computer is interfaced to a CAMAC system containing stepping motor modules, scalars, digital voltmeter interface and a limit switch modules. Programs for executing measurements are written in Basic (Skaarup 1979). On the Decwriter the results and a coarse plot of the data appear on-line.

Basically the triple-axis spectrometer set-up has been developed to the point where it can readily be used for experiments. In particular, it is worth noting that although only a horizontal aperture of 0.1-0.2 mrad is used, the intensity is sufficiently above conventional sources to enable new areas of research to be explored.

1.32 An x-ray energy-dispersive diffractometer for synchrotron radiation

(J. Staun Olsen*, B. Buras, S. Steenstrup* (*University of Copenhagen, Denmark) and L. Gerward (Technical University of Denmark))

A white-beam x-ray energy-dispersive diffractometer utilizing synchrotron radiation from the storage ring DORIS at DESY was built for the HAmburg SYnchrotron Radiation LABoratory (HASYLAB). The construction was a joint project by Physics Laboratory II, University of Copenhagen, Laboratory of Applied Physics III, Technical University of Denmark, and HASYLAB, all in collaboration with Risø National Laboratory.

A side- and top-view of the apparatus are shown in Fig. 29. A large table (1) with manually adjustable height carries the dif-

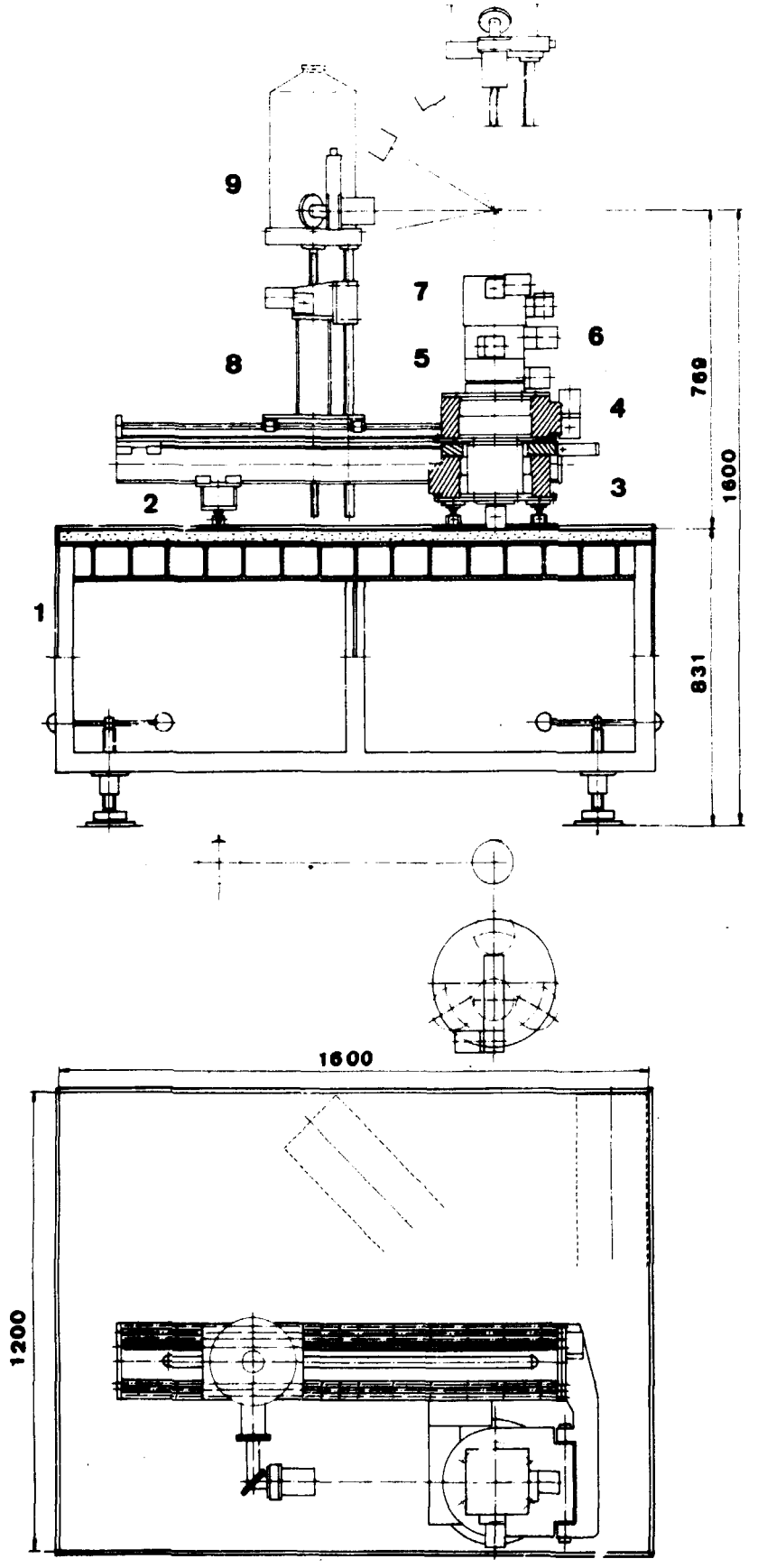

Fig. 29 A side- and top-view of the x-ray energy-dispersive diffractometer for synchrotron radiation.

fractometer equipped with 5 air cushions. By means of stepping motors, the diffractometer can be moved perpendicular to the direction of the incident beam, permitting high precision alignment. The bottom of the diffractometer consists of a (Huber) turntable (3) connected to the detector arm (2). By use of a stepping motor, the turntable enables high precision changes of the scattering angle to be made. On the table (3) a (Huber) turntable (4) is placed for rotating the sample. This table is provided with another table of variable height (5), on top of which a third table (6) is placed, enabling two mutually perpend_cular movements in the horizontal plane. Finally, the diffractometer is equipped with a large (Huber) goniometer head (7). The rotation of all turntables can be performed in steps of 0.0005^{o} and the translations in steps of 1/6 μm. The arrangement permits very precise placement of minute samples (of the order of micrometers) in the beam. This is especially important for high pressure studies using diamond anvil squeezers.

The semiconductor detector (9) of a Ge ultra-pure type is placed on a table of variable height controlled by a stepping motor (8). The support of the detector table can slide on the arm, which enables the distance of sample to detector to be remote-controlled. The diffractometer is constructed to operate by complete remote control in the horizontal scattering plane. However, after providing the diffractometer with a special detector, it may al_ be possible to work in the vertical scattering plane (Fig. 29), in which case the scattering angle should be set manually.

The motor control system is a Camac crate, using a PDP 11/03 computer. The computer-controlled stepping motor drives trigger translators of the SLO-SYN (ST 103 AX) type and controls the SLO-SYN stepping motors. Three motors at a time can be driven either manually or by the computer. The data-handling system is the JUPITER (Canberra) system, centered around the computer mentioned above, with two floppy discs. The programs are written in Fortran. The diffractometer is constructed mainly for white-beam diffractometry (single crystals, powders, amorphous samples, liquids), but can also be used for monochromatic beam diffraction if placed

at a monochromatic beam station. The diffractometer was tested and used during two two-week runs in 1980 at a temporary beam line, and will be installed at a permanent beam line in 1981.

1.33 References to section 1

AHARONY, A. (1973). Phys. Rev. B8, 3363-3370, and (erratum) B9, 3946.

AKELLA, J., JOHNSON, Q., THAYER, W. and SCHOCK, R.N. (1979). J. Less-common. Met. 68, 95-97.

ALS-NIELSEN, J. (1976). Phys. Rev. Lett. 37, 1161-1164.

ALS-NIELSEN, J. (1980). Risø-M-2268, 20 pp.

ALS-NIELSEN, J., BIRGENEAU, R.J., KAPLAN, M., LITSTER, J.D. and SAFINYA, C.R. (1977). Phys. Rev. Lett. 39, 352-355, and (erratum) 41, 1626-1627.

ALS-NIELSEN, J., LITSTER, J.D., BIRGENEAU, R.J., KAPLAN, M., SAFINYA, C.R., LINDEGAARD-ANDERSEN, A. and MATHIESEN, S. (1980). Phys. Rev. B22, 312-320.

AMBERGER, H.D. (1978). Z. Anorg. Allg. Chem. 439, 48-56.

ANISTRATOV, A.T., BEXNOSIKOV, B.V. and GUSAR, V.A. (1978). Sov. Phys. Solid State 20 (12), 2138-2139.

AVRAMI, M. (1940). J. Chem. Phys. 8, 212.

BARBARA, B., ROSSIGNOL, M.F., BOUCHERLE, J.X. and VETTIER, C. (1980). Phys. Rev. Lett. 45, 938-941.

BEAUVILLAIN, P., SEIDEN, J. and LAURSEN, I. (1980). Phys. Rev. Lett. 45, 1362-1365.

BHATTACHARYA, S. and LETCHER, S.V. (1980). Phys. Rev. Lett. 44, 414-417.

BIRGENEAU, R.J., HAMMONS, E.M., HEINEY, P. and STEPHENS, P.W. (1980). In: Proceedings of the International Conference on Ordering in Two Dimensions, Wisconsin, U.S.A., May 28-30 1980, 29-38.

BOND, R.A., ROSS, D.K., CARLILE, C.J. and ANDERSON, I.S. (1981). Low temperature order-disorder transitions in palladium deuteride. In: Proceedings of the EPS Conference, Antwerp, Belgium, April 1980. To be published.

BURAS, B., KOFOED, W., LEBECH, B. and BÄCKSTRÖM, G. (1977). Risø Report No. 357.

CAILLÉ, A. (1972). C.R. Hebd. Sean. Acad. Sci. B274, 891-893.

CHIN, M.D. and FAIN, S.C. (1977). Phys. Rev. Lett. 39, 146-149.

CLADIS, P.E. (1975). Phys. Rev. Lett. 35, 48-51.

CLADIS, P.E., BOGARDUS, R.K., DANIELS, W.B. and TAYLOR, G.N. (1977). Phys. Rev. Lett. 39, 720-723.

CLAUSEN, K.N. (1981). Magnetic excitations in Ho_2Co_{17} and Ho_2Fe_{17}. An inelastic neutron scattering study. Risø-R-426. To be published.

CLAUSEN, K.N. and NIELSEN, O.V. (1981). Magnetic anisotropy in single crystals of Ho_2Co_{17} and Ho_2Fe_{17}. Accepted for publication in J. Magn. Magn. Mater.

DE GENNES, P.G. (1963). In: Magnetism 3. Edited by G.T. Rado and H. Suhl. Academic Press, New York, 115-147.

DE GENNES, P.G. (1972). Sol. State Commun. 10, 753-756.

DE GENNES, P.G. (1974). The Physics of Liquid Crystals. Clarendon Press, Oxford, 333 pp.

DUNLAP, B.D. and SHENOY, H. (1974). Phys. Rev. B12, 2716-2724.

DUTTA, P., SINHA, S.K., NIELSEN, M., PASSEL, L. and BRETZ, M. (1980). In: Proceedings of the International Conference on Ordering in Two Dimensions, Wisconsin, U.S.A., May 28-30 1980, 169-174.

European Synchrotron Radiation News (1980), 4, 11. Available upon request from the European Science Foundation, 1 Quai Lezay-Marnésia, 6700 Strasbourg, France.

GILÁT, G. and RAUBENHEIMER, L.J. (1966). Phys. Rev. 144, 390-395.

HARDOUIN, F., SIGAUD, G., ACHARD, M.F. and GASPAROUX, H. (1979). Phys. Lett. A71, 347-349.

HOLMES, L.M., ALS-NIELSEN, J. and GUGGENHEIM, H.J. (1975). Phys. Rev. B12, 180-190.

HOLMES, L.M., JOHANSSON, T. and GUGGENHEIM, H.J. (1973). Solid State Commun. 12, 993-997.

IMRY, Y. and GUNTHER, L. (1971). Phys. Rev. B3, 3939-3945.

JANCOVICI, B. (1967). Phys. Rev. Lett. 19, 20-22.

JENSEN, S.J. KNAK, MOURITSEN, O.G., HANSEN, E. KJÆRSGAARD and BAK, P. (1979). Phys. Rev. B19, 5886-5901.

KELLER, J. and HOLZER, P. (1975). In: Proceedings of the 14th International Conference on Low Temperature Physics, Otaniemi, Finland, August 14-20 1975, 3, 438-440.

KEPA, H., GEBICKI, W., GIEBULTOWICZ, T., BURAS, B. and CLAUSEN, K. (1980). Solid State Commun. 34, 211-213.

KEPA, H., GIEBULTOWICZ, T., BURAS, B. and CLAUSEN, K. (1979). In: Physics Department, Annual Progress Report, Risø-R-414, 41-44.

KJEMS, J.K., DICKENS, M. and HUTCHINGS, M.T. (1978). In: Physics Department, Annual Progress Report, Risø-R-393, 41-42.

KOSTERLITZ, J.M. and THOULESS, D.J. (1973). J. Phys. C6, 1181-1203.

KUNC, K., BALKANSKI, M. and NUSIMOVICI, M.A. (1975a). Phys. Rev. B12, 4346-4355.

KUNC, K., BALKANSKI, M. and NUSIMOVICI, M.A. (1975b). Phys. Status Solidi B71, 341-349; B72, 229-248 and 249-254.

LANDAU, L.D. (1965). In: Collected Papers of L.D. Landau. Edited by D. ter Haar. Gordon and Breach, New York, 209 pp.

LAURSEN, I. and HOLMES, L.M. (1974). J. Phys. C7, 3765-3769.

LEBECH, B. (1981). J. Appl. Phys. 52 (3), 2018-2024.

LEBECH, B. and RAINFORD, B.D. (1972). J. Phys. (Paris) Colloq. 32 (C1), 370-371.

LEBECH, B., RAINFORD, B.D., BROWN, P.J. and WEDGWOOD, F.A. (1979). J. Magn. Magn. Mater. 14, 298-300.

LOEWENHAUPT, M. and HOLLAND-MORITZ, E. (1979). J. Appl. Phys. 50, 7456-7461.

McEWEN, K.A., STIRLING, W.G. and VETTIER, C. (1978). Phys. Rev. Lett. 41, 343-346.

McMILLAN, W.L. (1972). Phys. Rev. A6, 936-947.

MIKESKA, H.J. and SCHMIDT, H. (1970). J. Low Temp. Phys. 2, 371-381.

MØLLER, H. BJERRUM, SHAPIRO, S.M. and BIRGENEAU, R.J. (1977). Phys. Rev. Lett. 39, 1021-1025.

MOORUDIAN, A. and HARMAN, T.C. (1970). In: Proceedings of the Conference on the Physics of Semimetals and Narrow Gap Semiconductors, Dallas, Texas, U.S.A., 297-299.

MORITA, T. and HORIGUCHI, T. (1971). J. Math. Phys. 12, 981-986.

MYAELSKI, J., AZIZA, A., MYCIELSKI, A. and BALKANSKI, M. (1974). Phys. Status Solidi B67, 447-454.

NEVALD, R., VOSS, F.W., NIELSEN, O.V., AMBERGER, H.D. and FISCHER, R.D. (1979). Solid State Commun. 32, 1223-1225.

OLSEN, J. STAUN, BURAS, B., STEENSTRUP, S. and GERWARD, L. (1981). A spectrometer for x-ray energy dispersive diffraction using synchrotron radiation. Accepted for publication in J. Sci. Instrum.

PEIERLS, R.E. (1934). Helv. Phys. Acta 7, Suppl. 3-87.

PROST, J. (1981). Reflections on the re-entrant nematic and the S_A-S_A phase transition. In: Proceedings of the Conference on Liquid Crystals, Garmisch-Parten Kirchen, F.R.G., January 1980. To be published.

RATHMANN, O., ALS-NIELSEN, J. and BAK, P. (1974). Phys. Rev. B10, 3963-3987.

SCHWARTZ, R.W., WATKINS, S.F., O'CONNOR, C.J. and CARLIN, R.L. (1976). J. Chem. Soc. Farday Trans. II 72, 565-570.

SKAARUP, P. (1979). Risø-M-2184, 19 pp.

SKRIVER, H.L., ANDERSEN, O.K. and JOHANSSON, B. (1978). Phys. Rev. Lett. 41, 42-45.

SKRIVER, H.L., ANDERSEN, O.K. and JOHANSSON, B. (1980). Phys. Rev. Lett. 44, 1230-1233.

STEELE, W.A. (1973). Surf. Science 36, 317.

STEPHENS, P.W., HEINEY, P. and BIRGENEAU, R.J. (1979). Phys. Rev. Lett. 43, 47-51.

STEPHENS, R., STROMBERG, H.D. and LILLEY, E.M. (1968). J. Phys. Chem. Solids 29, 815-821.

SZPUNAR, J. (1976). At. Energy Rev. 14, 199-202.

VILLAIN, J. (1980). In: Proceedings of the International Conference on Ordering in Two Dimensions, Wisconsin, U.S.A., May 28-30 1980, 123-129.

VORA, P., SINHA, S.K. and CRAWFORD, R.K. (1979). Phys. Rev. Lett. 43, 704-708.

WARREN, B.E. (1941). Phys. Rev. 59, 693-698.

2. PLASMA PHYSICS

The plasma physics section operates under a contract of association between Risø National Laboratory and Euratom, and some staff members participate as members of or consultants in several of the committees concerned with the Euratom fusion programme. The research activities are centered on research in basic plasma physics (2.1-2.11) and on studies of technology of interest for future fusion reactors (2.12-2.27). In addition, a design of a single point Thomson scattering system for JET was carried out under a contract with JET (2.28).

The activities in basic plasma physics have mainly been concentrated on linear and non-linear wave phenomena and have covered experimental as well as theoretical investigations. The reconstruction of the main experimental facility - the Q-machine - was finished in the spring, and a study of the formation and stability of strong electrostatic double-layers in a current-carrying plasma was undertaken. In addition, a new device - a high density pulsed discharge plasma - was constructed and used for investigations of the excitation and propagation of electromagnetic waves. Particular interest was paid to the properties of whistler waves excited by a helical wave structure. The construction of a third experimental device - a DP-machine - facilitating the study of low frequency waves was continued and is expected to be finished during 1981. The theoretical studies were mainly concerned with non-linear wave phenomena and included investigations of the interaction between electromagnetic waves and inhomogeneous magnetized plasmas, solitary electron and ion phase space vortices, and numerical simulation of non-linear electron plasma waves with special attention to electron trapping effects.

The technological aspects of plasma physics are studied with one of the possible refuelling schemes for fusion reactors in mind. In this particular scheme, the fuel will be injected as high velocity pellets of solid hydrogen isotopes. Investigations of fundamental processes in the interaction between charged particles

of different energies and solid hydrogen isotopes are therefore of great interest. These studies have mainly been concerned with the interaction between beams of light ions and films of hydrogen, deuterium, and mixtures of different hydrogen forms. Among the results were measurements of the emission coefficients for positive and negative particles from solid HD and H_2-D_2 mixtures bombarded with keV electrons and hydrogen ions, determination of ranges and stopping powers of hydrogen and deuterium ions incident on H_2 and D_2 targets, and measurements of erosion of films of D_2 by keV light ions.

The direct interaction between pellets of deuterium and a plasma is studied in the tokamak "Dante". Small pellets (2.25 mm long and 0.6 mm diameter) are injected vertically into "Dante" with a speed of ~140-200 m/s. The pellets are produced and accelerated in a small gun and fed to "Dante" through a 5 m long guide tube. The plasma is totally quenched by the ablated pellet material, because the pellets contain more particles than the plasma, and a new pellet gun producing much smaller pellets is being built.

A new activity aimed at studying problems with the handling and acceleration of pellets of relevance for larger plasma and fusion experiments is in preparation. This project is supported by a grant from the Danish Ministry of Energy.

The scientific and engineering design of a single point Thomson scattering system for JET was performed in collaboration with the Electronics and Engineering Departments at Risø. This work was performed under a contract between JET and Risø. It is expected to be followed by a construction of the system under a new contract.

2.1 A helical wave structure for excitation of electromagnetic plasma waves

(A.A. Balmashnov (Patrice Lumumba University, USSR), J.P. Lynov, P. Michelsen and J. Juul Rasmussen)

A slow wave structure consisting of a helically wound Ta-wire (1 mm in diameter) surrounding the plasma column of our pulsed discharge afterglow plasma experiment (Balmashnov et al. 1979) was constructed in order to excite whistler waves, which are a special class of electromagnetic plasma waves. Although such helical slow wave structures have been successfully utilized in travelling wave tubes, to our knowledge they have not previously been used to excite waves in a plasma.

The helix forms four turns of radius 4.3 cm and the helix length is variable within the limits 4 to 12 cm. The helical wave structure is placed coaxially with the plasma column, so that there is no direct contact to the plasma, a fact which removes the problems of the common electric dipole or magnetic loop antennas (Sugai et al. 1978). The helical wave structure is fed in one end with a frequency, f = 278 MHz, corresponding to a vacuum wave-length which equals the total length of the wire of the helix. By varying the helix length, L, we were able to excite waves with different wave-lengths, λ, since we found a maximum coupling to the whistler waves if λ = L. Furthermore, we were able to excite waves at different radial positions due to the inhomogeneous radial plasma density in our experiment. Maximum wave amplitudes were observed at radial positions where (f,λ) satisfy the whistler dispersion relation for the local plasma density.

2.2 Linear and non-linear whistler wave propagation in a density crest

(A.A. Balmashnov (Patrice Lumumba University, USSR))

Whistler wave trapping in a density crest was investigated both theoretically and experimentally. Based on ray theory, conditions were derived for trapping the whistler wave in a density crest as well as in a trough. The oscillation length of the trapped ray

was calculated for the special case of a parabolic field-aligned density crest and the dependence on the point of wave excitation was found. Some hypotheses concerning the process of interference of the trapped rays and the possibility of linear-formed whistler wave filaments were made.

An experiment was performed in which whistler waves were excited in a plasma density crest by a helical wave structure (see 2.1). The measurements verified the characteristic behaviour of crest trapping and the process of linear filamentation. In addition, the process of whistler wave self-focusing in a radial inhomogeneous plasma was experimentally investigated. It was found that a whistler wave propagating along the plasma column with a density crest excited a longitudinal wave of the same frequency propagating across the external magnetic field. The amplitude modulation of the latter wave is accompanied by a density modification, which leads to the trapping of the whistler wave in a density trough in the centre of the plasma column.

2.3 Enhanced plasma confinement in a magnetic well by whistler waves

(A.A. Balmashnov (Patrice Lumumba University, USSR) and J. Juul Rasmussen)

The propagation of whistler waves in a magnetic field of mirror configuration was investigated experimentally. The waves were excited by the helical wave structure (see 2.1) in a region where the local cyclotron frequency, ω_c, was larger than the wave frequency, ω, and propagated to the region of cyclotron resonance $\omega = \omega_c$. The strong interaction between the wave and the electrons in this region increases the pitch angle of the leaking electrons and they may be reflected. When the resonance condition that the wave-length of the whistler wave was equal to the distance between two mirror points was satisfied, the confinement in the magnetic well was enhanced.

2.4 Numerical simulation of non-linear electron plasma waves: Trapping effects

(J.P. Lynov, P. Michelsen, H.L. Pécseli, J. Juul Rasmussen and K. Thomsen)

The electron Landau damping is considered to be one of the dominant absorption mechanisms of the wave energy for radio frequency waves applied as additional heating of fusion plasmas. Therefore, it is of great importance to study the non-linear effects on the damping and frequency shift in the initial phase of wave propagation. For a small but finite wave amplitude the initial damping is predicted to be given by the Landau damping rate γ_L (O'Neil 1965, Morales and O'Neil 1972), but the validity of these theories is restricted to the region $e\phi_o/T_e << /(v_e/v_p)^2$, where ϕ_o is the initial wave amplitude, T_e electron temperature, $v_e = (T_e/m)^{\frac{1}{2}}$, and v_p is phase velocity. For larger amplitudes, which will certainly be needed for heating experiments, the initial damping was predicted to increase strongly with increasing wave amplitude (Sugihara and Yamanaka 1975, 1979). The physical mechanism in the enhancement of the damping with increasing amplitude may be understood as follows: the number of strongly resonant particles will increase rapidly with increasing amplitude because, for a Maxwellian distribution, the slope, $\partial f_o/\partial v$, is not constant. The difference between the particles with velocities smaller and larger than the phase velocity is therefore larger than that given by linear theory, where this difference is proportional to $(\partial f_o/\partial v)_{v_p}$.

We have investigated the behaviour of non-linear electron waves using a numerical simulation based on the hybrid model of Denavit (1972) (Lynov et al. 1979b). For low amplitude waves ($e\phi_o/T_e < 10^{-5}$) we verified the linear dispersion relation. Increasing the wave amplitude, the initial damping was observed to increase and in Fig. 30 we have plotted the initial damping rate versus the wave amplitude for two different wave-numbers. The solid lines are the theoretical curves of Sugihara and Yamanaka (1979). The agreement is very good except for higher amplitudes ($e\phi_o/T_e \gtrsim 1.5$), where the damping rate of the simulation is larger than the theoretical one and the saturation anticipated by Sugihara and Yamanaka

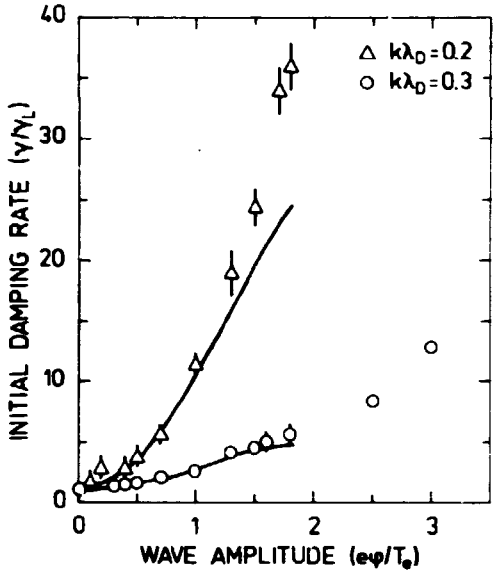

Fig. 30 Results of a numerical simulation of the initial damping rate of electron plasma waves as function of the wave amplitude for two different wave numbers $k\lambda_D$.

(1979) is not reflected in the simulation results. The enhancement in the damping rate is found to be particularly strong for small wave-numbers.

We further found that the frequency shift, $\delta\omega$, was positive within the initial time $t < \pi/\omega_B$, (ω_B is the bounce frequency = $k(e\phi_o/m)^{\frac{1}{2}}$) as predicted by Sugihara and Yamanaka (1979). For larger times, $\delta\omega$ becomes negative and follows the evolution predicted by Morales and O'Neil (1972).

2.5 Waterbag model of a solitary electron hole

(J.P. Lynov, P. Michelsen, H.L. Pécseli and J. Juul Rasmussen)

In connection with our experimental and numerical investigations of electron holes (Saeki et al. 1979, Lynov et al. 1979a) calculations were perfomed on a simple, theoretical model of a single electron hole (Lynov 1981). Electron holes are localized pulses of positive electrical potential which contain a large number of trapped electrons. In phase space, i.e. (x,v)-space, the electron holes appear as distinct vortex structures. The electron holes propagate as solitary waves in the sense that they preserve their shape and velocity, but two holes may coalesce upon collision

under certain conditions (Lynov et al. 1980) so that electron holes cannot be characterized as solitons.

In the single waterbag model, which was applied in the theoretical calculations, the normalized electron distribution function, $f(v,x,t)$, is assumed to have the values 0 or 1 only. This simplification leads to the contraction of the Vlasov and Poisson equations to a single non-linear first-order ordinary differential equation for the electrical potential, $\phi(x)$. Due to simple physical boundary conditions, maximum values of the hole velocity, v_h, and the hole amplitude, ϕ_o, are found. Thus, the hole's Mach number, $M_h \equiv |v_h|/v_t$, where v_t is the electron thermal velocity, must be smaller than $\sqrt{3/2}$, while the maximum value of ϕ_o decreases for decreasing wave guide radius. By numerical integration of the differential equation for $\phi(x)$, the half value width, Δx_h, of the hole potential can be found and the results are shown in Fig. 31. In this figure the shaded areas indicate the region of $\Delta x_h(\phi_o)$ derived from the waterbag model when varying M_h from 0 to

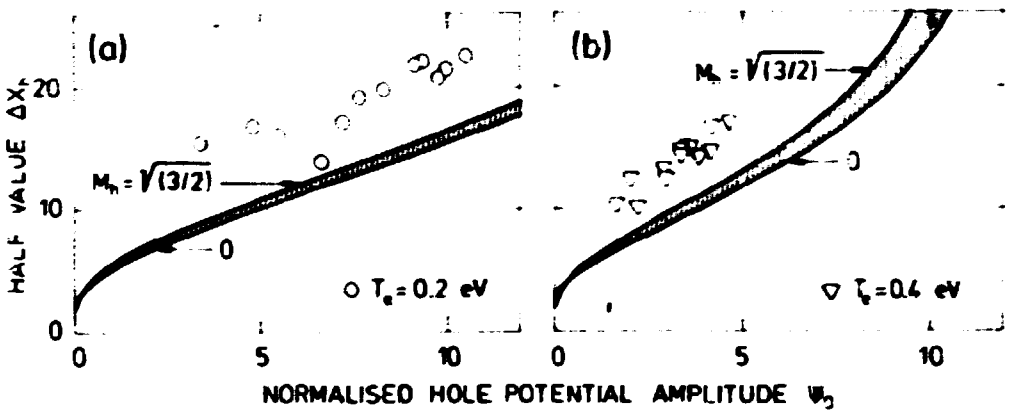

Fig. 31 Results of the waterbag model of a solitary electron hole. The shaded areas indicate the region of the normalized half-value width, Δx_h, of an electron hole as a function of the normalized hole potential amplitude, ϕ_o, derived from the theoretical waterbag model when varying the hole's Mach number, M_h, within its theoretical limits from 0 to $\sqrt{3/2}$. The discrete points show results obtained by numerical simulation of the experiment. The value of the electron temperature, T_e, is 0.2 eV in (a) and 0.4 eV in (b).

$\sqrt{3/2}$. The discrete points show results obtained by numerical simulation of our experiment and we note the qualitative agreement between waterbag theory and simulation. In both cases, Δx_h increases with ψ_o at approximately the same rate. This behaviour of the waterbag model is in clear contrast to t' small-amplitude limit of the more complex distribution function model of the electron hole by Schamel (1979) which predicts decreasing values of Δx_h for increasing ψ_o. More detailed investigations of the theoretical behaviour of $\Delta x(\psi_o)$ by application of the Schamel model without the small-amplitude assumption, which actually is not applicable in our experiments, are in preparation.

2.6 Ultra-strong stationary double-layers in a collisionless magnetized plasma

(R. Hatakeyama*, S. Iizuka*, P. Michelsen, J. Juul Rasmussen, K. Saeki*, N. Sato* (*Tohoku University, Japan) and R. Schrittwieser (University of Innsbruck, Austria))

Under certain circumstances large local potential jumps in plasmas appear to be caused by electrostatic double-layers (Carlquist 1979, Torven 1979). The double-layers belong to the class of Bernstein-Greene-Kruskal (BGK) solutions (Bernstein et al. 1957) of the Vlasov equation. Although the double-layer has been known for a long time, there is an increasing interest for a better understanding of this phenomenon, one reason being that the double-layer accelerates and confines charged particles and provides a mechanism for anomalous resistivity. Recent laboratory experiments and computer simulations have revealed some details of the double-layers. The experiments have been performed either in discharge plasmas where ionization processes were important, or in plasmas traversed by a strong electron beam. However, a double-layer may simply form when two plasmas of different potential are joined (Sato et al. 1981). To investigate this possibility, we performed experiments both in the Q-machine at Tohoku University and in the Risø Q-machine.

The double-layer is easily generated in the collisionless Q-machine plasma when the two plasma sources are appropriately

adjusted with respect to plasma production and a potential difference is applied between them. An example of the plasma potential along the column axis for a set of bias voltages is shown in Fig. 32. When the voltage is increased, the double-layer moves towards the positive plasma source and becomes narrower. An emissive probe is used to measure the plasma potential. When the bias of such a probe is negative with respect to the plasma potential, the emitted electrons are absorbed by the plasma. When the probe is positive it collects electrons from the plasma.

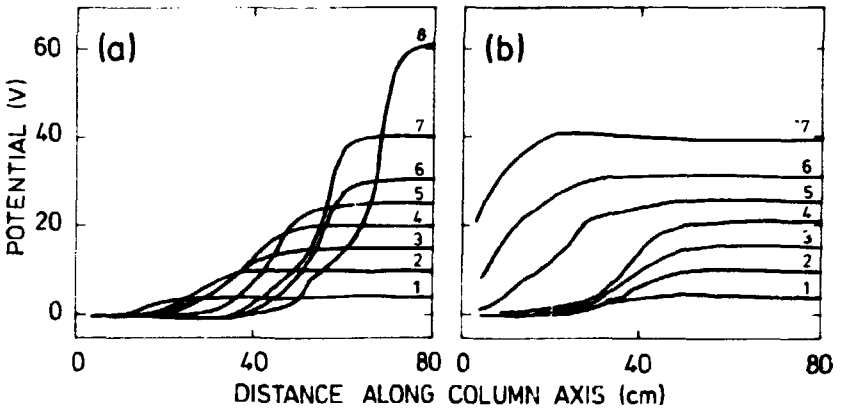

Fig. 32 Potential distributions along the plasma column for various values of bias voltage ϕ_0. 1: ϕ_0 = 5 V, 2: 10 V, 3: 15 V, 4: 20 V, 5: 25 V, 6: 30 V, 7: 40 V, 8: 60 V. The grounded source S_2 is placed at x = 0 and the biased source S_1 at x = 125 cm. The base pressure is p ≃ 10^{-6} torr in (a) and p = $2.5 \cdot 10^{-4}$ torr (He) in (b).

The double-layer position was found to depend on the ratio of the plasma production from the two sources. When the plasma production is increased at one plasma source, the double-layer moves towards the other plasma source. The maximum potential drop, ϕ, was limited by the electronics to ≃ 400 V, i.e. $e\phi/kT_e \simeq 2 \cdot 10^3$, a value between two and three orders of magnitude higher than that used in previous experiments. To investigate the effect of ionization by the electrons accelerated through the double-layer, the background pressure (He or Ar gas) was increased. It was found that when ionization processes were of importance, the

maximum size of the double-layer was limited to approximately the ionization potential of the background gas. In Fig.32b the double-layer is shown at constant background He-pressure for increasing applied potential differences. It is seen that the double-layer moves towards the plasma source on the low potential side when the potential jump exceeds the ionization potential of the gas and creates a normal sheath at the plasma source.

2.7 Moving double-layers and current suppression in a collisionless plasma

(S. Iizuka (Tohoku University, Japan), P. Michelsen, J. Juul Rasmussen and R. Schrittwieser (University of Innsbruck, Austria))

When a current passes through a plasma, several kinds of instabilities may arise. Such current driven instabilities have also been observed in single-ended Q-machines where the plasma flows from the plasma source towards the terminating target. We have performed new investigations of this instability. By use of a recently developed method (Schrittwieser et al. 1981) for time-resolved measurements of the plasma potential, we found that the instability is caused by a moving double-layer.

When a positive voltage is applied to the target, the plasma potential inside the column rises to a quasi-stable state within a very short time. Then a double-layer created in front of the plasma source moves through the plasma, and this relaxes the potential distribution. The double-layer gives rise to a current suppression which is due to a negative potential barrier on the low potential side of the double-layer. When the double-layer reaches the target, the barrier disappears causing a sudden increase of the current. This evolution, which repeats periodically, corresponds to one cycle of the instability. A very similar behaviour was found for the strong current oscillations of the thermionic converter (Burger 1965). The measurements were performed using an electron emissive probe, which could also be used as an ordinary Langmuir probe. The time resolved measurements were performed by detecting the zero-current points of the probe

characteristics sampled at a fixed time with respect to the instability cycle.

In Fig. 33 the time development of the current, I_T, the plasma potential, ϕ_s, and the ion, I_{is}, and electron, I_{es}, saturation currents are shown.

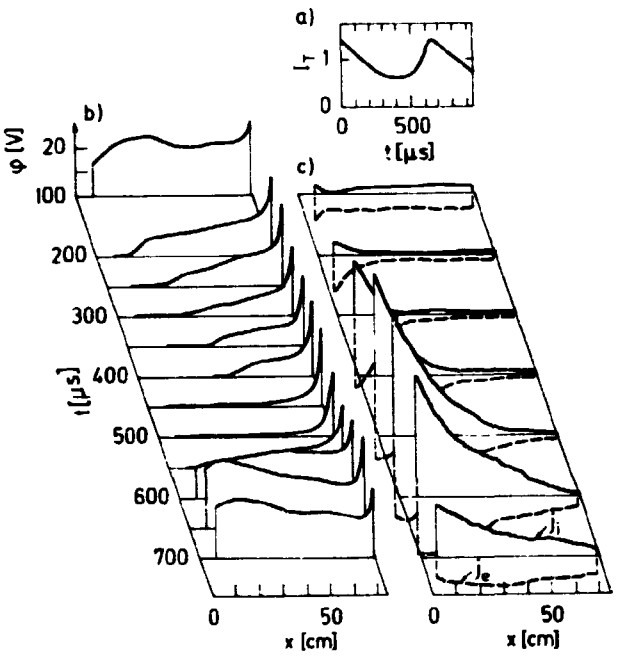

Fig. 33 The time development of currents and potential in a moving double-layer in a collisionless plasma. (a) Current to the target during one period of an oscillation. (b) The plasma potential along the axis measured at various times during the oscillation period. (c) Corresponding ion (I_{is}) and electron (I_{es}) saturation currents.

2.8 Observation of ion phase-space vortices

(R. Armstrong*, H.L. Pécseli and J. Trulsen* (*University of Tromsø, Norway))

The formation of ion phase space vortices was investigated experimentally in a conventional double-plasma (DP) device. The plasma densities were 10^7-10^8 cm^{-3} and temperatures T_e ~2 eV and T_i < 0.2 eV. The neutral background (Ar) pressure was $<10^{-4}$ torr.

The device has a diameter of 60 cm and a length of 120 cm. Ion acoustic shocks were excited as described by Ikezi et al. (1973). Ion phase space vortices developed behind the shock, separated from it by a region of heated ions, in good agreement with numerical results of Sakanaka (1972). We identified the vortex by actually measuring the ion velocity distribution at various positions behind the shock, using an electrostatic ion energy analyzer and a boxcar integrator.

To obtain more insight into the properties of ion phase space vortices, we considered a particularly simple model where the ion velocity distribution consists of two cold, counter-streaming ion beams, while the electrons are assumed to be Boltzmann distributed with T_e = constant at all times. Similar to the analysis of Kako et al. (1971), we obtained a relation for the non-linear potential variation (in normalized units)

$$1/2\left(\frac{d\psi}{dx}\right)^2 + V(\psi) = W, \tag{1}$$

where the pseudo-potential, V, is given by

$$V(\psi) = -e^{\psi} - \sigma\sqrt{-2\psi}, \quad \psi \lesssim 0. \tag{2}$$

Here W is an integration constant and σ is determined by the requirement of overall charge neutrality. Physically acceptable solutions to equation (1) require that $V(\psi)$ has a local minimum. It is demonstrated that this requirement is identical to the criterion of linear instability of the two ion beams, and that the corresponding solution of equation (1) is associated with a train of vortex-like formations in ion phase space. We may thus expect that a train of phase space vortices constitute the final, non-linear stage of an ion-ion beam instability. This conjecture was confirmed by a numerical particle simulation, which demonstrated that, once formed, these phase space vortices remain rather stable for at least hundreds of ion plasma periods. The model leading to equation (1) is extended to the corresponding waterbag model (see 2.5), allowing for a small but non-zero ion-temperature. The gross properties of stationary ion phase space configurations may be derived from this model. The currentless

double-layers of Perkins and Sun (1981) thus correspond to "one half of an infinitely long" ion phase space vortex.

2.9 A thermal oscillating two-stream instability

(K.B. Dysthe*, E. Mjølhus*, H.L. Pécseli and K. Rypdal* (*University of Tromsø, Norway))

A version of the oscillating two stream instability in which the ohmic heating of the electrons constitutes the non-linearity was developed theoretically for an inhomogeneous, magnetized plasma. The theory predicts the formation of strongly $\vec{B}$-field aligned striations, centered around the level of upper hybrid resonance. By applying our results to the conditions of ionospheric heating experiments (e.g. Fialer 1974) we can explain the development of the observed plasma irregularities. Also the non-linear, saturated stage of the striations is considered.

Plane disturbances nearly parallel to the magnetic meridan plane have the largest growth rates. The theory is an extension of ideas previously considered by Fejer and Das (1981). A new result in the present theory is that the instability also can be excited in an inhomogeneous plasma with constant amplitude pump, although with a higher threshold. A smaller threshold is obtained if the standing wave nature of the pump wave is taken into account. In the latter case, the phase of the pump enters as an important parameter. It can be demonstrated that the characteristics of the irregularities depend on the temperature-dependence of electron collision frequency. This dependence differs significantly for electron-ion and electron-neutral collisions. Since the composition of the ionosphere varies during the day, the relative importance of the two types of collision processes has a similar variation. Our results thus also account for the diurnal variation of the experimental results of Fialer (1974).

Our analysis is a promising start for a more general description of the interaction between electromagnetic waves and inhomogeneous magnetized plasmas.

2.10 Microwave scattering from cross-field irregularities

(M.J. Alport*, N. D'Angelo* (*University of Iowa, Iowa, U.S.A.) and H.L. Pécseli†)

The experiment was carried out in a weakly magnetized, partially ionized discharge plasma. Because of an externally imposed electric field in the radial direction, the electron component has an azimuthal $\vec{E}\times\vec{B}/B^2$ drift. The ion component, on the other hand, is hardly magnetized at all since the radius of the plasma column, R(~6 cm) is comparable to the ion Larmor radius, and in addition, the electron-neutral collision frequency is comparable to the ion gyro frequency. Unstable, cross-field fluctuations are excited by (i) the resulting azimuthal current, and (ii) the radial density gradient corresponding to the Farley-Buneman and the gradient driven instabilities known also in e.g. the equatorial electrojet.

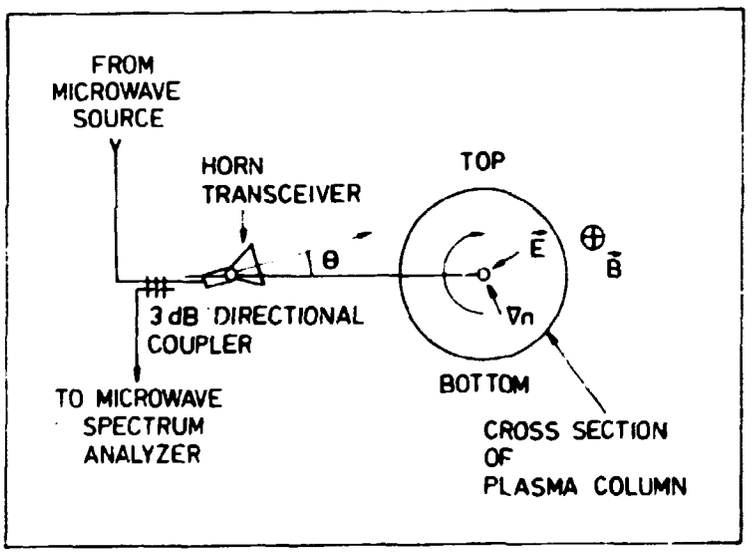

Fig. 34 Experimental set-up used to measure microwave scattering from cross field irregularities.

† Work performed as a visiting scientist at the University of Iowa, Iowa, U.S.A.

A rotatable microwave horn was mounted as shown schematically in Fig. 34 . The horn had a 3 dB width of ~24° and was operated at a frequency of 9.4 GHz (i.e. $\lambda_\mu \sim 3$ cm), using the same horn as emitter and receiver. Examples of back-scattered spectra are shown in Fig. 35 for various angles, θ, defined in Fig. 34. The

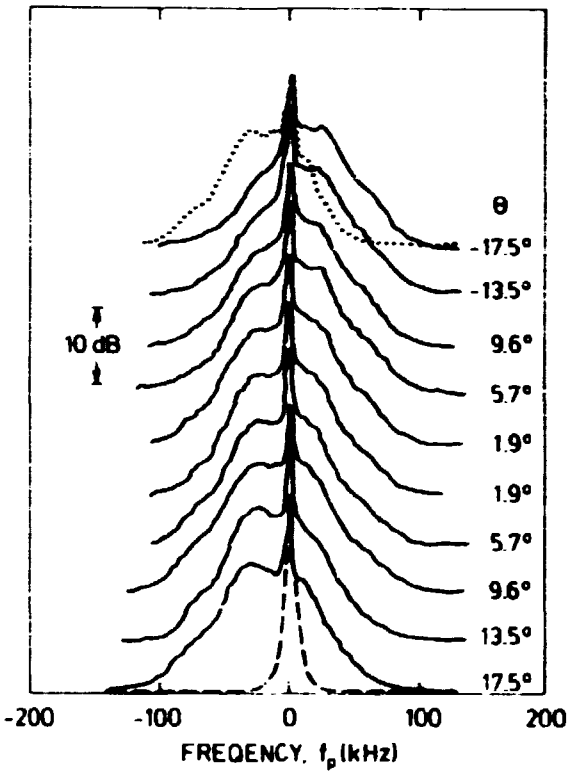

Fig. 35 Backscattered microwave spectra for various orientations (θ) of the microwave horn transceiver.

large peak corresponds to the signal back-scattered from the walls and the Doppler shifted part to back-scattering from fluctuations in the plasma with wave-lengths ~$\lambda_\mu/2$. The Doppler shift is a measure of the phase velocity of these fluctuations. Since the electron velocity is roughly proportional to radius we get a broad frequency band in the reflected signal, due to the finite angular resolution of the horn. Changing the sign of θ (see Fig. 35) we observe a change in the Doppler shift as expected for azimuthally propagating fluctuations. By varying the radial $\vec{E}$-field, we observe a corresponding variation in phase velocity, as expected for waves propagating with the electron drift. Varying the angle between the horn axis and the plane normal to $\vec{B}$, we

confirmed that the fluctuations were strongly $\vec{B}$-field aligned. The fluctuations in our setup thus propagate in good agreement with theoretical expectations (Rogister and D'Angelo 1970) in contrast to many electrojet observations where, e.g., the phase velocity is frequently seen to follow the ion-sound speed. We experienced that our microwave setup provided an easy, inexpensive and non-perturbing diagnostic for experiments of the present type.

2.11 Investigation of obliquely propagating electron Bernstein waves

(R.J. Armstrong*, J. Juul Rasmussen+ and J. Trulsen* (*University of Tromsø, Norway))

Electron Bernstein waves are electrostatic waves in a magnetized plasma (Bernstein 1958). They are known to be undamped when propagating perpendicular to the magnetic field. However, when the direction of propagation deviates from perpendicular, the waves are strongly damped. Only few observations of obliquely propagating Bernstein waves have been reported and in these cases the waves were excited by a point source, (e.g. Leiberge and Gonfalone 1978).

From a practical point of view, the electron Bernstein waves are expected to play a key role in connection with electron cyclotron heating of toroidal plasmas (e.g. Schuss and Hosea 1975). That is, an electromagnetic wave excited outside the plasma is converted into a Bernstein wave at some point in the plasma and then, in turn, is absorbed at the cyclotron frequency. It is therefore of great interest to perform a detailed study of the propagation characteristics in all propagation directions.

We have investigated the propagation of plane Bernstein waves oblique to the magnetic field. The experiment was performed in a

---

+ Work performed as a visiting scientist at the University of Tromsø, Norway.

large volume plasma in the Tromsø DP-machine, where a magnetic field was applied perpendicular to the axis. The waves were excited by a plane circular grid with a diameter much larger than the wave-length, and the waves were detected by a small grid probe. The wave dispersion was measured for different directions of propagation and was found to compare favourably with predictions based on the linear dispersion relation.

2.12 Secondary electron emission from solid HD and H_2-D_2 mixtures for incidence of keV electrons and hydrogen ions

(P. Børgesen, Chen Hao Ming, J. Schou and H. Sørensen)

The interactions between particle beams and surfaces of solid hydrogens are studied in order to obtain the information necessary for an understanding of the pellet plasma interaction. In principle it is possible to estimate, for instance, the secondary electron emission coefficient, δ, for solid T_2 and D_2-T_2 mixtures from similar data for solid H_2 and D_2. In order to make these estimates by extrapolation as reliable as possible, we have now also measured the secondary electron emission coefficients for solid HD and for H_2-D_2 mixtures (50/50) for incidence of hydrogen ions up to 10 keV and for electrons up to 2 keV. We present these results relative to the results for solid H_2 and D_2 by plotting them relative to the mean value of the results for H_2 and D_2, i.e.

$$R(E) = 2\delta(E)/(\delta_{H_2}(E) + \delta_{D_2}(E)),$$

and we find that within the experimental uncertainty the ratio R(E) is a constant for each combination of projectile and target. R is thus independent of the energy.

The R values found are shown in table 1. We see that R values for each target material are nearly the same for electron and ion incidence. Hence, the differences are in fact within the experimental uncertainties and the R value thus depends only on the target material. The R value for HD is 0.93 and 1.03 for H_2-D_2 (50/50).

Table 1.

	electrons	hydrogen ions
HD	0.94	0.92
H_2-D_2 (50/50)	1.01	1.05

2.13 Erosion of thin films of D_2 by keV light ions

(P. Børgesen, J. Schou and H. Sørensen)

The studies of erosion of thin films of D_2 by keV light ions (Børgesen et al. 1979) were continued. During the earlier experiments it was realized that the beam had to be very uniform across the irradiated area. Later it was realized that the normal method of collecting data was unsatisfactory for erosion measurements because it is important to record how the current collected by the target varies with time for irradiations lasting from tenths of seconds to several minutes. In the near future, measurements will be made using a new data acquisition system and a swept beam which will be more uniform. In addition, we plan to repeat the measurements using electron beams. The measurements will be made not only with targets of H_2 and D_2, but also with targets of N_2 and Ar in order to complement the measurements made on Ar (see 2.15).

The erosion measurements made so far are thus only provisional. In Fig. 36 it is seen how the coefficient for emission of positive particles, γ, varies with time when 200 Å films of H_2 and D_2 are irradiated. The H_2 films eroded much faster than the D_2 films. Average erosion yields for 200 Å films irradiated with 8 keV molecular ions were found to be: 760 D_2/D_3^+, 5500 H_2/D_3^+ and 21000 H_2/H_3^+. These yields are much larger than those reported for Ar. We have further observed that erosion of D_2 was temperature dependent and that this dependence was strongest for the thicker films.

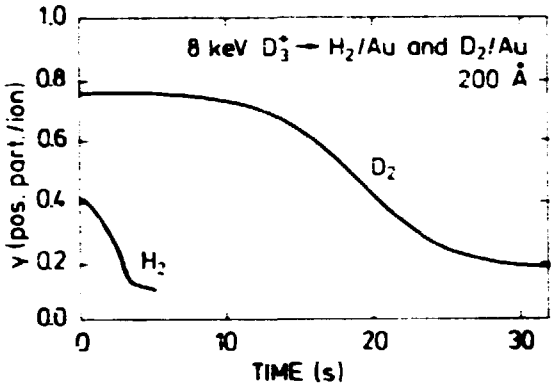

Fig. 36 Erosion of 200 Å films of H_2 and D_2 at 2.5 K. The emission coefficient γ is shown as a function of the irradiation time.

2.14 Erosion of frozen Ar by swift He ions

(F. Besenbacher*, J. Bøttiger*, O. Graversen*, J.L. Hansen*
(*University of Aarhus, Denmark) and H. Sørensen)

It has been known for some years that sputtering yields of frozen gases are orders of magnitude larger than the ones predicted by the theory of Sigmund (1969). In this theory, which accounts well for metals, the yields are associated with the energy deposited in nuclear collisions, i.e. with the nuclear stopping cross section. For frozen gases and other insulating materials, the yields seem rather to be associated with the energy lost to the electrons of the target, i.e. to the electronic stopping cross section, S_e.

The erosion yields for solid hydrogens (2.13), which are of importance for pellet-plasma interaction, are much larger than the yields found for Ar. It is, however, obvious that an understanding of the erosion of solid Ar is quite essential for an understanding of the erosion of solid hydrogens. Stopping power measurements for 0.5-3 MeV He ions in solid Ar were already in progress (2.16) and it was therefore appropriate to also study the erosion of Ar films with 0.1-3 MeV He ions (Besenbacher et al. 1979b). The Ar films were deposited on a well-polished metal plate (Al or Be) held at 6 K. The ion beam was made uniform by means of beam sweep and thereafter limited to 2×2 mm. The sputtering rate was measured by means of Rutherford back-scattering and a number of Bi-atoms were implanted in the metal substrate for

use as calibration markers. The erosion yields were found to increase with film thickness up to a thickness of 2×10^{17} atoms/cm^2 and thereafter it was independent of the film thickness. As an example, the yield for 750 keV $^3He^+$ is 68 atoms/ion. The yield is independent of the target temperature up to ~24-25 K, whereafter it increases very quickly with temperature. The yields as a function of the ion energy is found to scale well with the square of the electronic stopping power.

2.15 Ranges and stopping powers in solid H_2, D_2 and N_2

(P. Børgesen, Chen Hao Ming, J. Schou and H. Sørensen)

It has been described earlier (Børgesen et al. 1979b) how the range of low energy ions in solid H_2 and D_2 was determined by measuring the variation of the coefficient, γ, for emission of positive particles with film thickness, i.e. measurements could be made at particle energies much lower than previously done. So far, only one set of measurements (for gaseous targets) exists below 50 keV. It was suggested that the maximum range R(E) was given as

$$R(E) = 2T_\gamma(E) + R(E_{th}).$$

Here $T_\gamma(E)$ is the thickness at which γ reaches the bulk value and $R(E_{th})$ is a constant. Such range measurements were made for incidence of hydrogen and deuterium ions on H_2 and D_2 targets and later also for N_2 targets.

It is a problem that $R(E_{th})$ is unknown - although we expect it to be small - i.e. the lowest energy, E_{th}, at which particles back-scattered through a film may still be ionized is unknown. However, by differentiating $T_\gamma(E)$ it is possible to deduce stopping powers, dE/dR, which do not depend on $R(E_{th})$. In Fig. 37 are shown such stopping powers for hydrogen and deuterium ions in solid H_2 and D_2. We believe these to be the first stopping power measurements for solid hydrogens.

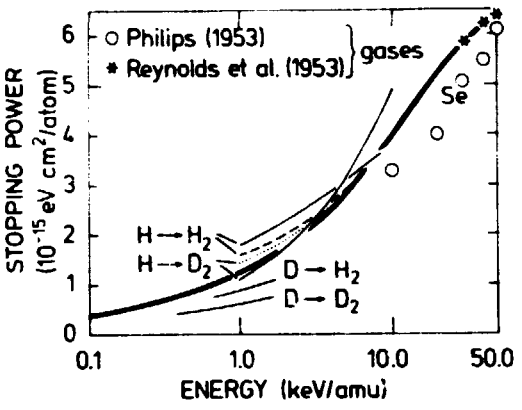

Fig. 37 Stopping powers for hydrogen and deuterium ions in solid H_2 and D_2. Thin solid curves: our measurements. Stopping powers for hydrogen ions in gaseous H_2 and D_2. Thick solid curve: electronic stopping power S_e (Andersen and Ziegler 1977). Broken curves: S_e plus nuclear stopping power (Lindhard et al. 1963). Experiment using gaseous targets o by Phillips (1953) and * by Reynolds et al. (1953).

In order to determine the energy E_{th} we still need to study the energy spectra of the back-scattered particles. For low energies and not too volatile targets, a study of the energy spectra arising from thin films will furthermore yield stopping power values based on quite different assumptions. An electrostatic analyzer was constructed for this purpose. The basic principle is described in textbooks on charged particle analysis and illustrated in Fig. 38. The voltage ΔV between the plates determines the energy of those (singly charged) particles which will follow the centre line through an angle of 90° to be detected in a channel electron multiplier. To minimize scattering inside the analyzer, the two limiting "plates" are formed by a series of razor blades.

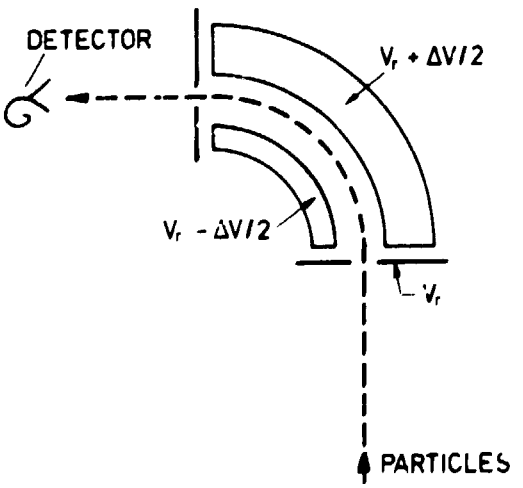

Fig. 38 Sketch of the electrostatic analyzer. The two "plates" are formed by a series of razor blades. The detector is a channel electron multiplier.

The energy window of the analyzer is proportional to the energy corresponding to the centre path indicated in Fig. 38. The energy resolution could therefore be improved by decelerating the ions to 10-20% of their original energy before analysis. This was accomplished by applying a retarding voltage, V_r, to the analyzer. The resulting defocussing was carefully corrected for by insertion of focussing apertures and by covering the retarding aperture with a fine grid. Tests showed the system to have an energy resolution of 1.5-3% of the original energy.

2.16 Stopping power of He ions in solid Ar

(F. Besenbacher*, J. Bøttiger*, O. Graversen*, J.L. Hansen*
(*University of Aarhus, Denmark) and H. Sørensen)

It is often discussed whether or not the stopping power cross section for a target material depends on its physical state, i.e. whether it is in the solid, liquid or gas state or bound in a chemical composition. Knowledge of such an effect is of course very important when one wishes to estimate data for chemical compounds and for target materials in various phase states. In his book on stopping power data of He ions, Ziegler (1978) presents semi-empirical curves that show differences between stopping power cross sections for solid and gaseous phases of various elements and materials.

Accurate measurements of stopping power cross sections for He ions in gaseous Ar do exist (Besenbacher et al. 1979a) and it is thus appropriate to do measurements on solid Ar as well. Such measurements were made by means of the set-up for studies of films of condensed gases now in use at the University of Aarhus (Besenbacher et al. 1979b). In this set-up, the stopping power cross section of Ar for 0.5-3 MeV He ions was then measured by means of the Rutherford back-scattering method to an accuracy of ~3%. There was no difference between the results for solid Ar and the ones obtained previously for gaseous Ar.

2.17 Corrosion inhibition by ion implantation

(L.G. Svendsen (NESELCO Ltd., Copenhagen, Denmark) and P. Børgesen)

Implantation of Al or Mg inhibits the corrosion of Cu, an effect which was investigated by Rutherford back-scattering spectrometry. In order to increase the oxidation rate, the Cu films were heated to 533 K in air for 15-240 minutes. Using a new numerical evaluation procedure (2.22), the target composition versus depth of an implanted target was evaluated, and this enabled a detailed study of the oxidation process. Unimplanted reference targets were found to oxidize to a stoichiometry of Cu_2O at a typical rate of $2 \cdot 10^{18}$ Cu atoms/cm^2 per hour. The corrosion of the implanted targets was strongly inhibited by the formation of protective implant-oxides. In the case of Mg, the corrosion was limited to a very shallow depth ($3 \cdot 10^{17}$) atoms/cm^2, whereas in the case of Al a thicker oxide layer developed, apparently due to diffusion of Cu through the implanted layer.

2.18 Preferential sputtering of TiN

(P. Børgesen, B.M.U. Scherzer (Max-Planck-Institute of Plasma Physics, Garching, F.R.G.) and H. von Seefeld (Technical University of Munich, Garching, F.R.G.))

For the purpose of studying the mechanism of preferential sputtering, thin films of TiN were deposited on carbon substrates. The target composition versus depth could then be evaluated by Rutherford back-scattering spectrometry (2.21). The films were then sputtered with 3.5 keV deuterons, where the energy was chosen to give a projected range of ~25% of the film thickness. This was designed to give not only the ratio of the resulting sputter yields, but also to show eventual variations in depth, etc.. N was seen to disappear much faster than Ti but, somewhat unexpectedly, enough Ti disappeared from all depths to maintain a uniform stoichiometry over the whole film. By means of the $D(^3He,p)^4He$ nuclear reaction, the implanted deuterium profile was found to extend through the whole film and even into the substrate.

In order to eliminate possible chemical effects, the experiment was repeated with 3.5 keV ^{3}He. The result was essentially the same, except that N disappeared at a slower rate than before. Finally, with 4 keV Ar, the ratio of the total N-content to the total Ti-content first decreased about 10%, and then remained constant. This agrees with the assumption of normal sputtering of an already N-depleted surface layer. Unfortunately, this layer would be too thin to resolve with Rutherford back-scattering.

2.19 Measurements of ^{3}He-profiles in Ta and Ta_2O_5 by nuclear reaction and Rutherford back-scattering; a discrepancy

(H. von Seefeld (Technical University of Munich, Garching, F.R.G.) and P. Børgesen)

The depth profiling of light elements in heavy targets is an important problem in many fields, including that of plasma-wall-interaction. The profiling of ^{3}He and D by means of the D(^{3}He,p)^{4}He nuclear reaction is by now a well-established method with well-defined uncertainties. The major uncertainty in this approach arises from the large discrepancies in the published nuclear reaction cross section data. An alternative, but uncommon method is based on the contribution of such an element to the total stopping power of the target. An element like ^{3}He contributes so little to the stopping power in heavy targets that this method is very uncertain, but these uncertainties are at least easy to estimate.

The two methods were compared. Thick targets of Ta and of Ta_2O_5 were implanted with 15 keV $^3He^+$. The implantation fluence was kept sufficiently low to avoid blistering and to avoid measurably changing the stoichiometry of the Ta_2O_5-targets. The distributions trapped in the targets were then determined by means of both methods. The resulting concentrations disagreed by factors of 2 (Ta-targets) to 3 (Ta_2O_5-targets), i.e. clearly beyond the combined uncertainties of the methods. We can only speculate as to the cause(s) of this discrepancy.

2.20 Permeation of deuterium through metals

(B.M.U. Scherzer (Max-Planck-Institute of Plasma Physics, Garching, F.R.G.) and P. Børgesen)

Diffusion and permeation of hydrogen isotopes are processes which are very important in fusion-reactor technology. The permeation of deuterium through Ni was investigated for the case of 8 keV D_2^+ implanted into foils of ~25 μm thickness. The permeating deuterium was collected in a Ti layer of ~200 Å thickness on the rear-side of the foil and detected by means of the $D(^3He,p)^4He$ nuclear reaction. The cleanliness of the Ni-Ti interface was seen to be of vital importance to the method, and great care was taken to clean the interface before depositing the Ti. The diffusion back out through the implanted surface was very sensitive to the cleanliness of this surface, so the target was sputter cleaned with low energy Ne just before implantation. The influence of surface composition was then investigated by contaminating it again with oxygen, after various lengths of time, during implantation. The permeation was seen to be influenced strongly by radiation damage.

It has been suggested by Zakharov et al. (1979) that hydrogen permeation through Mo is strongly enhanced by the formation and diffusion of complexes of hydrogen atoms and self-interstitial atoms. Implanting the same dose of 4 keV H^+-ions as Zakharov et al. (1979) into Mo-foils, we found much lower permeation rates by means of the $D(^3He,p)^4He$ nuclear reaction. Still following Zakharov et al. (1979) we then implanted Mo-foils with 9 keV $^3He^+$ and measured the resulting distribution. A larger dose of 4 keV H^+-ions implanted into the rear-side of the foil was then supposed to create a flow of self-interstitial atoms through the foil, resulting in a re-distribution of the ^3He at the front surface. The 40% decrease of the initial He-content observed by Zakharov et al. (1979) by sputter profiling should be clearly measurable with the $D(^3He,p)^4He$ reaction, but no change was found.

2.21 Depth profiling by ion beam spectrometry

(P. Børgesen, R. Behrisch* and B.M.U. Scherzer* (*Max-Planck-Institute of Plasma Physics, Garching, F.R.G.))

A formalism was developed for the evaluation of ion beam analysis energy spectra. A set of linear, simultaneous equations directly yield the stoichiometry of the target at a given depth. No previous knowledge of the target composition is necessary.

Two different procedures are available for solving the equations, depending on the input parameters: one may omit (i) one of the elemental signals, or (ii) the product of incident beam dose and detector solid angle. Extensive tests with synthesized spectra showed that with internally consistent input parameters both procedures always yielded the exact target composition for which the spectrum was generated.

To help choose the best procedure in a given case, the sensitivity of both statistical fluctuations and uncertainties in the input was demonstrated. The results are as follows:

(i) If the signal from a single target element is unavailable, the derived concentration of this element is very sensitive to small errors in the remaining input.

(ii) The set of equations may be treated as an eigenvector problem, and the accuracy of the results is of the same magnitude as the accuracy of the input.

When applicable at all, one will usually prefer (ii).

2.22 Computer program for evaluation of ion beam energy spectra

(P. Børgesen, B.M.U. Scherzer*, R. Behrisch* (*Max-Planck-Institute of Plasma Physics, Garching, F.R.G.), L.G. Svendsen (NESELCO Ltd., Copenhagen, Denmark) and S. Eskildsen (University of Aarhus, Denmark))

A very popular method of sample analysis is ion beam spectrometry. In many cases one may determine the composition of a target by solving an eigenvector problem (2.21). A computer program was developed which does this by inverse iteration. The program in-

cludes an automatic initial guess of eigenvector and eigenvalue. The iteration is very fast and usually converges sufficiently in 1 to 3 steps. The program determines first the stoichiometry of the target surface. By assuming this to be constant in a small depth interval, the program then determines the stoichiometry in the next depth step, and so forth. By taking sufficiently small steps the program retains essentially only the errors of the experimental spectrum. Various features are introduced to deal with or estimate resolution effects. The program was used extensively, both on the Amdahl 470 computer of the Max-Planck-Institute and on the NORD-system of the Institute of Physics, University of Aarhus.

2.23 Drag effect of a refuelling pellet

(C.T. Chang and P. Michelsen)

The drag effect of a refuelling pellet was studied in some detail (Chang and Michelsen 1981). As one of the illustrative examples, calculation was also made by considering the hypothetical injection of a 1 mm radius D_2-pellet into JET. In the computational work, the plasma temperature and density profiles were taken as

$$Te(keV) = 5(1-x^2)^2 \quad \text{and}$$

$$n_e(cm^{-3}) = 3\cdot10^{13}(1-x^2),$$

where $x = r/a$, $a = 1.25$ m is the plasma radius, and r is the radial distance measured from the magnetic axis. The results showed that at an injection speed of 3 km/s, the pellet penetration depth is ~0.45 cm from the magnetic axis, when using the neutral shielding theory by Parks and Turnbull (1978), and ~0.1 cm from the magnetic axis when using the ion-shielding theory by Gralnick (1973).

2.24 Line emission from the ablatant of a refuelling pellet

(C.T. Chang)

Up to the present, the only method available for the study of in situ ablation rate of the pellet is by measuring the H_α-line emission. Based on the collisional radiative model of Bates et al. (1962), the underlying atomic process was investigated. Preliminary analysis indicated that the diagnostic method used in the experiments on ORMAK (Oak Ridge Tokamak) (Foster et al. 1977) and ISX-A (Impurity Study Experiment at Oak Ridge) (Milora et al. 1979) implicitly assumed that the emission of the H_α-line comes mainly from the boundary of the ablated cloud. This implies that the emitting plasma is at a relatively high electron temperature and low electron density, and that the plasma can be treated as optically thin (with the possible exception of L_α-line). Once the ablatant is excited to the third excited level, it quickly ionizes and becomes trapped by the surrounding magnetic field lines, thus lost from the ablated cloud. In such a case, to a good degree of approximation, the H_α emission rate, dN_α/dt, is related to the pellet ablation rate, dN/dt, by

$$\frac{dN_\alpha}{dt} \propto \frac{K(1,3)}{K(1,c)} \cdot \frac{dN}{dt},$$

where $K(1,3)$ is the collisional rate coefficient from the ground level (1) to the excited level (3) and $K(1,c)$ is the ionization rate coefficient from the ground level. Furthermore, this ratio can be shown to be given by

$$\frac{K(1,3)}{K(1,c)} = C\left(1 + 4.88\frac{\chi_i}{T_e}\right)\left(\frac{\chi}{\chi_i}\right)^{\frac{1}{2}} \exp\left[\left(\frac{\chi_i - \chi}{T_e}\right)\right],$$

where C is a constant, χ (= 12.09 eV) is the excitation energy of the 1 to 3 transition and χ_i (= 13.6 eV) is the ionization energy. One observes that $K(1,3)/K(1,c)$ approaches a constant only if $T_e/\chi_i > 5$, i.e. a direct proportionality between the emission rate of H_α and the pellet ablation rate holds only if the electron temperature of the ablated cloud is greater than 70 eV. It is planned to examine whether such a restriction can be relaxed under more general emission conditions of the ablated plasma.

2.25 Development of a numerical computer code for the pellet ablation rate

(C.T. Chang)

In order to study the physical properties related to the emission process of the ablatant and to extend the validity of the neutral shielding model, the development of a computer code was undertaken. To develop the code, the original neutral shielding model of Parks and Turnbull (1978) was used as a check. It was found that because of the rapid attenuation of the incident electron energy flux in the subsonic region, a steep rise of flow parameters of the ablatant occurs near the vicinity of the pellet surface. The step size of integration is self-adjusted in the used procedure (RISOE/DIFFSUB/A). To locate the pellet surface accurately, this procedure is therefore more appropriate than the Runge-Kulta procedure (RISOE/RK5/A) where the step size integration is fixed during the integration. Two versions of the code were written, one using the radial distance as the independent variable, the other using the square of the Mach number as the independent variable. It is planned to extend the code to include the dissociation effect and variation of the specific heat rates.

2.26 Dante (Danish Tokamak Experiment)

(V. Andersen, H. Bcjder, M. Gadeberg, P.B. Jensen and P. Nielsen)

To study the pellet-plasma interaction in the tokamak plasma, pellets of frozen deuterium were shot into the plasma.

The pellet gun (Nordskov et al. 1979) is constructed for horizontal firing of the pellet, but to avoid certain problems when firing horizontally into the tokamak and to improve access for studying the interaction between the pellet and the plasma, vertical injection of the pellets was preferred. This was done by injecting the pellets into the tokamak through a 4 m long curved guide tube with an inner bore of 4 mm. Other advantages of the curved guide tube are that the pellet gun need not be lined up with respect to the ports of the tokamak, and that the vacuum systems for the tokamak and the pellet gun are well separated.

There are no measurable changes in the pellet size or velocity because of the curved guide tube. The time between the firing pulse for the pellet gun and actual launching of the pellet is somewhat uncertain, $\Delta t \approx 250$-500 ms. In addition, the pellet velocity varies from 140 to 200 m/s and hence there is uncertainty in the time of arrival of the pellet into the plasma. Two photodetectors immediately outside the gun sense when the pellet leaves the gun and the speed of the pellet. From these data a special calculator circuit produces a trigger-pulse to ignite the plasma. This ensures that the pellet enters the tokamak at a given time in the stable plasma period. A third detector at the entrance port of the tokamak gives, in connection with another calculator circuit, a trigger-pulse when the pellet is at a selected position. This device allows photography of the pellet ablation cloud.

Until now, results concerning ablation of frozen deuterium pellets in the hot plasma have been done in the type of discharges shown in Fig.39a. The pellets used in this experiment are much too large for the tokamak if all the pellet material is ablated. The number of particles in the pellet is ~20 times the total number of particles in the initial plasma. Figure 39b shows signals similar to those seen in Fig.39a, but with a pellet shot into the plasma at a time corresponding to a 4 ms delay after ignition. It is seen that the plasma is totally quenched by the ablated pellet material. The amount of ablated pellet material is detected by two different methods: (i) The unablated part of the pellet is collected in a collecting bottle placed beneath the tokamak at an exit port and a measurement of the pressure rise in this bottle gives the amount of unablated pellet material. (ii) The total amount of emitted H_α-light from the ablating pellet is detected. The number of emitted photons is proportional to the number of ionizations (Johnson and Hinnov 1973), so this measurement gives the total amount of ablated pellet material. The results of the two methods are in reasonable agreement, giving an ablation of about 60% of the pellet. Had the plasma remained alive, even more of the pellet might have been ablated because the pellet was still in the plasma region when the plasma was quenched.

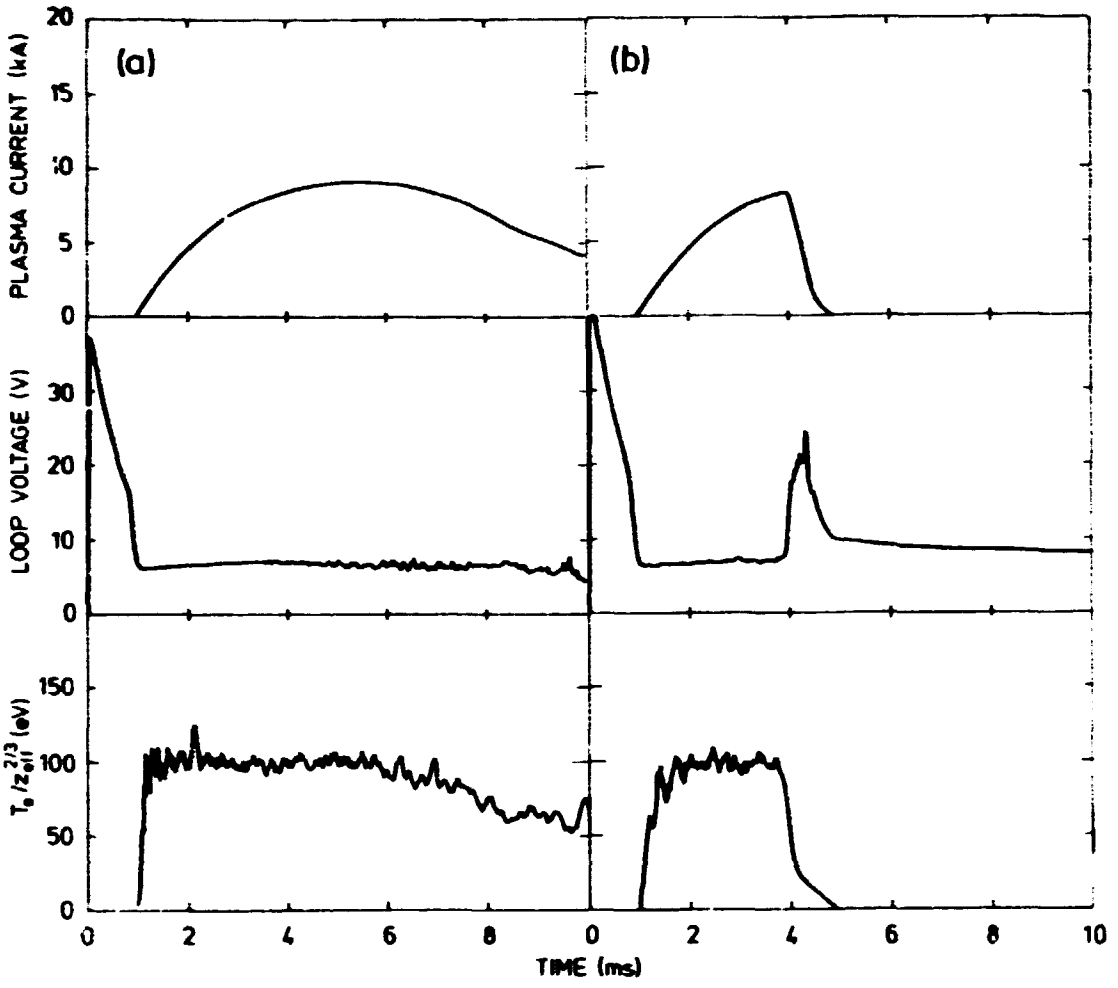

Fig. 39 Current, voltage and electron temperature ($T_e/z_{eff}^{2/3}$) of (a) reference shot no. 11, April 29, 1980, and (b) shot with pellet injection no. 14, April 29, 1980.

A rough comparison shows disagreement between our results and the theory of Parks and Turnbull (1978), but a more exact comparison has not been made because we need to gain more accurate knowledge of the electron temperature. Local measurements of the electron temperature is planned in the near future, using a double pulse ruby laser, Thomson-scattering system. Furthermore, a new pellet gun - producing smaller pellets - has been constructed (2.27), and will after a test period be installed at the tokamak.

In order to increase the possibilities of stabilizing the plasma before shooting the pellets, the plasma parameters of Dante have

been changed by dividing the ohmic capacitor bank, as well as the stabilizing capacitor bank, into smaller parts, which are fired successively. To create the final correction to the field we employ a pair of feedback amplifiers capable of delivering 20 kW. The amplifiers are coupled, so they can control both up-down and in-out movements. With these modifications, the discharge time is prolonged to 40 to 50 ms and we have used less than half of the flux in the ion core. Therefore, the discharge time may be prolonged even more by using additional capacitor banks.

A typical plot of plasma current, loop voltage and peak-electron-temperature ($T_{eo}/z_{eff}^{2/3}$), after these modifications, is shown in Fig. 40. The peak temperature can be calculated from the plasma resistivity assuming a parabolic current profile. The peak elec-

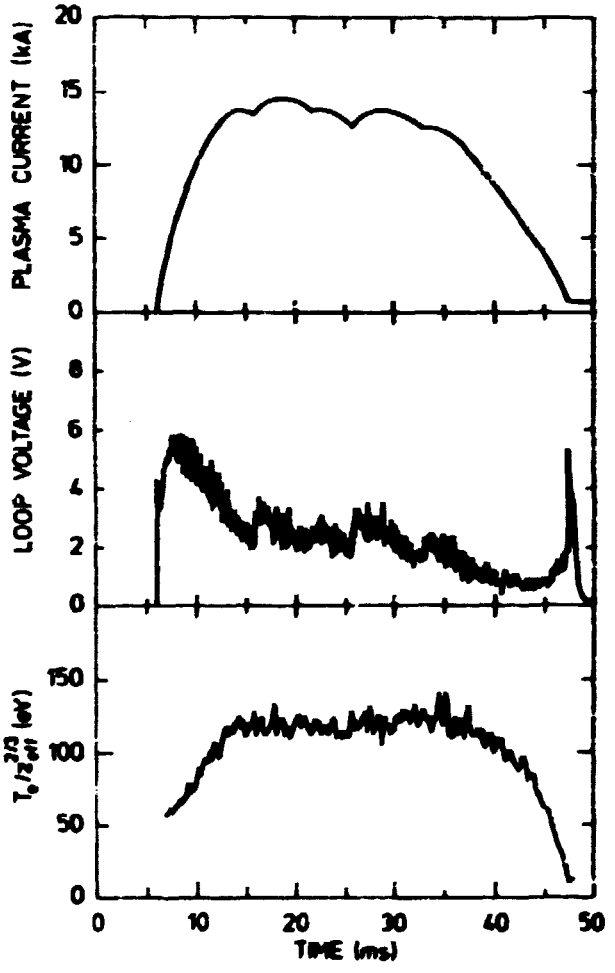

Fig. 40 Current, voltage and electron temperature ($T_e/z_{eff}^{2/3}$) of shot no. 13, November 24, 1980.

tron temperature measured with a soft x-ray spectrometer is ~170 eV, which, when compared to the temperature deduced from the resistivity, gives a $Z_{eff} \simeq 1.8$. Because of the longer discharge time of the plasma, it was necessary to elongate the pellet guide tube to get a reasonable delay in the time of arrival of the pellets. Furthermore, improvements of the curved guide tube technique are in progress in order to diminish the angular spread of directions of the pellets leaving the guide tube.

2.27 Pellet handling and acceleration

(S. Andersen, J. Knudsen, A. Nordskov, J. Olsen, B. Sass, H. Skovgård, H. Sørensen and K.V. Weisberg (Electronics Department, Risø))

As mentioned by Andersen et al. (1979) the pellet gun built for use at Dante (Nordskov et al. 1979) delivered pellets too large for the tokamak. We have therefore constructed a new gun that can deliver smaller pellets. Preliminary data from test runs with manual operation for this gun are given below.

Data for pellet gun

Pellet material	- solid D_2
Pellet dimensions	- 0.4×0.4 mm^2 cross section
	- 0.05 mm^3 - 0.01 mg - $1.6 \cdot 10^{18}$ molecules
Maximum velocity	- greater than 300 m/s
Barrel length	- 57 mm
H_2 propellant gas	- 5 bar cm^3 - $12 \cdot 10^{19}$ molecules

After the test runs, a unit for automatic operation of the gun was designed and built. Testing of the automatically operated gun is in progress.

An experimental programme for an extension of the work on pellet acceleration and handling was suggested to and approved by the Ministry of Energy. A grant to cover three years work was obtained under the energy research programme of the ministry. The purpose of the work done so far has been to build pellet guns for use at

Dante (Danish Tokamak Experiment). The purpose of the new work is more universal and aims at studying problems with handling and acceleration of pellets of relevance for larger plasma and fusion experiments, i.e. the pellets will be much larger than the ones needed for Dante.

2.28 Single point Thomson scattering system for JET (Joint European Torus)

(P. Nielsen)

A scientific and engineering design of a single point Thomson scattering system for JET was made in collaboration with the Electronics and the Engineering Departments at Risø.

The differential cross-section for scattering of photons on electrons is rather small, $\sigma = 8.8 \cdot 10^{-26}$ cm^2/steradian. With typical scattering lengths ~1 cm and F = 10 optics, we found that for a tokamak plasma with electron density $n_e \simeq 10^{13}$ cm^{-3}, of order 10^{19} - 10^{20} incident photons (light energy $\simeq$ 1-10 J are required to give a significant signal. Since the plasma emits continuous radiation (bremsstrahlung) of high intensity, the only available light source is a Q-switched laser. The choice of laser is a compromise between available laser energy and detector quantum efficiency at different wavelengths. In the design we chose a multi-pulse ruby laser, with a maximum energy of 20 J in each pulse. When scattering from a moving charge the light is doppler-shifted, the frequency shift being proportional to the velocity of the scattering electron. By analyzing the spectrum we can thus determine the electron temperature.

Figure 41 shows a general layout of the system. In order to overcome the problems associated with the expected neutron radiation dose of 10^8 rem in the torus hall, the most sensitive part of the system is placed on the first floor of the laboratory. The distance from the ceiling to the centre of the machine is ~18 m. The ruby laser light enters the torus hall through a trap system and is directed to a fixed mirror on an optical bench on the top of the torus. The mirror deflects the light along the bench onto

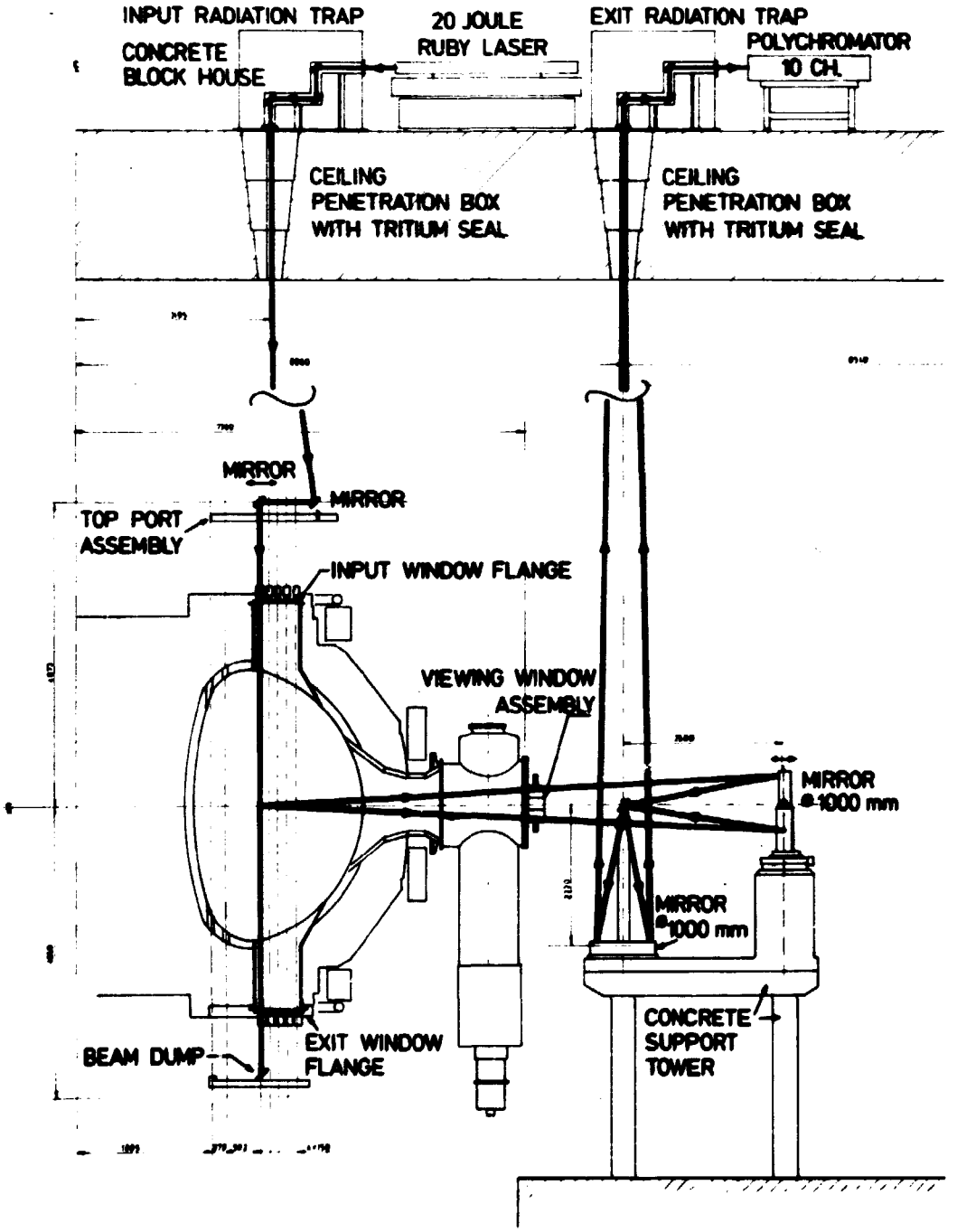

Fig. 41 General layout for the single point Thomson scattering system for JET.

a scanning mirror that can be moved to seven discrete radial positions. From the scanning mirror the light is passed through the torus to a dump below. The light is focussed in the centre of the machine. The width of the beam at the focal plane is less than 2 mm.

Two large mirrors (1 m in diameter) in a double newtonian configuration images the scattering volume to a point on the ceiling. The collected light is passed through another radiation trap and an aspheric achromatic lens re-images the scattering volume on the input slit of the analyzing instrument (polychromator). A field lens at the image on the ceiling forms a tritium seal.

The polychromator is a triple-prism polychromator, two prisms in positive and negative dispersion working as a notch-filter for the laser line, and the third prism dispersing the spectrum to 10 photo-multipliers. The entire system is auto-aligning and adjustable through the diagnostic computer system on JET. A number of photo-detectors supply the computer with information on the alignment status. Alignment is obtained by adjusting 23 step motors, controlling the tilt and position of the various mirrors.

A construction contract for the system between Risø and JET is expected to be signed in the spring of 1981.

2.29 References to section 2

ANDERSEN, H.H. and ZIEGLER, J.F. (1977). Hydrogen Stopping Power and Ranges in all Elements. Pergamon Press, New York, 317 pp.

ANDERSEN, V., GADEBERG, M., JENSEN, P.B. and NIELSEN, P. (1979). In: Physics Department, Annual Progress Report, Risø-R-414, 74-76.

BALMASHNOV, A., LYNOV, J.P., MICHELSEN, P., PÉCSELI, H.L. and RASMUSSEN, J. JUUL (1979). In: Physics Department, Annual Progress Report, Risø-R-414, 54-55.

BATES, D.R., KINGSTON, A.E. and McWHISTER, R.W.P. (1962). Proceedings of Roy. Soc. (London) A267, 297-312.

BERNSTEIN, I.B. (1958). Phys. Rev. 109, 10-21.

BERNSTEIN, I.B., GREENE, J.M. and KRUSKAL, M.D. (1957). Phys. Rev. 108, 546-550.

BESENBACHER, F., ANDERSEN, H.H., HVELPLUND, P. and KNUDSEN, H. (1979a). Mat. fys. Meddr. 40: 3, 33 pp.

BESENBACHER, F., BØTTIGER, J., HANSEN, J.L. and SØRENSEN, H. (1979b). In: Physics Department, Annual Progress Report, Risø-R-414, 67-68.

BØRGESEN, P., SCHOU, J. and SØRENSEN, H. (1979a). In: Physics Department, Annual Progress Report, Risø-R-414, 65-66.

BØRGESEN, P., SCHOU, J. and SØRENSEN, H. (1979b). In: Physics Department, Annual Progress Report, Risø-R-414, 66-67.

BURGER, P. (1965). J. Appl. Phys. 33, 1938-1943.

CARLQVIST, P. (1979). In: Wave Instabilities in Space Plasmas. Edited by P.J. Palmadesco and K. Papadopoulos. Astrophysics and Space Science Library 74, Kluwer Boston, Inc., Hingham, Massachusetts, U.S.A., 83-108.

CHANG, C.T. and MICHELSEN, P. (1981). On the drag effect of a refuelling pellet. Accepted for publication in J. Fusion Energy.

DENAVIT, J. (1972). J. Comput. Phys. 9, 75-98.

FEJER, J. and DAS, A.C. (1981). Resonance instability of small-scale field-aligned irregularities. To be published.

FIALER, P.A. (1974). Radio Sci. 9, 923-940.

FOSTER, C.A., COLCHIN, R.J., MILORA, S.L., KIM, K. and TURNBULL, R.J. (1977). Nucl. Fusion 17, 1067-1075.

GRALNICK, S.L. (1973). Nucl. Fusion 13, 703-713.

IKEZI, H., KAMIMURA, T., KAKO, M. and LONNGREN, K.E. (1973). Phys. Fluids 16, 2167-2175.

JOHNSON, L.C. and HINNOV, E. (1973). J. Quant. Spectrosc. Radiat. Transfer 13, 333-358.

KAKO, M., TANIUTI, T. and WATANABE, T. (1971). J. Phys. Soc. (Japan) 31, 1820-1829.

LEMBEGE, B. and GONFALONE, A. (1978). Plasma Phys. 20, 879-889.

LINDHARD, J., SCHARFF, M. and SCHIØTT, H. (1963). Mat. fys. Meddr. 33: 14, 42 pp.

LYNOV, J.P. (1981). Solitary electron density waves in a magnetized, plasma-loaded waveguide. Risø-R-432, 57-68.

LYNOV, J.P., MICHELSEN, P., PÉCSELI, H.L. and RASMUSSEN, J. JUUL (1980). Phys. Lett. 80A, 23-25.

LYNOV, J.P., MICHELSEN, P., PÉCSELI, H.L., RASMUSSEN, J. JUUL, SAEKI, K. and TURIKOV, V.A. (1979a). Phys. Scr. 20, 328-335.

LYNOV, J.P., MICHELSEN, P., PÉCSELI, H.L., RASMUSSEN, J. JUUL and THOMSEN, K. (1979b). In: Physics Department, Annual Progress Report, Risø-R-414, 58-59.

MILORA, S.L., FOSTER, C.A., EDMONDS, P.H. and SCHMIDT, G.L. (1979). Phys. Rev. Lett. 42, 97-101.

MORALES, G.J. and O'NEIL, T.M. (1972). Phys. Rev. Lett. 28, 417-420.

NORDSKOV, A., SKOVGÅRD, H., SØRENSEN, H. and WEISBERG, K.V. (1980). In: Physics Department, Annual Progress Report, Risø-R-414, 77-78.

O'NEIL, T. (1965). Phys. Fluids 8, 2255-2262.

PARKS, P.B. and TURNBULL, R.J. (1978). Phys. Fluids 21, 1735-1741.

PARKS, P.B. and TURNBULL, R.J. (1978). Risø Computer Library, Risoe/Diffsub/A; Risoe/RK5/A2.

PERKINS, F.W. and SUN, Y.C. (1981). Phys. Rev. Lett. 46, 115-118.

PHILLIPS, J.A. (1953). Phys. Rev. 90, 532-537.

REYNOLDS, H.K., DUNBAR, D.N.F., WENZEL, W.A. and WHALING, W. (1953). Phys. Rev. 92, 742-748.

ROGISTER, A. and D'ANGELO, N. (1970). J. Geophys. Res. 75, 3879-3887.

SAEKI, K., MICHELSEN, P., PÉCSELI, H.L. and RASMUSSEN, J. JUUL (1979). Phys. Rev. Lett. 42, 501-504.

SAKANAKA, P.H. (1972). Phys. Fluids 15, 1323-1327.

SATO, N., HATAKEYAMA, R., IIZUKA, S., MIENO, T., SAEKI, K., RASMUSSEN, J. JUUL and MICHELSEN, P. (1981). Ultra-strong stationary double layers in a non-discharge magnetoplasma. Phys. Rev. Lett. 46, 1330-1333.

SCHAMEL, H. (1979). Phys. Scr. 20, 336-342.

SCHRITTWIESER, R., IIZUKA, S., MICHELSEN, P., RASMUSSEN, J. JUUL, HATAKEYAMA, R., SAEKI, K. and SATO, N. (1981). A method for measuring fast time evolution of the plasma potential by means of a simple emissive probe. To be published.

SCHUSS, J.J. and HOSEA, J.C. (1975). Phys. Fluids 18, 727-734.

SIGMUND, P. (1969). Phys. Rev. 184, 383-416.

SUGAI, H., MARUYAMA, M., SATO, N. and TAKEDA, S. (1978). Phys. Fluids 21, 690-694.

SUGIHARA, R. and YAMANAKA, K. (1975). Phys. Fluids 18, 114-116.

SUGIHARA, R. and YAMANAKA, K. (1979). Nagoya University Research Report IPPJ-387, 21 pp.

TORVEN, S. (1979). In: Wave Instabilities in Space Plasmas. Edited by P.J. Palmadesco and K. Papadopoulos. Astrophysics and Space Science Library 74, Kluwer Boston, Inc., Hingham, Massachusetts, U.S.A., 109.

ZAKHAROV, A.P., GORODETSKY, A.E. and SHARAPOV, V.M. (1979). Z. Phys. Chem. NF 117, 245-256.

ZIEGLER, J.F. (1978). Helium Stopping Powers and Ranges in all Elements. Pergamon Press, New York, 365 pp.

3. PARTICIPATION IN THE UA2 COLLABORATION AT CERN

3.1 The UA2 collaboration at CERN

(O. Kofoed-Hansen, J. Dines Hansen*, P. Hansen*, B. Madsen* and R. Møllerud* (*Niels Bohr Institute, Copenhagen))

This group of researchers participate together with similar or larger groups from Bern, Switzerland, CERN, Geneva, Switzerland, Orsay, France, Pavia, Italy and Saclay, France, in the construction of a detector to study $p\bar{p}$ interactions at the SPS-collider. The goal is a search for Z^0 and W^+ and W^- particles resulting from high energy $p\bar{p}$-collisions. The work is described in a series of so-called $p\bar{p}$ notes and in the contribution to the 1980 Uppsala conference on LEP instrumentation and experimentation: A Detector to Study $p\bar{p}$ Interactions at the SPS-Collider, K. Borer et al. (45 authors from the above institutes).

4. METEOROLOGY

Investigations of the dispersive capability of turbulent flows, in particular of the atmospheric boundary layer, is the traditional domain of the work in the meteorology section. This kind of work has been strengthened during later years, from both a theoretical as well as an experimental point of view. This is evident from the number of publications that have appeared, as well as from the number of activities which are reported below.

A necessary component of these activities is an understanding of the turbulence structure of the dispersive medium, i.e. mainly the atmospheric boundary layer. Thus, experimental investigations with the aim of describing the turbulent fluxes of heat, momentum and matter have traditionally been pursued. These investigations have been performed under circumstances as close as possible to the ideal situation, with stationary and homogeneous surface conditions, or in situations with simple deviations. Thus, two-dimensional changes in surface roughness, surface temperature and surface elevation have been and are being studied. This work is being followed by theoretical studies and numerical modelling for evaluating various parameterizations of the higher order flux terms in the equations of motion.

Investigations of the dispersive capability of the atmosphere, considered on a statistical basis, has on the other hand led to a general interest in climatology. Work is being done on compilation of already existing information, with comprehensive data collection, and, in cooperation with the Danish Meteorological Institute, with the maintenance of approximately fifty automatic weather stations in Denmark and Greenland. These stations are erected typically for site evaluation purposes. At Risø, the 120 m meteorological tower has now been in operation for 24 years, and the length of the series of wind speed, wind direction and temperature data from various heights along the tower is now approaching the climatological standard of 30 years.

The action of the turbulent wind field on structures is a traditional area of application of micrometeorology, and a number of projects in this field have been carried out as a spin-off during the later years. After the advent of the National Wind Power Programme, however, this field has become a major activity in its own right. During the present year, activities have been further strengthened by the adoption of the test plant for small wind turbines. As an introduction to this new activity, a relatively detailed outline of the responsibilities of the test plant is given below.

The test plant is a project sponsored by the Ministry of Energy, with the Meteorology Section as project responsible. The purpose of the project is to assist danish wind turbine manufacturers and users to test and evaluate small wind turbines and to perform wind turbine research and development. The test facilities consist of seven foundations on which manufacturer's and users' turbines are erected and tested. One is permanently occupied by a Darrieus turbine of 4 m in diameter, intended for research only, and developed in collaboration with the Technical University of Denmark. The foundations are connected to a data collection system developed at Risø and based on a micro computer system (PDP11-03). It has 64 channels, some of which are connected to a central meteorological tower, and two mobile masts. A normal test procedure consists of three phases. (i) A mechanical testing of the turbine's capability to operate reliably, (ii) a determination of the turbine's power curve and (iii) more detailed and extensive measurements of specific phenomena. In practise, this separation of phases has not been rigorous since most of the turbines tested so far have been in the development stage.

Assistance to the manufacturers is given mainly as consultations on problems with blade design, power output and mechanical layout. Wind turbine users are informed by reports issued by the test plant, by meetings, and by courses and lectures. A newsletter source is being planned. Also, official authorities are supported by reports on various subjects, and by meetings. The test plant is responsible for the system's evaluation necessary in order to obtain government subsidy. During this activity, the test plant

has some influence on the development of reliable and safe system layouts. As part of the contribution to the danish wind turbine development, the test plant performs research and development in areas of common interest to the wind turbine manufacturers and users. Examples are the application of the induction machine as a wind turbine generator, power regulation by means of aerodynamic stall, and coupling of induction generators to the electric grid.

In conclusion, the work of the meteorology section may be divided into four major categories:

1) Atmospheric dispersion research (4.1 - 4.6),
2) Micro- and mesometeorological research (4.7 - 4.9),
3) Wind power research (4.10 - 4.15),
4) Climatology, measuring techniques and general applications (4.16 - 4.19),

the last of which comprises a fairly large spectrum of activities. Sections 4.1 through 4.19 report some of the work that has been done during the present year. It should be emphasized that this is by no means a comprehensive list of current research topics.

4.1 Use of a puff-model to calculate dose distributions from a source with variable rate of release

(T. Mikkelsen, S.E. Larsen and I. Troen)

We have estimated concentration dose distribution at distances up to 25 km downwind from an exponential decaying buoyant source, simulating a hypothetical accidental release into a stable atmosphere. The estimates have been obtained by use of a dynamical statistical trajectory model, a so-called puff-model, by which puff advection and growth are based on a record of the dispersing wind field. Comparison is made with an ordinary gaussian plume model. It was found that the ground level dose is strongly dependent on the rate of release in both types of models. Only the puff-model, however, produced a successive larger spread as a result of plume meandering when release time of some duration was considered.

Figure 42 shows iso-lines of the ground level concentration dose resulting from the passage of a puff chain, which was controlled by the wind at the source point. The time between the release of puffs was 200 s, a total of fifty puffs were released, each containing matter and buoyancy in accordance with an exponential decaying source strength with a time constant, τ, equal to 1800 s. 20 km downwind from the source, the instantaneous plume width represented by the lateral puff size, σ_p, was of the order ~600 m.

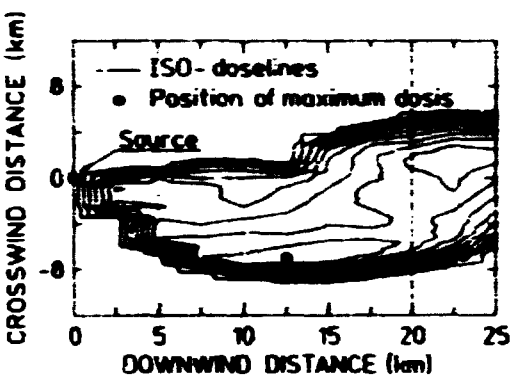

Fig. 42 Ground level concentration dose resulting from the puff-plume passage. The time constant for the source τ equals 1800 s. Iso-dose lines are shown for doses $D_{max}/2^n$; n = 1 to 9. The vertical broken line corresponds to the distance from the source, where results from the puff model and the gaussian plume model is compared in Fig. 43.

In Fig. 43 comparison is made between the gaussian plume model and the puff-model crosswind distributions at a line perpendicular to the mean wind direction 20 km downwind from the source. Where the gaussian plume model distributions have a constant width (σ_y = 560 m), the standard deviation of the crosswind dose distribution of the puff-model is approximately 3 km, i.e. ~5 times the

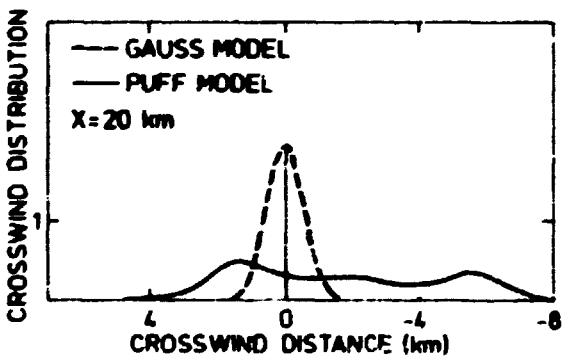

Fig. 43 Comparison of ground level crosswind dose distribution of the gaussian plume model at x = 23.2 km and the puff model at x = 20.0 km (puff trajectories = 23.2 km) under conditions of identical vertical spread. σ_z = 65 m. Gauss model: σ_y = 560 m, σ_z = 65.0 m (x = 23.2 km). Puff model: σ_p = 600 m, σ_z = 65.0 m.

width of the corresponding gaussian plume model's distribution. This enhanced spread comes because of large scale scatter in the puff centre positions, the so-called meandering.

4.2 Auto-regressive scheme for the simulation of wind variability on the mesoscale

(S.E. Larsen, T. Mikkelsen and I. Troen)

In principle, a puff-model is capable of describing dispersions under non-stationary and non-homogeneous conditions. An example is given in section 4.1. However, to utilize the capacity of the model fully, the necessary information about the flow field must be made available. We describe here a statistical model which can be used when a time series of the horizontal velocity components is available at the source point.

We used the findings of Smith (1968) and Hanna (1979) that both the lagrangian velocity of a particle and the single point eulerian velocity can be approximately described as first order auto-regressive processes. For example, for the one point eulerian velocity:

$$u(t+\Delta t) = \rho u(t) + n(t), \qquad (1)$$

where ρ is the correlation coefficient and $n(t)$ is a white noise process.

Equation (1) indicates that also the spatial variability of an eulerian velocity can be described by a first order auto-regressive process. Recently, some work has been done on coupling the spatial eulerian and the temporal lagrangian auto-regressive processes to yield a description of the spatial-temporal velocity field, see e.g. Durbin (1980) and Mikkelsen et al. (1980). We considered puffs with a constant release rate, and hence the puff velocity can be described by the puff number, i, and the flight time of the puff, $q\tau$, i.e. $u(q\tau,i)$, where τ is the time distance between each puff. We have considered two coupling schemes be-

tween the eulerian and the lagrangian auto-regressive processes controlling the puff velocities.

$$u((i+q)\tau,i) = \rho_L u((i+q-1)\tau,i) + u'((i+q)\tau,i)$$

$$u'((i+q)\tau,i) = \rho_E u'((i+q)\tau,i+1) + n((i+q)\tau,i) \qquad (2)$$

and

$$u((i+q)\tau,i) = \rho_E u((i+q)\tau,i+1) + u'((i+q)\tau,i)$$

$$u'((i+q)\tau,i) = \rho_L u'((i+q-1)\tau,i) + n((i+q)\tau,i) \qquad (3)$$

Here ρ_E and ρ_L are the eulerian and the lagrangian correlation coefficients, respectively, (assumed to be related through Pasquill's β. It is seen that puff number i leaves the source at time $i\tau$. Equation (2) corresponds to stating that while the velocities are lagrangianly correlated, the noise, u', perturbing the lagrangian velocity is eulerian correlated with the noises of the neighbouring puffs. In equation (3) the argument is turned around. n is a white noise process as in equation (1). Both processes (equations (2) and (3)) result in the same process for large flight times:

$$u((i+q)\tau,i) =$$

$$\rho_L u((i+q-1)\tau,i) + \rho_E u((i+q)\tau,i+1) - \rho_L \rho_E u((i+q-1)\tau,i+1) +$$

$$n((i+q)\tau,i), \qquad (4)$$

which is then taken as the basic process.

In practical use, we write the advecting velocity field as

$$V = u + V_o \qquad (5)$$

where u has zero mean value, which is controlled by equation (4), whilst V_o is the deterministic part of the field, which in its simplest form is determined as the mean velocity at the source

point, but which can also include a non-stochastic time and space variation of the advection as might, e.g. be determined from synoptic information.

The release velocity of puff number i, $u(i\tau,i)$, is measured at the source point. This, however, is not information enough to start equation (4) since determination of u, for the i'th puff at time step i+1, $u((i+1)\tau,i)$, demands the knowledge of $u(i\tau,i+1)$, as seen from equation (4), and this information is not available. By use of a forecast and backward forecast technique described in Box and Jenkins (1970), a special relation can be derived for $u((i+1)\tau,i)$, that is

$$(1 - \rho_L^2\rho_E^2)u((i+1)\tau,i) =$$

$$\rho_L(1 - \rho_E^2)u(i\tau,i) + \rho_E(1 - \rho_L^2)u((i+1)\tau,i+1) + n((i+1)\tau,i) \quad (6)$$

It should be noted that for simplicity we have kept a scalar notation. In practice, however, the notation should be vectorial and the ρ's are tensors. The values of the ρ's and the variance of n are determined from the velocity time series at the source point.

In conclusion, it may be said that the model in connection with the measured time series enables us to use a puff-model to describe dispersion from a point source, which is consistent with the actual known time series and which does incorporate statistically the remaining variability of the wind field, that is known to exist but not measured. As presented here, the model does not include the decrease of ρ_E as the puffs drift apart. This, however, is easily included by keeping track of the distance between the i'th and the i+1'th puff, and by letting ρ_E vary accordingly. A more serious restriction is that the model only includes the correlation between neighbouring puffs defined by their release number, and not by their distance. This calamity, if such it is, could be corrected, but implementation of the correction in the computer program would be extremely time consuming compared to the present scheme, which in practice operates as a very simple updating scheme for each time step.

4.3 Elevated source SF_6-tracer dispersion experiments in the Copenhagen area

(S.E. Gryning and E. Lyck (National Agency of Environmental Protection, Air Pollution Laboratory))

Atmospheric dispersion experiments are being carried out in the Copenhagen area under neutral and unstable meteorological conditions in order to investigate the effect of a built-up area on the atmospheric dispersion process. The tracer sulphurhexaflouride was horizontally released from a tower at a height of 115 m, and then collected at ground-level positions in up to three crosswind series of tracer sampling units, positioned 2 to 6 km from the point of release.

The lateral dispersion parameter, σ_y, was estimated from the measured tracer concentration distributions. Also, in addition to other parameters, the variance of the lateral wind fluctuations, σ_θ^2, was measured. Defining the normalized lateral spread, f_y, as $f_y = \sigma_y/\sigma_\theta \cdot x$, where x is the downwind distance from the source, Pasquill (1976) argued that f_y depends primarily on x. It can be argued that the f_y-function also depends on the wind speed (in addition to other parameters). Small values of f_y are associated with small wind velocities, and vice versa. The f_y-values that can be estimated from the experiment support the existence of a wind velocity dependence on the f_y-function, as shown in Fig. 44.

As the vertical distribution of the tracer was not measured in these experiments, the standard deviation of the vertical tracer concentration distribution, σ_z, could be inferred only indirectly from continuity considerations, (gaussian plume model). The values of σ_z are expected to be enhanced when compared with workbook values of σ_z as suggested by Turner (1970). The difference is expected to be most pronounced under neutral conditions, and insignificant under fully convective conditions. It can be seen from Fig. 45 that the experimental values of σ_z assigned Pasquill stability class D (neutral) are positioned above the D-curve, even when taking into account the calibration uncertainty in the tracer concentrations. Experimental values of σ_z assigned Pas-

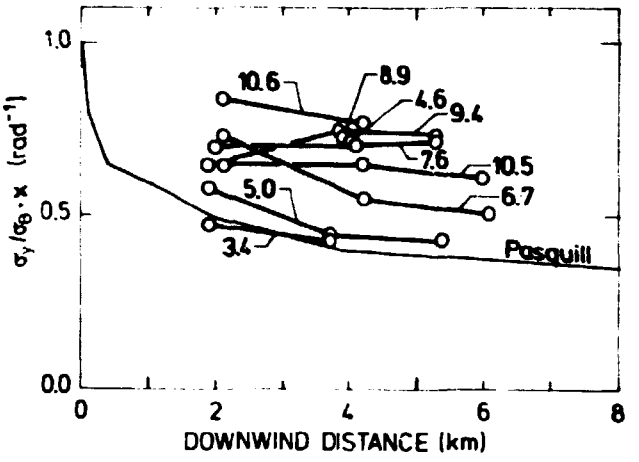

Fig. 44 The normalized lateral spread. $\sigma_y/\sigma_\theta \cdot x$, as a function of downwind distance. The mean wind velocity is indicated in units of m/s. Also shown is the f_y-function proposed by Pasquill (1976).

quill stability class C (slightly unstable) and stability class B-C (unstable) are seen not to be much different from the equivalent workbook values, although a substantial scatter is apparent. Based on the aforementioned results, improvements were devised on the methods of predicting σ_y and σ_z. The methods are offered by Gryning and Lyck (1980).

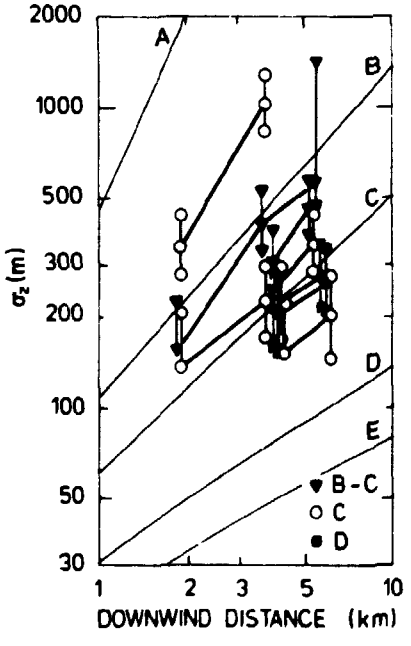

Fig. 45 Experimental values of σ_z, separated according to the Pasquill stability classification, versus downwind distance. The effect on σ_z that originates from the uncertainty in the calibration of the gaschromatograph, is shown as bars. For comparison, the workbook-curves (Turner 1970) for the Pasquill stability classes A-E are shown.

4.4 Joint experiment for verification of a small-scale puff model

(T. Mikkelsen, L. Kristensen and W.K. George)

During the years 1978-1979, the meteorology section, sponsored by the Danish Defence Research Establishment, developed a dynamical small-scale puff model intended for simulating ground-level released smoke diffusion in the atmospheric surface layer (Mikkelsen 1979). The intention is to develop a dynamical trajectory model for replacement of the gaussian plume model used hitherto for risk assessments of nuclear and chemical installations. In view of this, we participated in a joint experiment with the Danish Defence Research Establishment in order to validate the small-scale puff model. The experiment took place in late August, 1980, in a 1×1 km^2 flat moor terrain situated south of the town of Borris in western Jutland. The experimental site is ideal for micrometeorological experiments due to its flatness and homogeneity. The upwind fetch extends ~2.5 km, the downwind fetch ~3.0 km from the experimental site, the vegetation, which consists exclusively of grass and heather plants, constitutes a homogeneously distributed roughness of the order of ~1 cm over the entire terrain. The difference in level over the 1×1 km^2 test area is less than ~1 m.

The meteorological instrumentation was mounted on four 9 m high masts, placed on a crosswind line close to the smoke source as shown in Fig. 46. Each of the four masts were top mounted with a three axis sonic anemometer. With the relative position of the masts as indicated in the figures, we were able to obtain estimates of the spatial coherence of the horizontal velocity components at six, approximately logarithmically equidistant, lateral separations. A nearby permanent meteorological mast provided temperature and velocity measurements at levels 2, 22 and 45 m, from which the atmospheric stability was deducible.

It was of considerable interest to test the instantaneous dispersion scheme used with the puff model, since these dispersion parameters are dominant in the simulated concentration field when shorter averaging or release times are considered. From

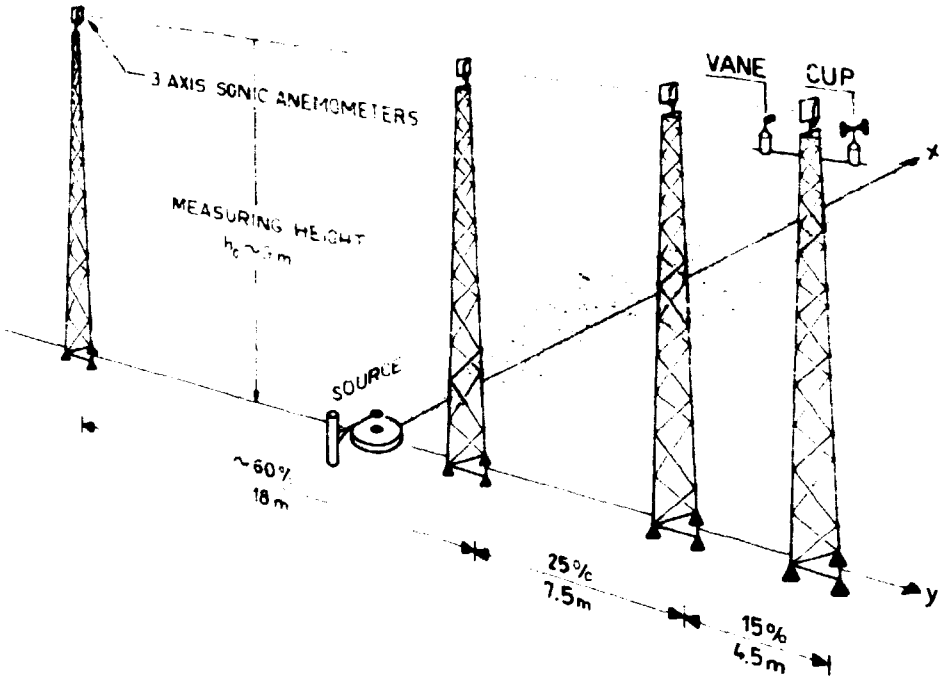

Fig. 46 Meteorological instrumentation.

a small propeller-aircraft photographs of the experimental site were taken during smoke release at 2 minute consecutive intervals from approximately 300 m height above ground-level. By referring to ground-placed markers, it was possible to depict the instantaneous lateral visible width of the smoke plume, and by use of the "opacity method" (Gifford 1980), the corresponding horizontal instantaneous standard deviation, σ_r, could be inferred by assuming a gaussian concentration distribution. Since the entire site was covered on each photograph, the instantaneous position and the instantaneous lateral spread of the smoke plume at downwind distances x up to 1 km from the source could be depicted. Averaged standard deviation, $\bar{\sigma}_r$, of the relative spread was obtained as an ensemble average of the instantaneous σ_r's from stationary runs.

In Fig. 47, we present measurements of the instantaneous standard deviation σ_r, from a 40 minute ground-level release to a convective boundary layer (bulk Richardson number $\simeq -0.07$). The mean wind speed measured at 9 m height was 5 m/sec, the horizontal turbulence intensity, i, was ~30%. Figure 48 shows $\bar{\sigma}_r(x)$ as well

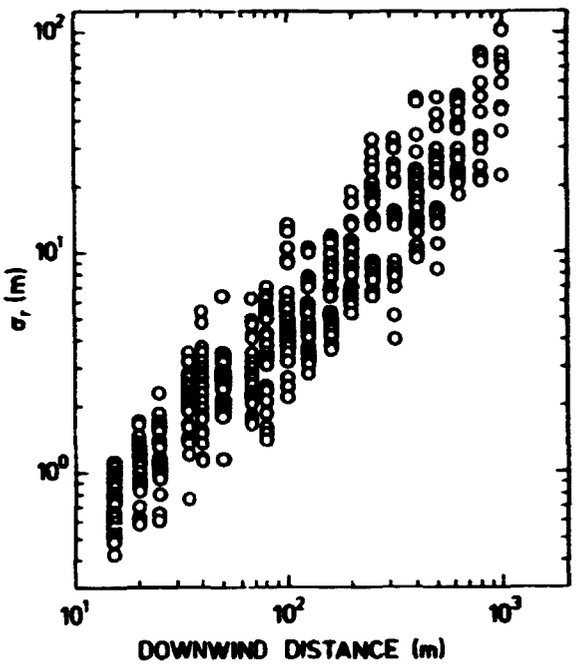

Fig. 47 Instantaneous standard deviation σ_r, as function of downwind distances x.

as the dispersion associated with the "centre-of-mass" fluctuations $(y_{cm}^2)^{\frac{1}{2}}$ of the plume over the 40 minute period. The latter is referred to a coordinate system aligned with the mean wind direction and could also be inferred from the photographs. The total lateral dispersion, $\bar{\Sigma}_y$, calculated as the geometric sum of

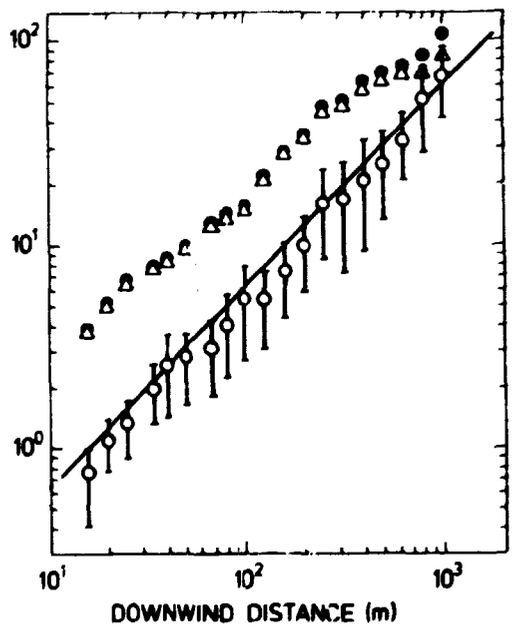

Fig. 48 The ensemble average of the standard deviations in Fig. 47 versus downwind distance x. The crossbars represent the ensemble standard deviation of the experiment. Dispersion associated with the centre-of-mass fluctuations $\left(\overline{(y'^2_{cm})}\right)^{1/2}$ is indicated by Δ, the total dispersion Σ_y by ●. The solid line is drawn from the formula of Smith and Hayes (1961) for the isotopic expansion of a gaussian puff.

the centre-of-mass dispersion and the instantaneous dispersion, is seen to be dominated entirely by the centre-of-mass dispersion over the 40 minute sampling period considered.

Finally, Fig. 48 shows the simulated value of σ_r calculated by the puff model on the basis of Smith and Hay's (1961) formula for isotropic expansion of a gaussian puff $\sigma_p = 0.22\ i \cdot x$. Reasonable agreement between measured and calculated values is observed over the downwind distance considered.

4.5 Lateral dispersion of pollutants in a very stable atmosphere

(L. Kristensen, N.O. Jensen and E.L. Petersen)

When the Richardson number is greater than ~0.2 (stable stratification and low wind speeds), observations have shown that turbulence cannot be maintained. Under such circumstances the turbulence will decay in such a way that the smallest eddies will be dissipated first. As a consequence, the length scale of the turbulence will increase with time. In the final stage of the decay only large horizontal eddies will usually be present. The air motion is then often called "meandering" because of the superficial similarity between the meandering of a river in flat terrain and the instantaneous shape of a plume from a continuous point source. Because of the absence of small eddies, the corresponding turbulent dispersion of a plume of pollutants will be negligible. However, if large horizontal eddies are present the time averaged concentrations at a fixed point can be rather low, even if the plume concentrations are high. This is so because the "bends" of the meandering plume move with the mean wind. If the large horizontal eddies have also disappeared then there is no process which will reduce the time averaged concentrations.

Three years of data, taken along the 123 m mast at Risø, and two years of data, taken along the 70 m mast on the small island of Sprogø in the Great Belt, have been analyzed in order to identify all situations in which the atmosphere was so stable that small-scale turbulence could not exist. The purpose was to see in how many situations meandering was also absent. This analysis showed

that meandering will be present in a strongly stable atmosphere. As can be seen from Fig. 49 the lateral spread, σ_y, given as the root mean square plume width, can easily be a factor of 4 to 6 too low if conventional methods are used.

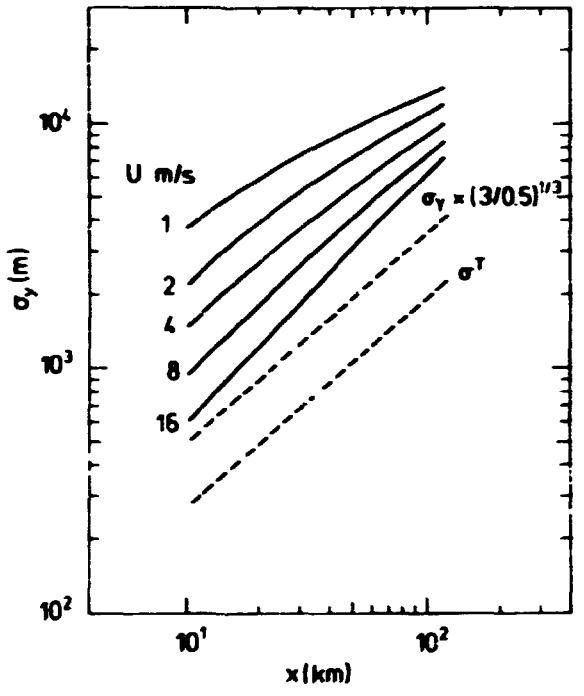

Fig. 49 The parameter σ_y (solid lines) as function of distance x for different values of windspeed U. Averaging time T is equal to three hours. The dashed lines show the values of σ_y given by Turner (1970), uncorrected and corrected for time averaging (Jensen et al. 1977).

4.6 Dilution of a puff denser denser than air

(N.O. Jensen)

After termination of the phase of gravity driven slumping of a heavy gas cloud (Jensen 1981), the height slowly starts to grow again. It was shown that this volume increase cannot be the result of entrainment through the side wall of the cloud but must be due to entrainment through the cloud's top.

As hazardous releases of heavy gases into the atmosphere is most often related to failure of pressurized vessels where the gas is stored in liquified form, the gas is typically quite cold relative to the ground temperature. Thus the initial entrainment is

driven by convective turbulence in the cloud rather than the ambient atmospheric turbulence. The strength of the turbulence in the cloud is controlled by the temperature difference, ΔT. The entrainment, on the other hand, is controlled by the density difference, $\Delta\rho$. The development in both of these differences is governed by the heat transfer at the surface and by the entrainment of atmospheric air. This coupled problem was given some analytical consideration in which some key parameters were identified. It was predicted that

$$\frac{\Delta T}{\Delta \rho} \propto \left(\frac{\Delta \rho}{\rho_o}\right)^{-(1/1+\beta)}$$

where β (~0.2) is an entrainment constant. Hence it is seen that, as entrainment goes on, the density difference vanishes faster than the temperature difference. As a consequence, the entrain-

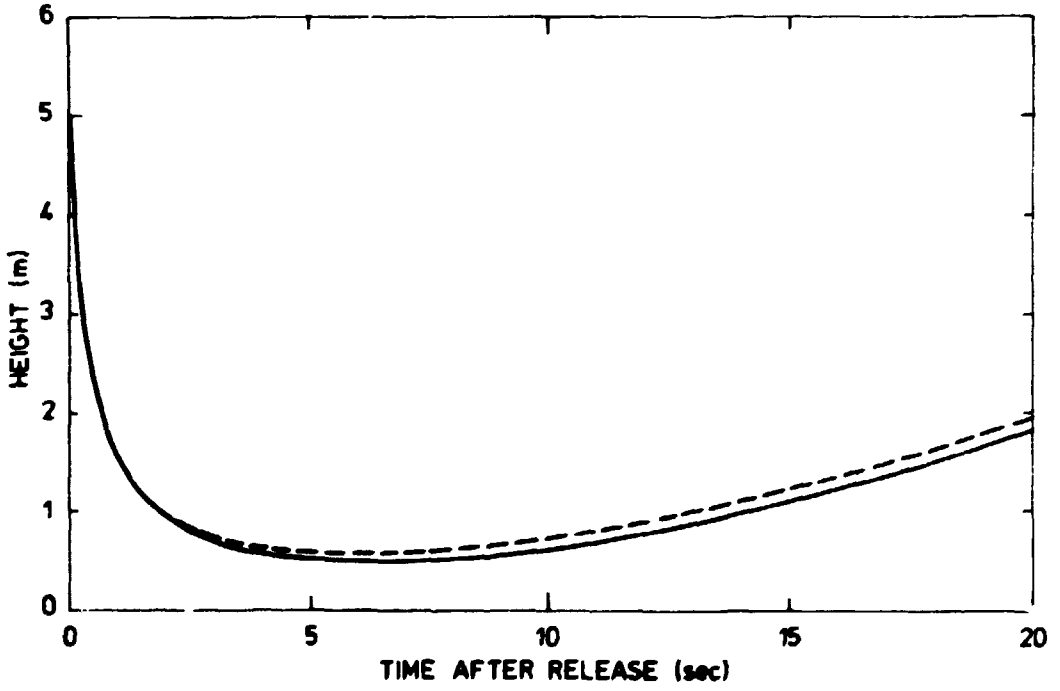

Fig. 50 The course of the height of a cloud of heavy gas, given as a function of time from release. At larger times, turbulent mixing of air will be dominant over the slumping process and the gas cloud's height will begin to grow. The dashed curve shows the accelerated growth resulting when the cloud is colder than the surface.

ment velocity is an increasing function of time in the interval of validity of the above analysis, and again consequently h(t), the height of the cloud, becomes a concave function of time (Jensen 1980).

In agreement with the above, Fig. 50 shows a numerical solution of the involved rate equations for $\Delta\rho$ and ΔT in combination with the gravity slumping - surface heat transfer - turbulence energy - and entrainment equations. The predicted region of accelerated growth is clearly seen.

4.7 Air-sea interaction

(S.E. Larsen, N.E. Busch and O. Mathiassen (Danish Meteorological Institute))

The meteorology section participated in the surface layer part of the JONSWAP 1975 experiment. In the experiment the section co-operated with groups from the University of Hamburg and the Dutch Meteorological Service. The aim of the experiment was to study the structure of the turbulent marine surface boundary layer. For this purpose, the vertical profiles of temperature, velocity and humidity were measured simultaneously with measurements of the turbulent variations of the same signals. The measurements were taken at a mast erected on the sea bed and projecting approximately 10 m above the sea surface.

The meteorology section used wind-vane mounted three-dimensional hot-wire sensors, cold-wire and Lyman-α humidiometers to obtain the structure of turbulence of the three components of the velocity vector, temperature and humidity (Busch and Larsen 1975).

The measurements were performed 5 to 7 m above sea level, dependent upon the tide level. Data were obtained for the wind velocity between 2 and 8 m/s, and for stabilities: $-0.3 < z/L < 0.25$, where z is the measuring height and L the Monin-Obuchov length.

Analysis has been performed of twenty runs, each of 20 minutes duration. For ten of the runs, only integral statistics were obtained, while spectra and cross-spectra were also calculated for the remaining ten runs. In the course of the analysis a number of technical difficulties were encounted: the hot-wires corroded, making pre-calibration useless. This was solved by calibrating the hot-wire signals against the profile velocities run by run (Larsen et al. 1979). Contamination caused the cold-wires to lose frequency response and gave rise to cold-spikes, as reported by several authors, (e.g. Larsen et al. 1980). These phenomena destroyed the high-frequency part of the temperature spectra but seemed to have little influence on the heat-flux estimates. The Lyman-α humidiometer showed an unexpected signal attenuation for frequencies higher than 10 Hz, a phenomenon which has been reported by Schmitt et al. (1979). Finally, flow deformation around the three-dimensional hot-wire probe showed itself to be an appreciable problem, giving rise to 25% over-estimates of the vertical velocity, apart from other differences. Based on a wind-tunnel test it was found, however, that this problem could be solved by a simple linear correction scheme (Rasmussen et al. 1981).

Of the results, only the spectral ones will be commented upon. All spectra conformed exactly to the parametrization and forms which have been established for over land spectra. The only deviation from this simple picture is in relation to the humidity spectrum, which is usually considered to follow the form and scaling of the temperature spectrum. It was found that the combined humidity spectra of several runs increased with decreasing frequency. This corresponds to a situation where the phenomena influencing the humidity variations is of a considerably larger scale than those influencing the temperature and velocity variations.

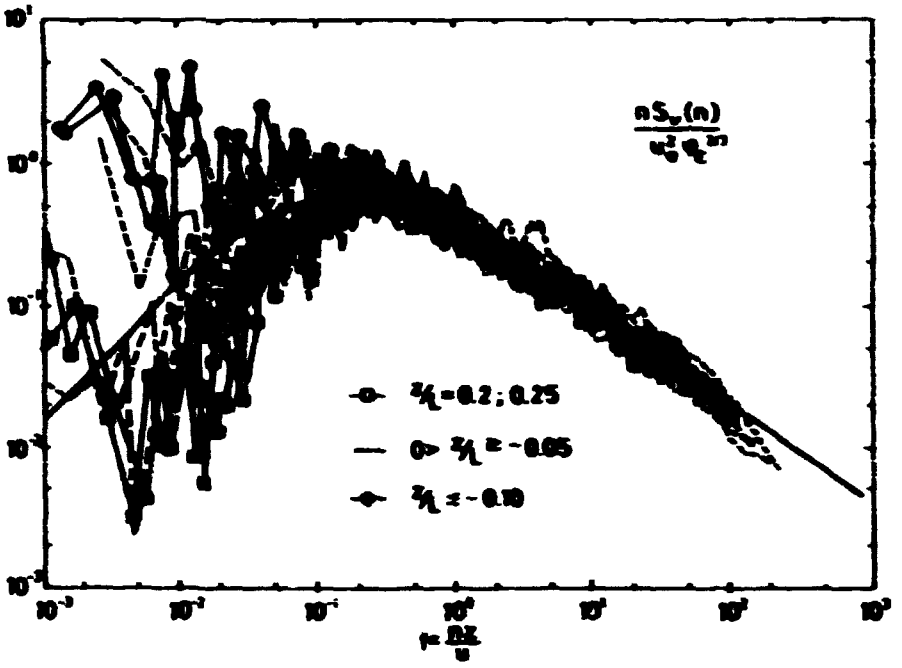

Fig. 51 Spectra of the lateral velocity component, scaled by the friction velocity, u_*, and the dissipation function, ϕ_ε, and plotted versus the dimensionless frequency, f = nz/u, where n is the frequency in Hz, z is the measuring height and u is the mean velocity. The curve is the analytical expression given by Kaimal et al. (1972) for neutral stability.

Owing to the high frequency resolution (100 Hz) and the small spatial scale (~1 mm) of the hot-wire system, it has for the first time been possible to obtain spectra of all three velocity components for wave numbers high enough to show the onset of dissipation. This is illustrated in Fig. 51, which shows the spectra of the lateral velocity for all ten runs. That the high-frequency reduction in intensity reflects the beginning of the dissipation range is further illustrated in Fig. 52, where the ratio between the spectra for the lateral and the longitudinal components is shown and compared with the theoretical prediction.

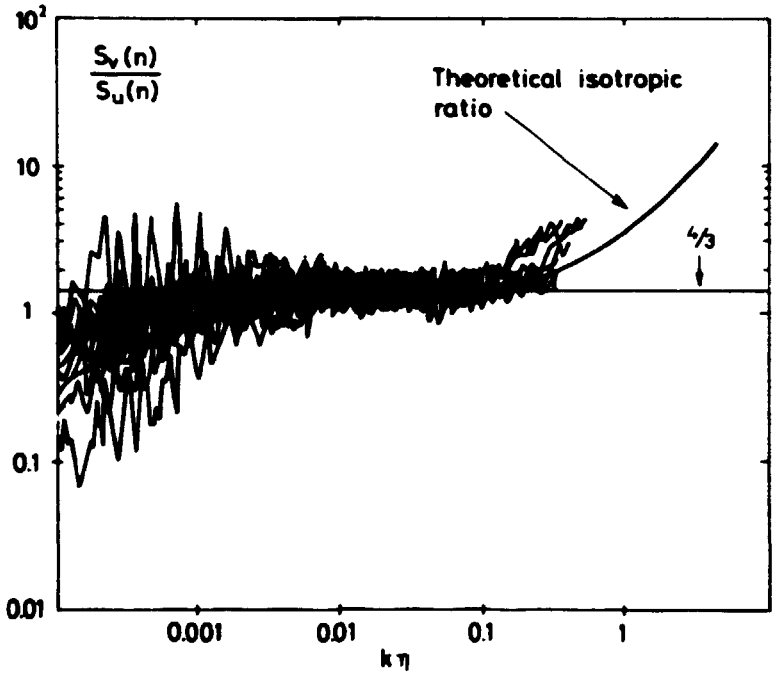

Fig. 52 The ratio between the spectra for the lateral component, v, and the longitudinal component, u, plotted versus kη, where k is the wave number and η is the Kolmogorov scale. The curve corresponds to the theoretical prediction given by Wyngaard (1968).

4.8 Lateral coherence in the atmospheric boundary layer

(L. Kristensen and D.H. Lenschow (National Centre for Atmospheric Research, Boulder, Colorado, U.S.A.))

With the purpose of studying the spatial structure of velocity, temperature and humidity fluctuations in the entire atmospheric boundary layer, a series of airplane measurements were planned in the summer and carried out in the fall of 1979.

In the period from September 10th to 18th, a number of formation flights were performed in the relatively flat area around Boulder with NCAR's two Queen Airs. A single flight could consist of several flight legs, each of which had a typical duration of 10 minutes. For a particular flight leg, the pilots tried to maintain a constant height and a constant relative lateral displacement with respect to each other. This displacement could be anywhere between approximately 30 to 1600 m (1 mile). For displace-

ments up to 300 m it was possible to monitor the relative displacement vector by means of a photographic technique: the starboard airplane had a camera mounted in the rear port window and this took photographs of the port airplane at a constant rate of approximately one per second. From the photographs, the relative displacement vectors were determined by a manual technique.

Constant lateral displacements of 1 mile could be obtained by allowing the two aeroplanes to fly directly over two adjacent highways. Both airplanes were equipped with inertial navigation systems (INS) and the signals from these were recorded, together with the signals from a number of sensors measuring velocity, temperature, etc.. By comparing the relative displacement vectors determined by means of the photographs and the inertial platforms, it turned out that the instrumental trend and bias of the INS-determination could be corrected for, so that it became possible to update the relative displacement vector twenty times per second, the general sampling rate of the sensors.

The spatial structure of the turbulence - elucidated by the spectral coherence (a normalized measure of the cross spectrum) between velocity components, temperatures and humidities, measured perpendicular to the mean wind direction - is usually obtained by means of instruments mounted on an array of masts perpendicular to the mean wind direction. By using two airplanes, a great deal of flexibility is obtained. Height and displacement can easily be changed and, most importantly, it is not necessary to wait until the wind blows perpendicular to an array of masts, since the relevant wind direction is given as the true air velocity, seen from the airplane. The main purpose of the formation flight study is to be able to predict theoretically two-point turbulence statistics from one-point measurements, and theories for this will be tested by means of the data obtained from these flights.

4.9 Change of terrain roughness for long fetches

(S.E. Larsen, K. Hedegaard (Danish Meteorological Institute), N.O. Jensen and I. Troen)

The response of the atmospheric boundary layer to a step change in surface roughness is usually estimated by use a numerical/ analytical models, which are based on surface boundary layer theory. It has been pointed out (Jensen 1978) that, for large fetches, the predictions of these models do not match the predictions for the corresponding homogeneous boundary layer. This lack of matching gives rise to problems in connection with wind-technological applications (Petersen et al. 1981), and Action on Building Structures 2 (Wind load, 2nd edition October 1977. Dansk Standard DS 410.2, translated edition November 1978).

We will describe a simple change of terrain roughness model, which for neutral stability covers the behaviour of the flow for large fetches. It is based on a simple surface layer theoretical model which is described in Panofsky (1973) and Jensen (1978).

The height of the interface between the old and new boundary layer, h, grows as

$$\frac{dh}{dt} = \bar{u}(h)\,\frac{dh}{dx} = A\,\sigma_w, \tag{1}$$

where x is the fetch, $\bar{u}$ the mean velocity, and the entrainment velocity is considered proportional to the standard deviation of the vertical velocity. A is a constant of O(1).

The variables $\bar{u}$ and σ_w are presumed to vary with height, z, as in an equilibrium boundary layer.

$$\bar{u}(z) = (u_{*_o}/\kappa)(\ln(z/z_o) - 2z/H) \tag{2}$$

$$\sigma_w/u_{*_o} = (1 - z/H)^4 \tag{3}$$

Equations (2) and (3) can be deduced from Panofsky (1973) and Wyngaard et al. (1974), respectively; u_{*_o} is the surface value of the friction velocity and $H = u_{*_o}/f$, is the scaling height

of the planetary boundary layer, with f being the Coriolis parameter. The roughness length is z_o, and κ the von Karman constant.

By means of equations (2) and (3), equation (1) can be interpreted to read

$$C\frac{x}{z_o} - 1 = \frac{h/z_o}{1-\frac{h}{H}}\left(\left(\ell n\frac{h}{z_o} - 1\right) - \left[1 + \frac{(1-\frac{h}{H})}{h/H}\ \ell n(1 - \frac{h}{H})\right]\right), \qquad (4)$$

where C is a constant of O(1). The term in the square bracket can be replaced by h/H with a maximum deviation of 0.2 at $h/H \simeq 0.7$.

The corresponding surface layer model (Panofsky 1973) is obtained by letting $H \to \infty$. Within the surface layer this model is known to work well, provided one uses the z_o-value pertaining to the rougher surface (Jensen 1978). Therefore, the same rule should be applied to equation (4). For a roughness change, smooth-to-rough, the same principles can be used for the choice of H. For the change rough-to-smooth, we first notice that it will take a fetch of $x \simeq \bar{u}/f \simeq 100$ km for the planetary boundary layer eddies to die. This indicates that also here H_{rough} should be used in equation (4). However, another constraint is that $h(x \to \infty) = H_{smooth} < H_{rough}$. As equation (4) is too primitive to give information about h's final approach to H_{smooth}, the most reasonable choice for the rough-to-smooth transition is to let $H = H_{rough}$ and to stop the development of h as soon as it reaches H_{smooth}. The change in surface stress can be found by matching the two velocity profiles in h(x). We denote upstream parameters by 1 and downstream parameters by 2. We first consider the smooth-to-rough transition and obtain for $h < H_1 < H_2$

$$\frac{u_{*o2}}{u_{*o1}} = 1 - \frac{m}{\ell n(h/z_{o2})}, \qquad (5)$$

with $m = \ell n(z_{o1}/z_{o2})$. For $H_1 < h < H_2$ we find that

$$\frac{u_{*o2}}{U_g} = \kappa\left[\ell n\ \frac{h}{z_{o2}} - 2\ \frac{h}{H_2}\right]^{-1}, \qquad (6)$$

where U_g is the u-component of the geostrophic wind, and where u_{*o2} is seen to approach its geostrophic equilibrium as $h \to H_2$ for $x \to \infty$. For the rough-to-smooth case, u_{*o2} is forced to its equilibrium value as soon as h reaches H_2, in accordance with the arguments above.

Finally, the ratio between two velocities, measured at the same height z in the two boundary layers, can be written

$$\frac{\bar{u}_2(z)}{\bar{u}_1(z)} = \frac{u_{*o2}}{u_{*o1}} \frac{\ln(z/z_{o2}) - 2z/H_2}{\ln(z/z_{o1}) - 2z/H_1} \qquad (7)$$

The available data on flow response to roughness change for large fetches is quite limited. Based on climatological measurements at two locations 10 km apart in Jutland, Hedegaard and Larsen (1981) have compiled data on the velocity ratio in equation (7) for fetches up to 10 km. These data, together with the predictions of equations (4,5,7), are shown in Fig. 53. As test material

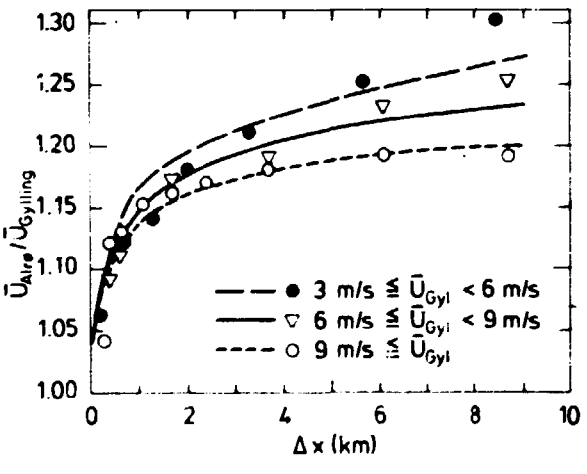

Fig. 53 The ratio between the velocity measured over water and over land as a function of water fetch, Δx (Hedegaard and Larsen 1981). The data are obtained at two measuring stations in Jutland and represent the average during 18 months. $u_{Alrø}$ refers to measurements on an island, Alrø, and is interpreted as the velocity over water. $u_{Gylling}$ refers to measurements on a peninsula, Gylling Næs, and is interpreted as land data.

for equation (7) the data are not overwhelmingly good. The datapoints represent average values of the velocity ratios for a sampling period of 1½ years, and include all stabilities. The data describe the rough-to-smooth transition, and the controlling parameters for each velocity interval have been estimated by

deriving the geostrophic wind and H_1 from the land data and the z_{o1}-value estimated for the land, by use of the drag law for neutral stability given by Jensen (1978). Based on the same drag law and Charnock's formula, the z_{o2} and H_2 values for water have subsequently been derived. With the derived parametric values (Hedegaard and Larsen 1981), the model results are compared to the data in Fig. 53, and the model is seen to give a fairly good description of the data, in spite of the simplicity of the model and the complexity of the different situations which have contributed to the average data in Fig. 53.

4.10 The application of gauge function analysis to the neutral atmospheric boundary layer

(W.K. George and N.O. Jensen)

Asymptotic analysis has long played an important role in the development of similarity laws in fluid mechanics. In turbulence problems, even though the techniques used have been primarily heuristic, the results have been quite successful. Examples include the deduction of the $k^{-5/3}$ scaling law for the energy spectrum and the logarithmic friction law for the zero pressure gradient boundary layer.

Asymptotic techniques have also been applied to the atmospheric boundary layer with some success. However, unlike the examples cited above, the choices for the scaling parameters are not unique, and alternative models can be formulated which lead, for example, to power law velocity and friction laws instead of the usual logarithmic ones. Unfortunately, the experimental data are not sufficiently accurate to distinguish between these different models. Moreover, in view of the non-uniqueness of asymptotic solutions, there exists the possibility that the solutions are complementary.

In an effort to sort out these apparent conflicts and place the similarity scaling for the neutral planetary boundary layer on more objective foundations, a gauge function analysis (Nayfeh

1973) is in progress. The velocity, for example, is written in *outer variables as*

$$u = u_o[\Delta_o(\varepsilon)F_o(\tilde{z}) + \Delta_1(\varepsilon)F_1(\tilde{z}) + ...]$$

and in inner variables as

$$u = u_s[\delta_o(\varepsilon)f_o(z^+) + \delta_1(\varepsilon)f_1(z^+) + ...]$$

where u_o and u_s are scaling variables, and $\tilde{z} = z/h$, $z^+ = z/z_o$ and $\varepsilon = z_o/h$. z_o is the surface roughness and h is an undetermined boundary layer height. The gauge functions, $\Delta_o(\varepsilon),...$ and $\delta_o(\varepsilon),...,$ are determined by the equations of motion and the matching of inner and outer solutions subject to the boundary conditions and to the constraint that

$$\frac{\Delta_{n+i}}{\Delta_n} \to 0 \text{ and } \frac{\delta_{n+1}}{\delta_n} \to 0 \text{ as } \varepsilon \to 0$$

This matching is accomplished by matching the inner limit of the outer solution to the outer limit of the inner solution. The result of such an analysis is determination of the scaling laws and matched layer profiles which depend only on the manner in which the physics has been allowed to control the dynamics of the problem.

4.11 Analysis of data from the Gedser wind turbine, 1977-1979

(S. Frandsen, C.J. Christensen and P. Lundsager)

The measurements on the Gedser wind turbine were terminated in November 1979. The data were processed and the results reported this current year (Lundsager et al. 1980). The analysis included power production characteristics based on ten minute averages, coherence between measurements of wind and electric power output based on high frequency scanning, drive train oscillations and structural responses of the rotor. To conclude the analysis, a comparison of the Gedser wind turbine with modern Danish, Swedish and American experimental wind turbines was carried out. The four

turbines are shown to the same scale in Fig. 54 to impart the relative scale of the various installations. The two Danish designs are three bladed with upwind rotors, while the Swedish and American turbines are two bladed with their rotors situated downwind of the tower.

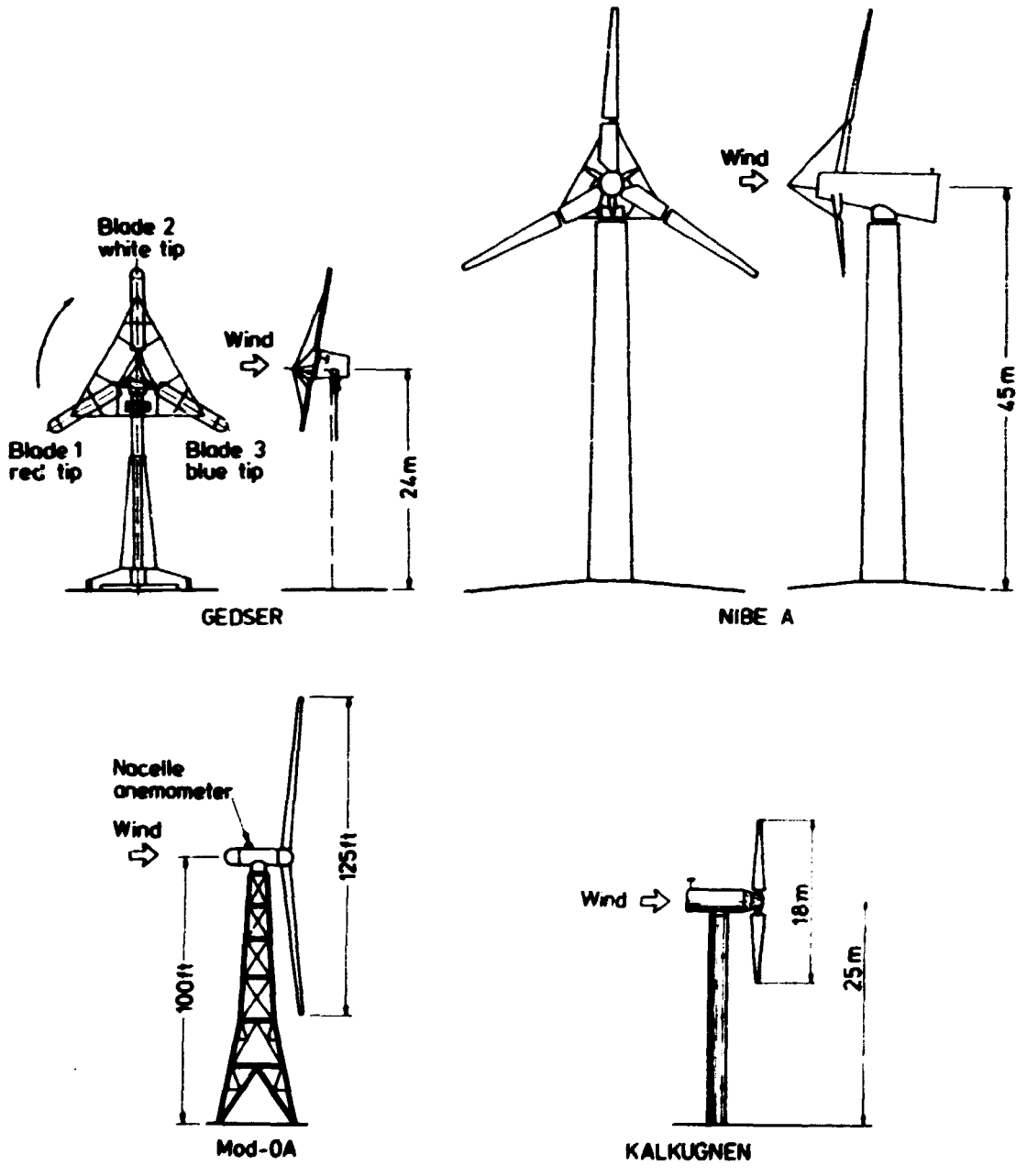

Fig. 54 The Gedser wind turbine and three modern experimental wind turbines. All figures are in scale 1:850.

All four designs are simple, horizontal axis propeller turbines, which can be shown to have a theoretical maximum efficiency of 59%. In practise the efficiency is somewhat lower due to the drag on the airfoils, the limited number of blades, finite rotational speed of the rotor, power losses both in the gearbox and electrical generator, etc.. Figure 55 shows the overall ef-

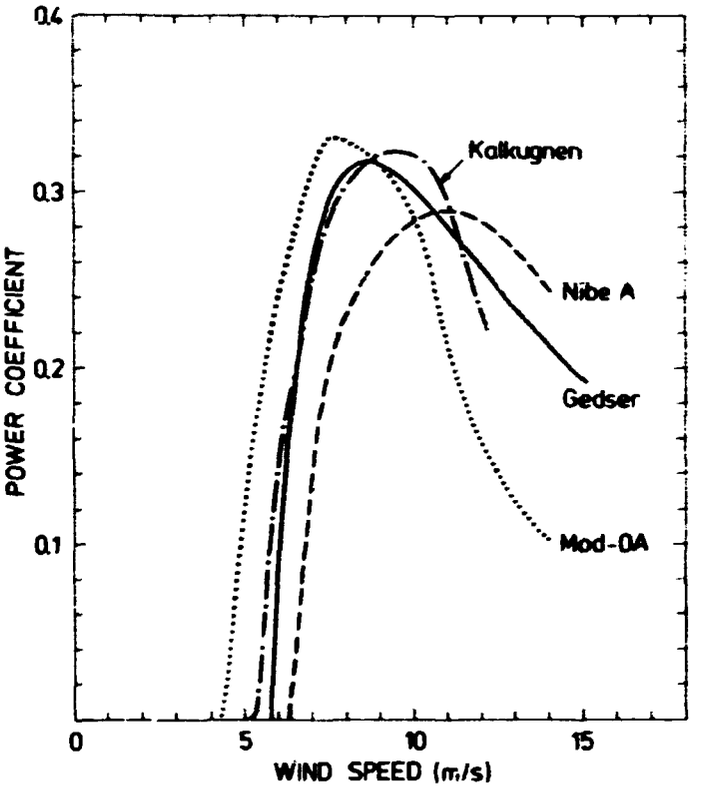

Fig. 55 Power coefficient curves.

ficiencies for the four turbines considered as a function of windspeed. The maximum efficiency is found to be a good measure of the "level of development", and it is seen that the American Mod-OA has the largest maximum efficiency 0.33, whilst Nibe A has the smallest at 0.29. However, since the uncertainties of the estimated efficiencies are probably of the same order as the differences, the turbines must be considered equal in productive capability, although the operational ranges are unequal.

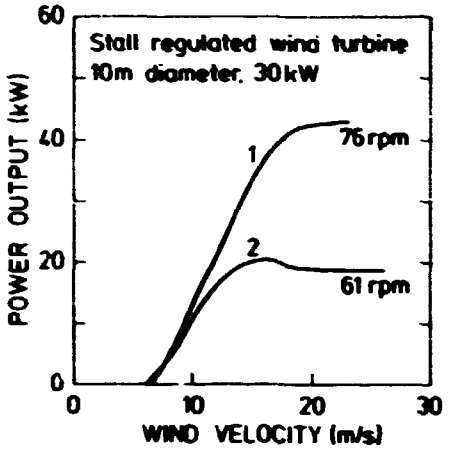

Fig. 56 Power curves, measured for one stall regulated wind turbine at two different rotor speeds.

4.12 Power regulation of wind turbines by aerodynamic stall

(T. Friis Pedersen)

A typical feature of small Danish wind turbines is the regulation of the power by aerodynamic stalling of the blades. On such turbines, the prediction of the maximum power and hence the largest loads on the entire turbine is dependent on the ability to predict the stall properties of the blades. These properties depend on a number of parameters of the blade design, of which the most important seems to be the aerodynamic properties of the profile used.

A reliable prediction of the stall properties of a given blade design has proved difficult to obtain in practice. Therefore, a series of measurements are being made on two of the wind turbines erected at the test plant. The measurements comprise the variation of parameters such as speed of revolution and blade pitch angle in order to clarify their influence. Figure 56 shows the influence of rotor speed on the power output of a 30 kW machine, which is heavily overloaded in high winds at one rotor speed, whilst it shows satisfactory behaviour at another rotor speed, even at very high wind speeds.

4.13 Aerodynamic brake for small wind turbines

(J. Krogsgaard)

System-evaluated wind turbines are required to have aerodynamic braking as a part of the safety system. A wing brake is under development, intended for use in new designs as well as earlier designs without wing brakes.

Since even small aerodynamic drag has a large effect on the annual power production of a wind turbine operating at constant rotor speed, a wing brake is being developed that is built into the blade, flush with the aerofoil surface. The design of common

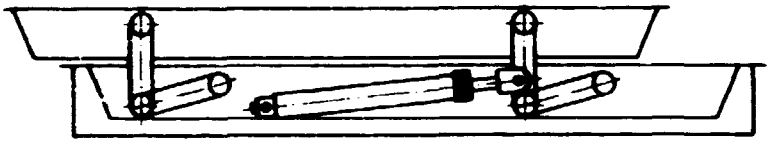

Fig. 57 The aerodynamic brake for small wind turbines (glider plane air-brake design).

glider plane air-brakes is adopted (Fig. 57), and the brake is activated by centrigugal forces in order to prevent overspeeding of the rotor. The acceleration at which the brake is activated may be adjusted by means of a spring assemby, and the brake may therefore be applied to a variety of wind turbines.

4.14 Computer models for a stationary description of the induction machine applied in wind turbines

(P. Hjuler Jensen and P. Rasmussen)

Usually induction machines are modelled with respect to their behaviour as motors. Because the behaviour of induction machines, when used in wind turbines, is somewhat different, new models need to be develcped for the application of induction machines as generators in wind turbines. The behaviour in the two applications is shown in Fig. 58, which shows the terminal voltage as

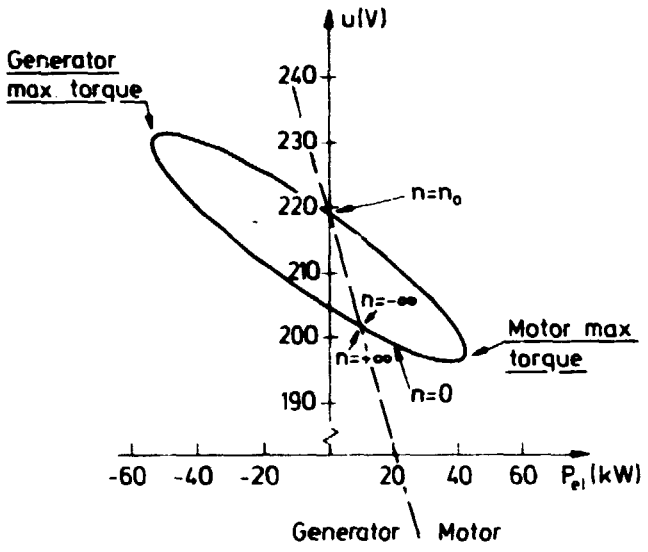

Fig. 58 Diagram showing the terminal voltage versus electric power for an induction machine. The diagram covers all operational conditions with the shaft rpm (n) parameter.

a function of the electric power as predicted by one of the models described below.

For one of the models, the input data is the mechanical power delivered by the rotor and, based on this data and that of the generator, a number of mechanical and electrical quantities such as electric power, rotor speed, etc. are calculated. Another model computes the electric and mechanical parameters based on a prescribed percentage of slip. This model includes an option for prescribing passive external components. A third model deduces approximate values of electric properties such as impedance for an induction machine used as a generator from the data for the machine when applied as a motor.

4.15 Coupling of wind turbine generators to the electric grid

(P. Rasmussen)

During the coupling of a wind turbine induction generator to the electric grid, strong transients in the mechanical and electrical parameters arise to the extent that they may be described as shocks. This is a source of heavy loads on the structure, and in several cases failures may be explained by this phenomenon. Figure 59 shows an example of a recorded pattern during coupling, measured on a machine erected at the test plant.

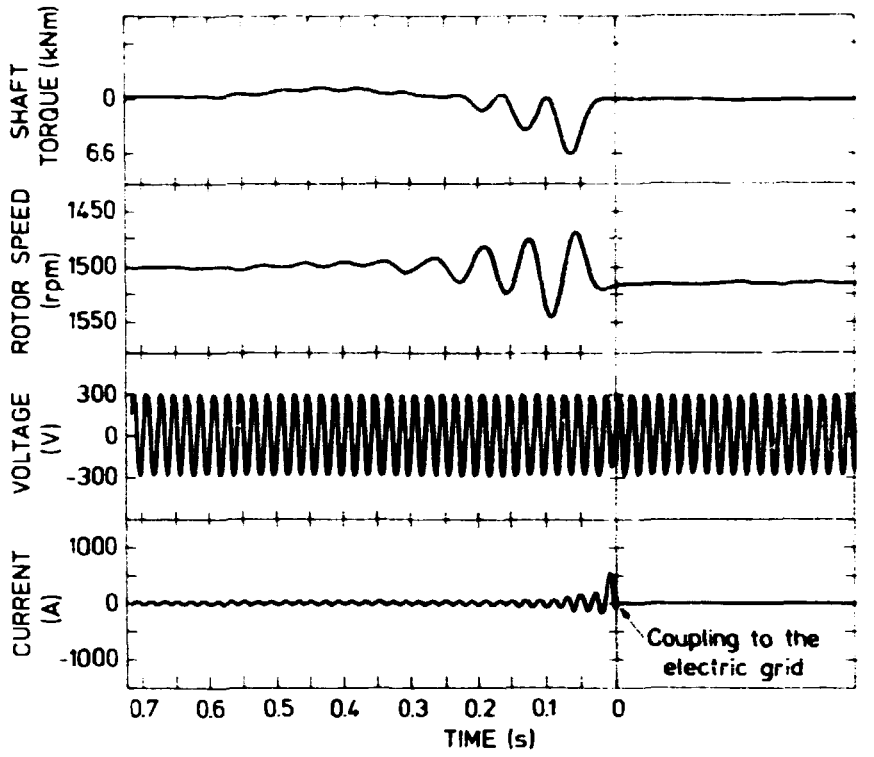

Fig. 59 Transients recorded during coupling to the grid of a 10 m diameter, 30 kW wind turbine.

A series of measurements of the effect of two-stage couplings are being made, together with investigations of the efficiency of a thyristor-controlled coupling developed at the Technical University of Denmark.

4.16 Nibe wind turbine measurements

(C.J. Christensen, O. Christensen, S. Frandsen, S.O. Hansen and P. Lundsager)

Under contract to the Danish wind power programme, a fast six-channel strip chart recorder system that can record any of forty sensors on each of the two Nibe turbines was supplied. We ran this system to measure critical parameters such as strains on the wings during the running-in, and safety-testing of the turbines. As the computerized data collecting system described previously (Hansen et al. 1979) was finished, the recorder was also

used for an extensive check of the computer system. As of now, the computer system is in operation and the experiments are being transferred to this much more powerful system. A number of observations (i.e. flapwise stall-connected oscillations of large amplitudes at high winds on the turbine A-wings or a too heavy-handed braking procedure on the B-turbine) were made and described in unpulished, internal notes to the contractor. A review of these measurements is being written in cooperation with the contractor.

4.17 Mean power output and choice of wind turbine parameters

(S. Frandsen, I. Troen and E.L. Petersen)

For many applications it is useful to have a simple method for the estimating of the mean power output of a wind turbine. Knowing the frequency distribution of the windspeed, the long-term average power output can be calculated as

$$P_M = \int_0^\infty f(V) \cdot p(V) dV, \qquad (1)$$

where p(V) is the power curve (i.e. the power output from a wind turbine as a function of windspeed), and f(V) is the Weibull distribution (see 4.18)

$$f(V) = \left(\frac{C}{A}\right)\left(\frac{V}{A}\right)^{C-1} \times \exp\left(-\left(\frac{V}{A}\right)^{C}\right), \qquad (2)$$

where C and A are parameters.

In general, the integral in equation (1) does not have an analytical solution and P_M must be determined by means of numerical integration. However, for many purposes the following simplified method for the calculating of the potential power output from a wind turbine could be valuable: assume that the power curve has the simple shape indicated in Fig. 60, where the power output is linearly dependent on the windspeed in the speed range with highest energy density,

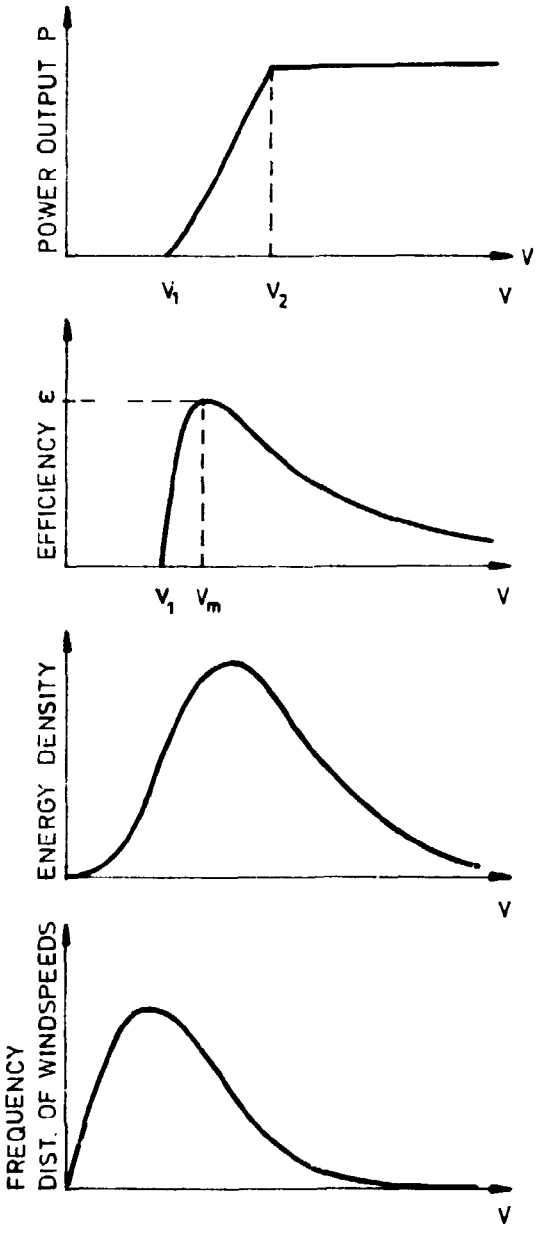

Fig. 60 The two upper figures show, respectively, the idealized power curve and the efficiency curve, while the lower figures show the distribution of energy at different wind speeds and the frequency distribution of wind speeds. It is obviously important that the efficiency is high at the wind speeds with the largest energy.

$$P(V) = k(V-V_1), \tag{3}$$

where k is a constant and V_1 is the starting windspeed. The available energy flux within the rotor area is $1/2\ \rho V^3 \cdot A_R$, ρ is the air density and A_R the rotor area. The efficiency is then defined as

$$\varepsilon(V) = P(V)/(1/2\ \rho V^3 \cdot A_R). \tag{4}$$

Differentiating equation (4) with respect to V yields that the maximum efficiency ε_m will be obtained at the windspeed

$$V = V_m = 3/2\ V_1. \tag{5}$$

On the other hand, if it is assumed that the maximum efficiency $\varepsilon_m = \varepsilon(V_m)$ is known, then the slope k of the power curve can be found from equation (4) and (5) to be

$$k = 3/2\ \rho\varepsilon_m A_R V_m^2. \tag{6}$$

The expression for the power curve in equation (3) can now be rewritten as

$$P(V) = 3/2\ \rho\varepsilon_m A_R V_m^2 (V - 2/3\ V_m) \text{ for } V_1 \leq V \leq V_2 \tag{3a}$$

With these simplifications the integration of equation (1) can be performed, resulting in an expression for the mean power output

$$P_m = 1/2\ \rho\varepsilon_m A_R \cdot A^3 [3(\frac{V_m}{A})^2 \{G_C(\frac{V_2}{A}) - G_C(2/3\ \frac{V_m}{A})\}], \tag{7}$$

where V_2 is the windspeed above which the power output becomes constant and $G_C(\alpha) = 1/C\ \gamma(1/C, \alpha^C)$, γ being the incomplete gamma function. If we assume a linear power curve, it can be shown that the optimal choice of V_m is given by

$$\frac{V_m}{A} = ((\frac{C+2}{C})^{1/C} - 0.15). \tag{8}$$

The assumption of linear power seems to be an excellent approximation when dealing with horizontal axis, stall-regulated propeller turbines, which make up the greater part of wind turbines in Denmark. If V_m is chosen in accordance with equation (8), equation (7) provides a good estimate of the mean power output. Deviations of V_m from its optimal value enlarge the error. To calculate P_m, the actual windspeed distribution and the wind turbine characteristics must be known.

The means to derive the windspeed distribution at the specific site and height is described in "Windatlas for Denmark" (Petersen et al. 1981); values of the parameters A and C result from the calculation. From the wind turbine only V_m, ε_m and A_R have to be known, since P_M is not too sensitive to V_2. While V_m for the optimal turbine is given by equation (8), ε_m must be estimated in each case.

4.18 Wind climatological investigation for wind power assessment

(E.L. Petersen, I. Troen, S. Frandsen and K. Hedegaard (Meteorological Institute))

The basis of the method which was used in the wind climatological investigation for wind power assessment is the geostrophic resistance law. This law expresses the frictional force at the earth's surface as a function of the geostrophic wind, which is treated as an external driving force (Tennekes and Lumley 1972). The method requires a long series of surface pressure observations from a reasonably dense network, and was applied in Denmark, using thirteen years of data from 55 synoptic stations. A

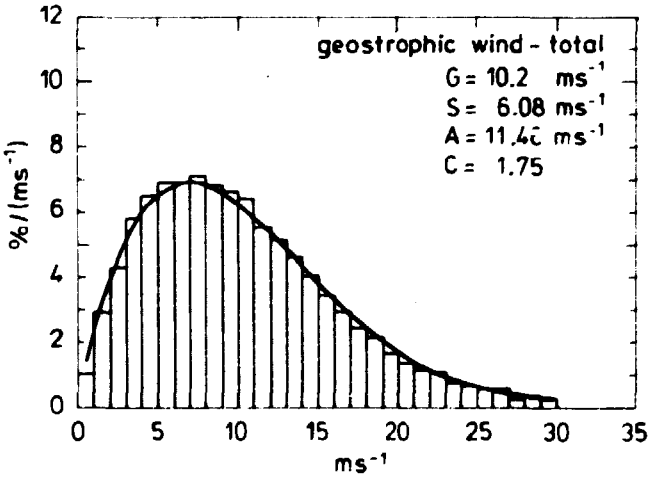

Fig. 61 The distribution of the geostrophic wind obtained from the synoptic pressure analysis (histogram). The parameters listed are the mean, standard deviation, scale and shape parameters of the fitted Weibull distribution (unbroken line).

third order polynomial surface was fitted to the pressure values using the method of least squares; the magnitude and direction of the geostrophic wind was then determined from the gradient utilization of log-linear wind profiles (Businger 1973), the frequency distribution of the windspeed was computed as function of height up to 200 m for four typical types of terrain and with the eight 45° wind direction sectors centered around N, NE, etc.. The Weibull distribution was found to give excellent fit to the distribution of the geostrophic wind (Fig. 61) and to the calculated windspeed distributions. The result of the analysis is a set of graphs giving the Weibull parameters for the windspeed as function of type of terrain, wind direction sector and height (Petersen et al. 1981).

The main purpose has been to provide a method well-suited for wind power assessment. Simple computational procedures have been devised which make it possible to estimate the wind distribution over homogeneous terrain, and in the presence of topographical and shelter effects (Petersen et al. 1981).

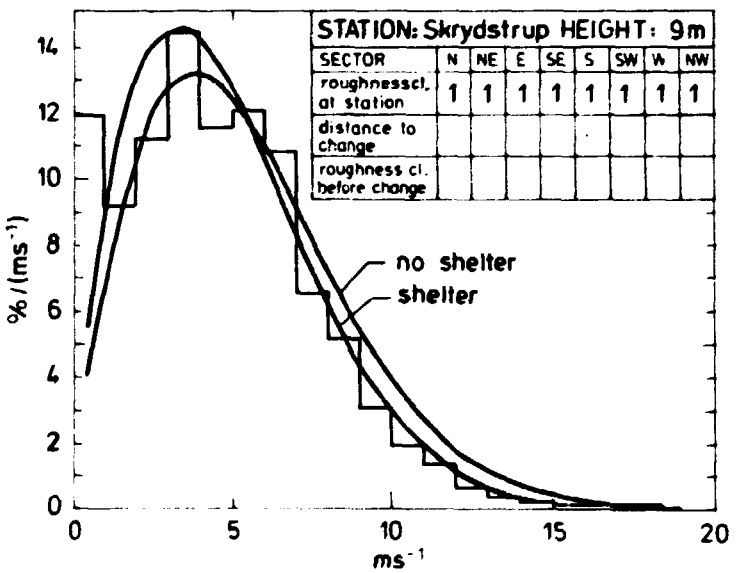

Fig. 62 The observed distribution of windspeed at the airport Skrydstrup (histogram) and the computed distribution ("shelter"). Also shown is the result should the shelter correction not be included ("no shelter"). From Windatlas for Denmark (Petersen et al., 1980, see section 4.18).

4.19 Radiation errors on temperature measurements

(S.E. Larsen and L. Kristensen)

Climatic measurements for environmental projects usually include measurements of the vertical temperature gradient along a mast. Because the measuring stations often have to be battery powered, forced ventilation radiation shields are not mounted, for power-saving reasons. When unventilated shields are used, it is well-known that temperature measurements can be in error several degress (^{o}C) due to radiational heating or cooling of the shield.

Most of the climatic stations established by the meteorology section also include in their programme temperature measurements in a standard Stevenson screen. These measurements are performed at the same height as the lowest level temperature measurement on the mast.

A comparison between the temperatures in the Stevenson screen and at the lowest level of the mast reveals that the Stevenson screen is a much more efficient radiation shield; indeed, the comparison indicated that although the temperature measured in the Stevenson screen is not of course the true air temperature, it is so much closer to this than the temperature measured within the radiation shield that data improves drastically when all shield temperatures are corrected by means of the Stevenson screen measurements.

This idea has been used to correct the mast temperatures as follows: the heat balance for a temperature shield can be written

$$A_1 R = A_2 h \Delta T, \tag{1}$$

where R is the incoming radiation, h is the heat transfer coefficient for the shield, ΔT is the temperature of the shield minus that of the air. A_1 is the exposed area combined with the shield's absorbtivity, while A_2 is the total area of the shield; h is a function of the air velocity, which is usually written

$$h(u) = a(1 + (u/u_o)^b), \tag{2}$$

where a is a weak function of the temperature. Equations (1) and (2) combine to

$$\Delta T = T_{Sh} - T_{St} = A_1 R/[A_2 a(1 + (u/u_o)^b)], \qquad (3)$$

where the indices St and Sh stand for Stevenson's screen and shield, respectively. The velocity dependency of equation (3) has been extracted from several years of data from Greenland and Denmark. For the type of shield used by the meteorology section, $u_o \simeq 3$ m/s and $b \simeq 2$. These values have been obtained through studies of ΔT versus u for different times of the day, different seasons and different locations. Here we have avoided an influence on the estimates of u_o and b by correlations between $A_1 R/A_2 a$ and u.

With u_o and b in equation (3) established, the temperature gradient can, at each instant, be corrected for radiation error because the incoming radiation is the same at the two levels. Let $T(z_1)$ be the temperature at the upper level of the mast and $T(z_2)$ the temperature at the level of the Stevenson screen. By use of equation (3) we now obtain

$$T_m(z_2)-T_m(z_1) =$$

$$T_t(z_2)-T_t(z_1) - (T(z_1)-T_{St})\frac{(u_2/u_o)^b - (u_1/u_o)^b}{1 + (u_2/u_1)^b}, \qquad (4)$$

where m and t refer to measured and true values, respectively, and $u_2 = u(z_2)$ and $u_1 = u(z_1)$. It is seen that the simultaneously measured temperature difference $(T(z_1)-T_{St})$ yields the necessary information about the unknown incoming radiation.

The radiation errors as described in equation (4) have been found to influence the overall temperature gradient climatology very little. However, some situations exist where the errors might be appreciable, and from equation (4) it is seen that such situations might typically be, for example, stable nighttime conditions with strong radiational cooling and light to medium

windspeed, or daytime conditions with strong radiational heating and medium windspeed.

4.20 Forecasting road surface frost

(N.O. Jensen)

The nocturnal trend of the road surface temperature results mainly from four different factors: infrared radiational exchange with water in the atmosphere, evaporation and condensation of water on the surface, turbulence heat transport in the atmosphere, and heat conduction from lower layers of the road.

The influence of the phase transition of water has not been considered in the present investigation, because a typical situation with strong cooling is also dry (clear sky). Order of magnitude estimates of the remaining terms showed that the heat conduction term would typically be one order of magnitude less than the remaining terms A simplified heat budget could thus be written as

$$\frac{\Delta T}{\Delta t} = [R_n + c_H(T-T_o)u]/[\rho c d] \qquad (1)$$

where ΔT is the temperature change of the road surface over time Δt, R_n is the net radiation, T_o is the surface temperature, T is the air temperature measured at the same height, z, as the windspeed u, and c_H is the heat transfer coefficient corresponding to this height. The density and heat capacity of the road is denoted by ρ and c, respectively, and d is the thickness of that upper layer of the road that effectively takes part in the heat exchange process. This parameter, as well as c_H, has to be determined from a series of measurements from the particular site in question, although approximate values can be guessed from theory. Thus, c_H is

$$c_H = \rho_a c_{pa} \left(\frac{0.4}{\ln z/z_o}\right)^2, \qquad (2)$$

where ρ_a and c_{pa} are density and heat capacity of the air, respectively, z is height above ground, and z_o is the aerodynamic roughness of the surface (~0.1 cm). The thickness d is approximately

$$d = \left(\frac{\lambda\tau}{\rho c}\right)^{1/2} , \qquad (3)$$

where λ is the heat conductivity of the road and τ is a characteristic time scale for the surface temperature variation (24 hours).

This slab model was tested experimentally during the spring of 1980, where a little more than one month of data was gathered. A characteristic feature in the data is the relatively constant net loss by radiation during the night. Figure 63 shows an example corresponding to clear skies.

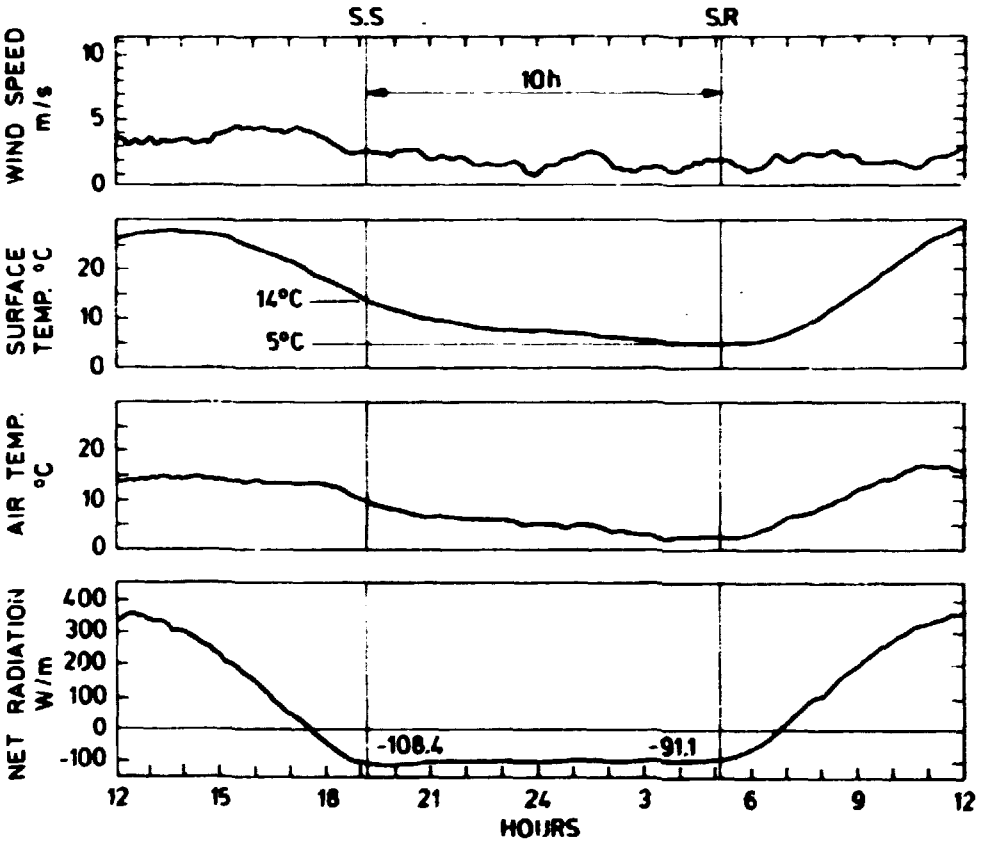

Fig. 63 Typical development of the road surface temperature during a diurnal period. Also shown are the corresponding time series of windspeed, air temperature and net radiation.

The conclusions drawn from the data analyses are first of all that the temperature gradient in the upper part of the road is so large that the small depth in which the thermometer for measuring T_o is necessarily placed causes significant (~1 ^oC) deviations from the "true" surface temperatures; and secondly that the two terms in the heat budget (equation (1)) always come out as a small difference so that the small heat conduction term becomes significant after all.

After empirical corrections for the above, further analyses of the data show that the slab model is a usable approximation and that the fitting constants d and c_H take on values in agreement with expectation (equations (2) and (3)).

4.21 References to section 4

BOX, G.E.P. and JENKINS, G.M. (1970). Time series analysis, forecasting and control. Holden-Day, San Francisco, 572 pp.

BUSCH, N.E. and LARSEN, S.E. (1975). In: Physics Department, Annual Progress Report, Risø-R-334, 68-70.

BUSINGER, J.A. (1973). In: Workshop on Micrometeorology. Edited by P.A. Haugen. American Meteorological Society, Boston, Massachusetts, 67-100.

DURBIN, P.A. (1980). J. Fluid Mech. 100, 279-302.

GIFFORD, F.A. (1980). Atmos. Environ. 14, 1119-1121.

GRYNING, S.E. and LYCK, E. (1980). Danish National Agency of Environmental Protection, Air Pollution Laboratory, Risø, MST LUFT A40, 32 pp.

HANNA, S.R. (1979). J. Appl. Meteorol. 18, 518-525.

HANSEN, S.O., CHRISTENSEN, O., CHRISTENSEN, C.J., LUNDSAGER, P., FRANDSEN, S. and KRISTENSEN, L. (1979). In: Physics Department, Annual Progress Report, Risø-R-414, 112-113.

HEDEGAARD, K. and LARSEN, S.E. (1981). Wind speed and direction changes due to terrain effects as revealed by climatological data from two sites in Jutland. Risø-R-434. To be published.

JENSEN, N.O. (1978). Q. J. R. Meteorol. Soc. 104, 351-356.

JENSEN, N.O. (1981). Entrainment through the top of a heavy gas cloud. 11th International Technical Meeting on Air Pollution. Modelling and its application. NATO/CCMS Air Pollution Pilot Study, Amsterdam, The Netherlands, October 22-26. To be published.

JENSEN, N.O. (1981). On the calculus of heavy gas dispersion. Risø-R-439. To be published.

JENSEN, P.H., PETERSEN, E.L., THYKIER-NIELSEN, S. and VINTHER, F.H. (1977). Risø-R-356, 120 pp.

KAIMAL, J.C., WYNGAARD, J.C., IZUMI, Y. and COTÉ, O.R. (1972). Q. J. R. Meteorol. Soc. 98, 563-589.

LARSEN, S.E., HØJSTRUP, J. and GIBSON, C.H. (1980). In: Air-Sea Interaction. Edited by F. Dobson, L. Hasse and R. Davis. Plenum Press, New York, 269-292.

LARSEN, S.E., MATHIASSEN, O. and BUSCH, N.E. (1979). In: Proceedings of the Dynamic Flow Conference, Marseille, France, September 1978. DISA, Skovlunde, Denmark, 591-598.

LUNDSAGER, P., FRANDSEN, S. and CHRISTENSEN, C.J. (1980). Risø-M-2242, 136 pp.

MIKKELSEN, T. (1979). Simulation of obscuration smoke diffusion. Work done under contract to the Danish Defence Research Establishment/Risø, 73 pp.

MIKKELSEN, T., LARSEN, S.E. and TROEN, I. (1980). In: Proceedings of seminar on radioactive releases and their dispersion in the atmosphere following a hypothetical reactor accident, Risø, April 22-25, 1980, 595-614.

NAYFEH, A.H. (1973). Perturbation methods. John Wiley and Sons, New York, 437 pp.

PANOFSKY, H.A. (1973). In: Workshop on Micrometeorology. Edited by D.A. Haugen. American Meteorological Society, Boston, Massachusetts, 151-176.

PASQUILL, F. (1976). Environmental Protection Agency, EPA-600/4-76-030b, PB-258 036/3GA, 55 pp.

PETERSEN, E.L., TROEN, I., FRANDSEN, S. and HEDEGAARD, K. (1981). Risø-R-428, 229 pp.

RASMUSSEN, K. RØMER, LARSEN, S.E. and JØRGENSEN, F.E. (1981). DISA, Skovlunde, Denmark, 26, 27-35.

SCHMITT, K.F., FRIEHE, C.A. and GIBSON, C.H. (1979). J. Atmos. Sci. 36, 602-618.

SMITH, F.B. (1968). Atmos. Environ. 2, 491-508.

SMITH, F.B. and HAY, J.S. (1961). Q. J. R. Meteorol. Soc. 87, 82-101.

TENNEKES, H. and LUMLEY, J.L. (1972). A first course in turbulence. MIT Press, Cambridge, Massachusetts and London, 300 pp.

TURNER, D.B. (1970). Workbook of atmospheric dispersion estimates. Public Health Service, Division of Air Pollution, Cincinnati, Ohio, PHS-Pub-999-AP-26, PB-191 482, 88 pp.

WYNGAARD, J.C. (1968). J. Sci. Instrum. (J. Phys. E) 1, 1105-1108.

WYNGAARD, J.C., COTÉ, O.R. and RAO, K.S. (1974). In: Turbulent Diffusion in Environmental Pollution. Proceedings of a synposium held at Charlottesville, Virginia, U.S.A., April 8-19, 1973. Edited by F.N. Frenkill and R.E. Munn. Academic Press, New York, 193-211.

5. LIQUID N_2 AND He PLANT

The production of liquid N_2 and He amounted to 220 000 and 19 000 litres, respectively. Out of these amounts, 10 000 litres of liquid He were delivered to laboratories in Copenhagen, Odense and Aarhus.

6. PUBLICATIONS AND EDUCATIONAL ACTIVITIES

6.1 Publications

ALS-NIELSEN, J. (1980). Synchrotron x-ray diffraction using triple axis spectrometry. Progress Report for 1980, Risø-M-2268, 23 pp.

ALS-NIELSEN, J., LITSTER, J.D., BIRGENEAU, R.J., KAPLAN, M., SAFINYA, C.R. LINDEGAARD-ANDERSEN, A. and MATHIESEN, S. (1980). Observation of algebraic decay of positional order in a smectic liquid crystal. Phys. Rev. B22, 312-320.

ALS-NIELSEN, J., SAFINYA, C.R., KAPLAN, M., BIRGENEAU, R.J., DAVIDOV, D., LITSTER, J.D., JOHNSON, D.L. and NEUBERT, M.E. (1980). High resolution x-ray study of a smectic-A - smectic-C phase transition. Phys. Rev. B21, 4149-4153.

ANDERSEN, N. HESSEL (1980). Electrical resistivity investigations on metallic rare earths. In: Crystalline Electric Field and Structural Effects in f-Electron Systems. Edited by J.E. Crow, R.P. Guertin and T.W. Mihalisin. Plenum Press, New York and London, 373-387.

ANDERSEN, N. HESSEL, KJEMS, J.K. and VOGT, O. (1980). Temperature variation of the magnetic structure of HoSb. J. Phys. C13, 5137-5144.

ANDERSEN, O.K., SKRIVER, H.L., NOHL, H. and JOHANSSON, B. (1980). Electronic structure of transition metal compounds; ground state properties of the 3d-monoxides in the atomic sphere approximation. Pure and Appl. Chem. 52, 93-118.

ANDERSEN, V. (1980). Tokamakken - en beholder til 100 millioner grader varmt plasma (The tokamak - a container for a 100 million degrees hot plasma). T1-Teknikeren 60: 10, 4-8.

ANDERSEN, V. (1980). DANTE - Dansk Tokamak Eksperiment (DANTE - Danish Tokamak Experiment). Gamma No. 44, 26-38.

BALMASHNOV, A.A. (1980). On the self-focusing of whistler waves in a radial inhomogeneous plasma. Phys. Lett. 79A, 402-404.

BØRGESEN, P., BEHRISCH, R. and SCHERZER, B.M.U. (1980). Evaluation of ion beam spectra for surface analysis of probes exposed in fusion devices. In: Proceedings of the EUROPHYSICS

Conference on Nuclear Physics Methods in Materials Research, Darmstadt, F.R.G., September 23-26, 1980, 363-366.

BØRGESEN, P., SCHOU, J. and SØRENSEN, H. (1980). Ion-induced emission of charged particles from solid hydrogen and deuterium. J. Nucl. Mater. B93/94, 701-703.

BØRGESEN, P., SCHOU, J. and SØRENSEN, H. (1980). Erosion of thin films of D_2 by keV light ions. In: Proceedings of the Symposium of Sputtering, Perchtoldsdorf, Vienna, Austria, April 28-30, 1980, 822-831.

BOULET, R.M., DUNSWORTH, A.E., JAN, J.P. and SKRIVER, H.L. (1980). De Haas-van Alphen effect and LMTO bandstructures of NiSi. J. Phys. F. 10, 2197-2206.

BRAUDE, A., LINDEGAARD-ANDERSEN, A., CARNEIRO, K. and PETERSEN, A. STEEN (1980). Diffuse x-ray scattering from several platinum chain compounds. Solid State Commun. 33, 365-369.

BOHR, J., NIELSEN, M. and ALS-NIELSEN, J. (1980). Commensurate-incommensurate phase transition in Kr-monolayer adsorbed on graphite. In: Proceedings of the 3rd European Conference on Surface Science, 1, 112-116.

BURAS, B. (1980). Synchrotron radiation and energy-dispersive diffraction. In: Proceedings of the Symposium on Accuracy in Powder Diffraction. Edited by S. Bloch and C.R. Hubbard. National Bureau of Standards, Washington D.C., U.S.A., June 11-15, 1979. NBS Special Publication 567, 33-54.

BURAS, B., FARGE, Y. and THOMPSON, D.J. (1980). Large synchrotron radiation sources. European Great Projects, International Seminar, Rome, Italy, March 26-27, 1979. European Physical Society, Rome, 79-103.

BURAS, B., OLSEN, J. STAUN and GERWARD, L. (1980). On the use of wide-angle energy-sensitive detectors in white beam x-ray single crystal diffraction. Nucl. Instrum. Methods 178, 131-135.

BUSCH, N.E., CHRISTENSEN, O., KRISTENSEN, L., LADING, L. and LARSEN, S.E. (1980). Cups, propellers and laser anemometers. In: Air-Sea Interactions. Instruments and Methods. Edited by F. Dobson, L. Hasse and R. Davis. Plenum Press, New York, 11-46.

CHANG, C.T., JØRGENSEN, L.W., NIELSEN, P. and LENGYEL, L.L. (1980). The feasibility of pellet refuelling of a fusion reactor. Nucl. Fusion 20, 859-893.

CLAUSEN, K. NØRGAARD and LEBECH, B. (1980). Spin waves in Ho_2Co_{17}. J. Magn. Magn. Mater. 15-18, 347-348.

COWLEY, R.A. and CARNEIRO, K. (1980). Critical properties of pure and random antiferromagnets: CoF_2, Co/ZnF_2, KMn/NiF_3. J. Phys. C13, 3281-3291.

DUTTA, P., SINHA, S.K., VORA, P., NIELSEN, M., PASSELL, L. and BRETZ, M. (1980). Neutron diffraction studies of melting of physisorbed monolayers of CD_4 on graphite. In: Proceedings of the International Conference on Ordering in Two Dimensions, Wisconsin, U.S.A., May 28-30, 1980. Edited by S.K. Sinha. North-Holland, 169-174.

ETHELFELD, J. (1980). Statusrapport vedrørende bremseaktiverings-system - centrifugaludløser - af 30 kW Riisagermølle (Description of the brake activating system for the 30 kW Riisager windmill). Risø-M-2220, 18 pp.

ETHELFELD, J., JENSEN, F., KJØLLER, J. and LYSTRUP, Aa. (1980). Arbejdsrapport og vejledning vedrørende reparation af tre stykker vinger til 30 kW Riisagermølle (Report on the repair of the blades for the 30 kW Riisager windmill). Risø-M-2207, 20 pp.

FRANDSEN, S. and CHRISTENSEN, C.J. (1980). On wind turbine power measurements. Proceedings of the Third International Symposium on Wind Energy Systems, Copenhagen, August 26-29, 1980. BHRA Fluid Engineering, 207-222.

GRYNING, S.E. (1980). Meteorological measurement programs for air pollution studies. Risø-M-2259, 26 pp.

GRYNING, S.E. and LYCK, E. (1980). Comparison between dispersion calculation methods based on in-situ meteorological measurements and results from elevated source tracer experiments in an urban area. Danish National Agency of Environmental Protection, Air Pollution Laboratory, Risø, MST LUFT A40, 32 pp.

GRYNING, S.E. and LYCK, E. (1980). Medium-range dispersion experiments downwind from a shoreline in near neutral conditions. Atmos. Environ. 14, 923-931.

GRYNING, S.E. and LYCK, E. (1980). Elevated source SF_6-tracer dispersion experiments in the Copenhagen area; Preliminary

results II. In: Seminar on Radioactive Releases and Their Dispersion in the Atmosphere Following a Hypothetical Reactor Accident, Risø, April 22-25, 1980. Edited by F. van Hoeck and P. Recht. Commission of the European Communities, Luxembourg, Vol. 2, 905-924.

CRYNING, S.E., PETERSEN, E.L. and LYCK, E. (1980). Elevated source SF_6-tracer dispersion experiments in the Copenhagen area; Preliminary results I. In: Proceedings of the Tenth International Technical Meeting on Air Pollution Modelling and its Application. NATO/CCMS Air Pollution Pilot Study, Rome, Italy, October 23-26, 1980, 119-132.

GUNNESKOV, O. and LUNDSAGER, P. (1980). Static deflection and Eigen-frequency analysis of the Nibe wind turbine rotors. Analysis procedures and results. Risø-M-2200, 42 pp.

JAN, J.P., MACDONALD, A.H. and SKRIVER, H.L. (1980). Prediction of Fermi surface pressure dependence in Rb and Cs. Phys. Rev. B21, 5584-5593.

JENSEN, N.O. (1980). The simple approach to deposition. In: Seminar on Radioactive Releases and Their Dispersion in the Atmosphere Following a Hypothetical Reactor Accident, Risø, April 22-25, 1980. Edited by F. van Hoeck and P. Recht. Commission of the European Communities, Luxembourg, Vol. 1, 331-343.

JENSEN, N.O. (1980). A simplified diffusion-deposition model. Atmos. Environ. 14, 953-956.

JENSEN, P. HJULER (1980). Effektmålinger på 15 kW vindmølle fra Jysk Vindkraft (Power measurements on a 15 kW wind turbine from Jysk Vindkraft). Risø-M-2269, 33 pp.

JENSEN, V.O. (1980). Dansk deltagelse i JET-projektet (Danish participation in the JET-project). Gamma No. 43, 33-38.

JENSEN, V.O. (1980). Fusionsenergi - fremtidens energikilde (Fusion energy - the energy source of the future). Tl-Teknikeren 60:5, 8-13.

JOHANSSON, B., SKRIVER, H.L., MÅRTENSSON, N., ANDERSEN, O.K. and GLÖTZEL, D. (1980). Presence and character of the 5f electrons in the actinide metals. Physica B+C 102, 12-21.

KARPMAN, V.I., LYNOV, J.P., MICHELSEN, P., PÉCSELI, H.L., RASMUSSEN, J. JUUL and TURIKOV, V.A. (1980). Modification of plasma solitons by resonant particles. Phys. Fluids 23, 1782-1794.

KEPA, H., GEBICKI, W., GIEBULTOWICZ, T., BURAS, B. and CLAUSEN, K. (1980). A neutron study for phonon dispersion relations in HgTe. Solid State Commun. 34, 211-213.

KNORR, K., LOIDL, A. and KJEMS, J.K. (1980). Soft modes and mode splitting in paramagnetic TbP. In: Crystalline Electric Field and Structural Effects in f-Electron Systems. Edited by J.E. Crow, R.P. Guertin and T.W. Mihalisin. Plenum Press, New York and London, 141-152.

KRISTENSEN, L. (1980). The Existence and Effect of Meandering on Dispersion of Pollutants. In: Seminar on Radioactive Releases and Their Dispersion in the Atmosphere Following a Hypothetical Reactor Accident, Risø, April 22-25, 1980. Edited by F. van Hoeck and P. Recht. Commision of the European Communities, Luxembourg, Vol. I, 93-113.

LARSEN, S.E. (1980). Meteorologiske overvejelser i forbindelse med beregninger af konsekvenser af frigørelse af radioaktivt materiale til atmosfæren fra Risø (Meteorological considerations in connection with calculation of consequences of radioactive releases into the atmosphere from Risø. Risø-I-18, 21 pp.

LARSEN, S.E. and BUSCH, N.E. (1980). On the humidity sensitivity of hot-wire measurements. DISA Information No. 25, 4-5.

LARSEN, S.E., HØJSTRUP, J. and GIBSON, C.H. (1980). Fast-response temperature sensors. In: Air-Sea Interactions. Instruments and Methods. Edited by F. Dobson, L. Hasse and R. Davis. Plenum Press, New York, 269-291.

LARSEN, S.E., HØJSTRUP, J. and JENSEN, N.O. (1980). Meteorologisk eksperiment i Holland (Meteorological experiment in The Netherlands. Vejret 1, 26-29.

LEBECH, B. and ALS-NIELSEN, J. (1980). A neutron and x-ray diffraction study of Nd metal. J. Magn. Magn. Mater. 15-18, 469-470.

LEBECH, B., CLAUSEN, K. and VOGT, O. (1980). First-order transitions and the magnetic phase diagram of CeSb. In: Crystalline Electric Field and Structural Effects in f-Electron Systems. Edited by J.E. Crow, R.P. Guertin and T.W. Mihalisin. Plenum Press, New York and London, 103-107.

LEBECH, B., CLAUSEN, K. and VOGT, O. (1980). First-order transitions and the magnetic phase diagram of CeSb. J. Phys. C13, 1725-1733.

LEBECH, B., RAINFORD, B.D., BROWN, P.J. and WEDGWOOD, F.A. (1979). Magnetic form factors of praseodymium and neodymium metals. J. Magn. Magn. Mater. 14, 298-300.

LINDGÅRD, P.A. (1979). Theory of static and dynamic properties of crystal field systems including correlation effects. In: Proceedings of the International Conference on Crystalline Electric Field and Structural Effects in f-Electron Systems. Edited by J.E. Crow, R.P. Guertin and T.W. Mihalisin. Plenum Press, New York, 153-164.

LINDGÅRD, P.A., ALS-NIELSEN, J. and HUTCHINGS, M.T. (1980). Renormalization of long wavelength spin waves in the 2d ferromagnet Rb_2CrCl_4. J. Magn. Magn. Mater. 15-18, 343-344.

LINDGÅRD, P.A. and YANG, D. (1980). Correlation theory of static and dynamic properties. J. Magn. Magn. Mater. 15-18, 1037-1038.

LOIDL, A., KNORR, K., KJEMS, J.K. and HAUSSÜHL, S. (1980). Inelastic neutron scattering by coupled rotational and translational modes in CsCN. J. Phys. C13, L349-355.

LUNDSAGER, P., FRANDSEN, S. and CHRISTENSEN, C.J. (1980). Analysis of data from the Gedser wind turbine 1977-1979. Risø-M-2242, 136 pp.

LUNDSAGER, P. and GUNNESKOV, O. (1980). Static deflection and eigen-frequency analysis of the Nibe wind turbine rotors. Theoretical background. Risø-M-2199, 25 pp.

LUNDSAGER, P., PETERSEN, H. and FRANDSEN, S. (1980). The dynamic behaviour of the stall regulated Nibe A wind turbine. Measurements and a model for stall-induced vibrations. Risø-M-2253, 61 pp.

LYNOV, J.P. (1980). Modifications of KdV solitons by reflected particles. In: Proceedings of the International Conference on Plasma Physics, Nagoya, Japan, April 7-11, 1980, 1, 400.

LYNOV, J.P. (1980). Solitary electron density waves in a magnetized plasma-loaded waveguide. Risø-R-432, 107 pp.

LYNOV, J.P., MICHELSEN, P., PÉCSELI, H.L. and RASMUSSEN, J. JUUL (1980). Interaction between electron holes in a strongly magnetized plasma. Phys. Lett. 80A, 23-25.

LYNOV, J.P., MICHELSEN, P., PÉCSELI, H.L. and RASMUSSEN, J. JUUL (1980). Hvad er plasma - og hvad kan det bruges til? (What is a plasma - and what can it be used for?). Tl-Teknikeren 60:8, 4-7.

LYNOV, J.P., MICHELSEN, P., PÉCSELI, H.L., RASMUSSEN, J. JUUL and THOMSEN, K. (1980). Modulational instability of electron plasma waves. In: Proceedings of the International Conference on Plasma Physics, Nagoya, Japan, April 7-11, 1980, 1, 233.

LYNOV, J.P., RASMUSSEN, J. JUUL and THOMSEN, K. (1980). Recurrence of long wavelength electron plasma waves. In: Proceedings of the International Conference on Plasma Physics, Nagoya, Japan, April 7-11, 1980, 1, 401

MACKENZIE, G.A. (1980). Analysis of neutron powder diffraction data: User's guide. Physics Department, Internal Note.

MAHRT, L., LARSEN, S.E. and GRYNING, S.E. (1980). Studier af faldvinde på Risø (Studies of gravity flows at Risø). Vejret 4, 26-28.

MAHRT, L. (1980). On the dynamics of gravity flows. Risø-R-420, 33 pp.

MAHRT, L. (1980). Comment on "Gravity wind on a snow patch". J. Meteorol. Soc. (Japan) 58, 93.

MAHRT, L., HEALD, R.C., LENSCHOW, D.H., STANKOV, B. and TROEN, I. (1979). An observational study of the nocturnal boundary layer. Boundary-Layer Meteorol. 17, 247-264.

McTAGUE, J.P., NIELSEN, M. and PASSELL, L. (1980). Structure and phase transitions in physisorbed monolayers. In: Proceedings of the NATO Advanced Study Institute on Strongly Fluctuating Condensed Matter Systems held in Geilo, Norway, April 16-27, 1979. Edited by T. Riste. Plenum Press, New York and London, 195-220.

MICHELSEN, P. (1980). Laboratory plasma physics. In: Proceedings of the International Conference on Plasma Physics, Nagoya, Japan, April 7-11, 1980, 2, 122-137.

MIKKELSEN, T., LARSEN, S.E. and TROEN, I. (1980). Some puff modelling principles relevant for dispersion calculations in the atmosphere. Risø-M-2258, 28 pp.

MIKKELSEN, T., LARSEN, S.E. and TROEN, I. (1980). Use of a puff-model to calculate dispersion from a strongly time dependent source. In: Seminar on Radioactive Releases and Their Dispersion in the Atmosphere Following a Hypothetical Reactor Accident, Risø, April 22-25, 1980. Edited by F. van Hoeck and P. Recht. Commision of the European Communities, Luxembourg, Vol. 2, 575-614.

MIKKELSEN, T. and PÉCSELI, H.L. (1980). Strong turbulence in partially ionized plasmas. Phys. Lett. 77A, 159-162.

MØLLENBACH, K. (1980). Studies in small angle scattering techniques. Experimental methods and examples of their use. Risø-R-396, 99 pp.

NIELSEN, M., ALS-NIELSEN, J. and McTAGUE, J.P. (1980). Powder diffraction patterns from superstructures in adsorbed monolayers near commensurate-incommensurate phase transitions. In: Proceedings of the International Conference on Ordering in Two Dimensions, held in Wisconsin, U.S.A., May 28-30. Edited by S.K. Sinha. North-Holland, 135-141.

NIELSEN, M., McTAGUE, J.P. and PASSELL, L. (1980). Neutron scattering studies of physisorbed monolayers on graphite. In: Proceedings of NATO Advanced Study Institute on Phase Transitions in Surface Films, held at Ettore Majorana Centre of Scientific Culture, Erice Sicily, Italy, June 11-25, 1979. Plenum Press, New York and London, 127-163.

NIELSEN, P. and SØRENSEN, H. (1980). Brændstofpåfyldning på kommende fusionsreaktorer (Refuelling of future fusion reactors). Tl-Teknikeren 60:13, 12-17.

NORDSKOV, A., SKOVGÅRD, H., SØRENSEN, H. and WEISBERG, K.V. (1980). A light-gas gun for acceleration of pellets of solid D_2. Risø-M-2245, 19 pp.

OTT, H.R., and KJEMS, J.K. (1980). Experimental test for ε-expansion with n = 4: the magnetic ordering of Ce monochalcogenides. J. Magn. Magn. Mater. 15-18, 401-402.

PÉCSELI, H.L. and RASMUSSEN, J. JUUL (1980). Nonlinear electron waves in strongly magnetized plasmas. Plasma Phys. 22, 421-438.

PEDERSEN, K.S. (1980). The liquids nitrogen, oxygen and helium-4 studied by neutron scattering. PhD thesis, Technical University of Denmark, 108 pp.

PEDERSEN, K.S. and CARNEIRO, K. (1980). Collective excitations of normal liquid ^{4}He at 3.1 K, studied by neutron inelastic scattering. Phys. Rev. B22, 191-194.

PEDERSEN, T. FRIIS (1980). Bremsefaldskærm til vindmøller med fast bladindstilling (Brake parachute for fixed pitch wind turbines). Risø-I-34, 9 pp.

PEDERSEN, T. FRIIS and JENSEN, P. HJULER (1980). Samfundsøkonomisk analyse af mindre vindmøller (National economics of small wind turbines). Risø-M-2215, 44 pp.

PETERSEN, E.L., TROEN, I. and FRANDSEN, S. (1980). Vindatlas for Danmark (Wind atlas for Denmark). Risø (August), 149 pp. (Popular version in Danish; available from DEFU, Lundtoftevej 100, Bldg. 325, 2800 Lyngby.)

PETERSEN, H. (1980). The test plant for and a survey of small Danish wind turbines. Risø-M-2193, 52 pp.

PETERSON, E.W., TAYLOR, P.A., HØJSTRUP, J., JENSEN, N.O., KRISTENSEN, L. and PETERSEN, E.L. (1980). Risø 1978: Further investigations into the effect of local terrain irregularities on tower-measured wind profiles. Boundary-Layer Meteorol. 19, 303-313.

RASMUSSEN, F. (1980). Effektmålinger på SJ-10 kW - R vindmølle (Power measurements on the SJ-10 kW - R wind turbine) Revised edition. Risø-M-2225, 26 pp.

RASMUSSEN, F. (1980). Effektmålinger på 15 kW gyromølle (Power measurements on the 15 kW gyromill). Risø-M-2226, 13 pp.

RASMUSSEN, F. (1980). Effektmålinger på 30 kW Riisagermølle (Power measurements on the 30 kW Riisager wind turbine). Risø-M-2227, 13 pp.

RASMUSSEN, P. (1980). Slæberingsasynkronmaskinen som vindmøllegenerator (The slip ring asynchronous machine used as a wind turbine generator). Risø-I-9, 9 pp.

RASMUSSEN, P. (1980). Togeneratordrift på vindmølle (Dual-generator operation on a wind turbine). Risø-I-10, 9 pp.

RASMUSSEN, P. (1980). Status over energiproduktionen fra mindre vindkraftanlæg (Status of the energy production from small wind turbines). Risø-I-26, 10 pp.

RASMUSSEN, P. (1980). Accelerationsberegning for stallregulerede vindmøller uden belastning (i friløb) (Calculation of acceleration of stall-regulated wind turbines without load (idle). Risø-I-27, 7 pp.

SCHOU, J. (1980). Transport theory for kinetic emission of secondary electrons from solids. Phys. Rev. B22, 2141-2174.

SCHOU, J. (1980). Transport theory for kinetic emission of secondary electrons from solids by electron and ion bombardment. Nucl. Instrum. Methods 170, 317-320.

SKRIVER, H.L., ANDERSEN, O.K. and JOHANSSON, B. (1980). 5 f-electron delocalization in americium. Phys. Rev. Lett. 44, 1230-1233.

SKRIVER, H.L., ANDERSEN, O.K. and JOHANSSON, B. (1980). Calculated specific volumes and magnetic moment of the 3d transition metal monoxides. J. Magn. Magn. Mater. 15-18, 861-862.

SKRIVER, H.L. and JAN, J.P. (1980). Electronic states in thorium under pressure. Phys. Rev. B21, 1489-1496.

STEINER, M., KJEMS, J.K., KAKURAI, K. and DACHS, H. (1980). Neutron scattering of nonlinear excitations in the 1-D ferromagnet $CsNiF_3$. J. Magn. Magn. Mater. 15-18, 1057-1058.

TCHEN, C.M., PÉCSELI, H.L. and LARSEN, S.E. (1980). Strong turbulence in low-β plasmas. Plasma Phys. 22, 817-829.

TROEN, I., MIKKELSEN, T. and LARSEN, S.E. (1980). Comments on "Generalization of K-theory for turbulent diffusion" (II). J. Appl. Meteorol. 19, 117-118.

TROEN, I., MIKKELSEN, T. and LARSEN, S.E. (1980). Note on spectral diffusivity theory. J. Appl. Meteorol. 19, 609-615.

6.2 Contract reports

CHRISTENSEN, O. and FRANDSEN, S. (1980). Rockwool A/S A-tagpladens aerodynamiske modstand mod afblæsning under storm, når pladerne er udlagt tæt sammen på et fladt tag med kun randvis fastgørelse til dette (The aerodynamic resistance of Rockwool A/S A-roof-tiles against blowing off during a storm when the tiles are placed close together on a flat roof, fastened at edges only). Work done under contract to Rockwool A/S.

JENSEN, N.O. (1980). Frigørelses og spredningsbetragtninger vedrørende klor (Considerations regarding the release and spreading conditions of chlorine). In: Risikoanalyse af den planlagte ændring af klortappestationen på Grindsted Products A/S anlæg i Grenå. Edited by J.R. Taylor. Work done under contract to Grindstedværket A/S.

JENSEN, N.O. (1980). Eksempler på spredning af klor (Examples of chlorine spreading). In: Risikovurdering af Dansk Sojakagefabriks Kloralkalianlæg. Edited by D.S. Nielsen. Work done under contract to the City of Copenhagen (Københavns Magistrats 5. afdeling), 90-98 and J1-J32.

JENSEN, N.O. (1980). Dispersion of large releases of H_2S. Appendix C in: Danish Natural Gas Transmission System Treatment Plant,

Preliminary Risk Analysis Report. Work done under contract to DONG (Dansk Olie og Naturgas A/S). Cl + 9 pp.

JENSEN, N.O. (1980). Undersøgelse af en mikrometeorologisk model for temperatur udviklingen i en vejoverflad (Investigation of a micrometeorological model for temperature development in a road surface). Work done under contract to Vejlaboratoriet. 36 pp.

JENSEN, N.O. and HANSEN, F.Aa. (1980). Første statusrapport vedrørende vindmålinger på Sprogø (Wind measurements on Sprogø: First progress report). Work done under contract to Vejdirektoratet. 8 pp.

KRISTENSEN, L. (1980). Statusrapport nr. 1 vedrørende meteorologiske målinger ved Kvanefjeld (Progress report no. 1 concerning meteorological measurements at Kvanefjeld). 10 pp.

KRISTENSEN, L. (1980). Statusrapport nr. 2 vedrørende meteorologiske målinger ved Kvanefjeld. Data fra perioden september 1979 til september 1980 (Progress report no. 2 concerning meteorological measurements at Kvanefjeld. Data for the period September 1979 to September 1980). 121 pp.

LARSEN, S.E. (1980). Meteorologi, Pladsansøgning, Gylling Næs (Site evaluation of Gylling Næs for a nuclear power plant). Section 3.3.3. Work done under contract to ELSAM. 102 pp.

PETERSEN, E.L., TROEN, I. and HEDEGAARD, K. (1980). Vindatlas for Danmark (Wind atlas for Denmark). Risø (May). Contract report for the Wind Power Programme of the Danish Energy Ministry and the Danish Utilities. 201 pp.

6.3 Conference contributions

ALPORT, M.J., D'ANGELO, N. and PÉCSELI, H.L.. Scattering of EM-waves from plasma irregularities and wave packets. AGU Chapman Conference on Formation of Auroral Arcs, Fairbanks, Alaska, U.S.A., July 21-27.

ALS-NIELSEN, J.. Resolution in diffraction. An outline of the method of conjugate diameters. European Science Foundation, Summer School on Synchrotron Radiation, Vienna, Austria, September.

ALS-NIELSEN, J.. Liquid crystals studied by perfect crystals. Colloque Pierre Curie, École Supérieure de Physique et de Chimie, Paris, France, September.

ALS-NIELSEN, J.. Concept and experiments illustrating upper marginal dimensionality. Conference on Magnetic phase transitions, London, U.K., September.

ALS-NIELSEN, J.. Liquid crystals studied by perfect crystals. Danish Physical Society, Annual Meeting, Odense, Denmark, November 12.

ANDERSEN, N. HESSEL and KREBS-LARSEN, F.. Characterization of the solid ionic conductor $LiI \cdot D_2O$. 16th Meeting of Danish Crystallographers, Aarhus, Denmark, May 21-22.

ANDERSEN, N. HESSEL, KJEMS, J.K. and VOGT, O.. Temperature variation of the magnetic structure of HoSb. Danish Physical Society, Topical Meeting on Magnetism, Risø National Laboratory, Denmark, December 9.

ANDERSEN, V., GADEBERG, M., JENSEN, P.B. and NIELSEN, P.. Pellet ablation studies in DANTE. IEEE International Conference on Plasma Science, Madison, Wisconsin, U.S.A., May 19-21.

ANDERSEN, V., GADEBERG, M., JENSEN, P.B., NIELSEN, P. and SØRENSEN, H.. Acceleration and injection of D_2-pellets. 11th Symposium on Fusion Technology, Oxford, England, September 15-19.

BALMASHNOV, A.A.. Whistler wave propagation in a plasma column with nonequilibrium density distribution. Danish Physical Society, Spring Meeting, Helsingør, Denmark, May 30-31.

BØRGESEN, P., SCHOU, J. and SØRENSEN, H.. Range and stopping power for hydrogen isotopes in solid hydrogens; a method. Danish Physical Society, Topical Meeting on Atomic Physics and Plasma Physics, Risø National Laboratory, Denmark, January 25-26.

BØRGESEN, P., SCHOU, J and SØRENSEN, H.. Erosion of thin films of D_2 by keV light ions. Symposium on Sputtering, Perchtholdsdorf/Vienna, Austria, April 28-30.

BØRGESEN, P., SCHOU, J. and SØRENSEN, H.. Ion induced emission of charged particles from solid hydrogen and deuterium. Fourth International Conference on Plasma Surface Interaction in Controlled Fusion Devices, Garmisch-Partenkirchen, F.P.G., April 21-25.

BØRGESEN, P., BEHRISCH, R. and SCHERZER, B.M.U.. Evaluation of ion beam spectra for surface analysis of probes exposed in fusion devices. EUROPHYSICS Conference, Nuclear Physics 7th Divisional Conference on Nuclear Physics Methods in Material Research, Darmstadt, F.R.G., September 23-26.

BURAS, B.. Instrumentation proposed for the European synchrotron radiation facility. Nordic Symposium on Research with Synchrotron Radiation in Physics, Chemistry and Biology, Gysinge, Sweden, June 13-15.

BURAS, B.. X-ray energy-dispersive diffraction in x-ray scattering with synchrotron radiation. European Science Foundation Summer School on Synchrotron Radiation, Vienna, Austria, September.

CLAUSEN, K.. Magnetic excitation in Ho_2Fe_{17} and Ho_2Co_{17}. Danish Physical Society, Spring Meeting, Helsingør, Denmark, May 30-31.

DUTTA, P., SINHA, S.K., VORA, P., NIELSEN, M., PASSELL, L. and BRETZ, M.. Neutron diffraction studies of melting of physisorbed monolayers of CD_4 on graphite. International Conference on Ordering in Two Dimensions, Wisconsin, U.S.A., May 29-30.

FRANDSEN, S. and CHRISTENSEN, C.J.. On wind turbine power measurements. Third International Symposium on Wind Energy Systems, Copenhagen, Denmark, August 26-29.

GIEBULTOWICZ, T., KEPA, H., BURAS, B., CLAUSEN, K. and GALASKA, R.. Magnetic ordering in $Cd_{1-x}Mn_xTe$. Danish Physical Society, Topical Meeting on Magnetism, Risø National Laboratory, Denmark, December 9.

GRYNING, S.E. and LYCK, E.. Elevated source SF_6-tracer dispersion experiments in the Copenhagen area. Preliminary results II. EEC Conference on Radioactive Releases and Their Dispersion in the Atmosphere Following a Hypothetical Reactor Accident, Risø National Laboratory, Denmark, April 22-25.

HANSEN, S.O.. Cross wind vibrations of a 130 m tapered concrete chimney. Fourth Colloquium on Ind strial Aerodynamics, Aachen, F.R.G., June 18-20.

HEILMANN, I.U., KJEMS, J.K., SHIRANE, G., ENDOH, Y., BLUME, M., REITER, G. and BIRGENEAU, R.J.. Spin dynamical properties of the linear-chain antiferromagnet TMMC in a magnetic field. Danish Physical Society, Spring Meeting, Helsingør, Denmark, May 30-31.

JENSEN, N.O.. The simple approach to deposition. EEC Conference on Radioactive Releases and Their Dispersion in the Atmosphere Following a Hypothetical Reactor Accident, Risø National Laboratory, Denmark, April 22-25.

JENSEN, N.O.. Entrainment through the top of a heavy gas cloud. 11th International Technical Meeting on Air Pollution Modelling and its Application. NATO/CCMS Air Pollution Pilot Study, Amsterdam, The Netherlands, October 22-26.

JENSEN, V.O.. Denish participation in the JET-project. Danish Physical Society, Topical Meeting on Atomic Physics and Plasma Physics, Risø National Laboratory, Denmark, January 24-25.

JENSEN, V.O.. Plasma and fusion physics at Risø. 15th Nordic Symposium on Plasma and Gas Discharge Physics, Oppdal, Norway, February 18-20.

KEPA, H., GEBICKI, W., GIEBULTOWICZ, T., PUŹNIAK, R., BURAS, B. and CLAUSEN, K.. A neutron study of lattice dynamics in mercury telluride. Tenth Polish Seminar on Semiconductor Compounds, Jaszowiec, Poland, April 22-30.

KJEMS, J.K.. Dynamic Huang-scattering in fast ionic conductors. A neutron scattering study of CaF_2. 16th Meeting of Danish Crystallographers, Aarhus, De mark, May 21-22.

KJEMS, J.K., KAKURAI, K. and STEINER, M.. Neutron scattering studies of the 1-D ferromagnet $CsNiF_3$. Danish Physical Society, Spring Meeting, Helsingør, Denmark, May 30-31.

KJEMS, J.K.. The influence of superconductivity on the crystal field excitations in $La_{1-x}Tb_xAl_2$. Danish Physical Society, Topical Meeting on Magnetism, Risø National Laboratory, Denmark, December 9.

KNUDSEN, G.P., VOSS, F. WULFF, NEVALD, R. and MØLLER, H. BJERRUM. Tectragonal phase transitions and other structural aspects of cubic $Cs_2NaLnCl_6$. 16th Meeting of Danish Crystallographers, Aarhus, Denmark, May 21-22.

KRISTENSEN, L.. The existence and effect of meandering in dispersion of pollutants. EEC Conference on Radioactive Releases and Their Dispersion in the Atmosphere Following a Hypothetical Reactor Accident, Risø National Laboratory, Denmark, April 22-25.

LARSEN, S.E., MATHIASSEN, O. and BUSCH, N.E.. Spectra of turbulence in the marine surface layer. AMS Conference on Ocean-Atmosphere Interaction, Los Angeles, California, U.S.A., January 30-February 2.

LEBECH, B.. Nd, an example of a substance where both x-ray and neutron diffraction experiments have been essential for solving the magnetic structure. 16th Meeting of Danish Crystallographers, Aarhus, Denmark, May 21-22.

LEBECH, B.. Neutron diffraction studies of the modulated magnetic structures of CeSb and Nd metal. 26th Annual Conference on Magnetism and Magnetic Materials, Dallas, Texas, U.S.A., November 11-14.

LEBECH, B.. The modulated magnetic structure of Nd metal. Danish Physical Society, Topical Meeting on Magnetism, Risø National Laboratory, Denmark, December 9.

LINDGÅRD, P.A.. Correlation theory of static and dynamic properties of multi-level systems. Annual Conference on Condensed Matter, Antwerp, Belgium, April 9-11.

LINDGÅRD, P.A.. Theory of static and dynamic properties of multi-level systems. Danish Physical Society, Topical Meeting on Magnetism, Risø National Laboratory, Denmark, December 9.

LUNDSAGER, P.. The Test Plant for small windmills. 3rd International Symposium on Wind Energy Systems, Copenhagen, Denmark, August 26-29.

LUNDSAGER, P. and PETERSEN, H.. Status of small Danish windmills. Seminar on Small Scale Wind Energy Systems, Enköping, Sweden, December 1-2.

LYNOV, J.P., RASMUSSEN, J. JUUL and THOMSEN, K.. Recurrence of long wavelength electron plasma waves. International Conference on Plasma Physics, Nagoya, Japan, April 7-11.

LYNOV, J.P.. Modification of KdV solitons by reflected particles. International Conference on Plasma Physics, Nagoya, Japan, April 7-11.

LYNOV, J.P., MICHELSEN, P., PÉCSELI, H.L., RASMUSSEN, J. JUUL and THOMSEN, K.. Modulational instability of electron plasma waves. International Conference on Plasma Physics, Nagoya, Japan, April 7-11.

LYNOV, J.P.. Recurrence of sinusoidal waves in nonlinear, dispersive systems. Danish Physical Society, Spring Meeting, Helsingør, Denmark, May 30-31.

MICHELSEN, P.. Laboratory Plasma Physics. International Conference on Plasma Physics, Nagoya, Japan, April 7-11.

MIKKELSEN, T., LARSEN, S.E. and TROEN, I.. Use of a puff-model to calculate dispersion from a strongly time-dependent source. EEC Conference on Radioactive Releases and Their Dispersion in the Atmosphere Following a Hypothetical Reactor Accident, Risø National Laboratory, Denmark, April 22-25.

MILLHOUSE, A.H., STEINER, M. and KJEMS, J.K.. Critical neutron scattering in the 3-D-Ising metamagnet $DyPO_4$. 26th Annual Conference on Magnetism and Magnetic Materials, Dallas, Texas, U.S.A., November 11-14.

MØLLER, H. BJERRUM. The magnetic properties of the mixed valence system TmSe. Danish Physical Society, Topical Meeting on Magnetism, Risø National Laboratory, Denmark, December 9.

NIELSEN, M.. The phase transition between commensurate and incommensurate hexagonal structures in physisorbed layers on graphite. International Conference on Ordering in Two Dimensions, Wisconsin, U.S.A., May 28-30.

NIELSEN, P.. Dante (Danish Tokamak Experiment). Danish Physical Society, Topical Meeting on Atomic Physics and Plasma Physics, Risø National Laboratory, Denmark, January 25-26.

OLSEN, J. STAUN, BURAS, B., STEENSTRUP, S. and GERWARD, L.. Spectrometer for x-ray energy dispersive diffraction. 16th Meeting of Danish Crystallographers, Aarhus, Denmark, May 21-22.

OLSEN, J. STAUN, BURAS, B., STEENSTRUP, S. and GERWARD, L.. Spectrometer for x-ray energy d spersive diffraction. Danish Physical Society, Spring Meeting, Helsingør, Denmark, May 30-31.

PÉCSELI, H.L.. Nonlinear electron waves in a weakly magnetized, partially ionized plasma. IEEE International Conference on Plasma Science, Madison, Wisconsin, U.S.A., May 19-20.

PÉCSELI, H.L. and MIKKELSEN, T.. Experimental investigation of turbulence in a magnetized, partially ionized plasma. AGU Chapman Conference on Formation of Auroral Arcs, Fairbanks, Alaska, U.S.A., July 21-25.

PÉCSELI, H.L., ALPORT, M.J., D'ANGELO, N. and MIKKELSEN, T.. Laboratory investigation of cross field instabilities. 22nd Annual Meeting of the Division of Plasma Physics, San Diego, California, U.S.A., November 10-14.

PEDERSEN, T. FRIIS. On rotor, transmission and generator layout for optimal power production of stall-regulated wind turbines. Wind Meeting, Herning, Denmark, May 17.

RASMUSSEN, J. JUUL. Nonlinear plasma waves; particle trapping effects. Danish Physical Society, Spring Meeting, Helsingør, Denmark, May 30-31.

RASMUSSEN, F.. The power production of wind turbines in view of latest measurements. Methods and results. Wind Meeting, Herning, Denmark, May 17.

RASMUSSEN, P.. On the application of dual generator operation and slip ring induction generators in wind turbines. Wind Meeting, Herning, Denmark, May 17.

SCHOU, J.. Transport theory for kinetic emission of secondary electrons from solids by electron and ion bombardment. Danish Physical Society, Topical Meeting on Atomic Physics and Plasma Physics, Risø National Laboratory, Denmark, January 25-26.

SKRIVER, H.L.. Band structure and cohesion of the actinide metals. International Symposium on the Physical Properties of Actinide and Related 4f Materials, Zürich, Switzerland, April 9-11.

SKRIVER, H.L.. Band structure and cohesion of the actinide metals. Journies des Actinides, Stockholm, Sweden, May 27-28.

TROEN, I.. Vindatlas for Danmark (Windatlas for Denmark). 12th Meeting of Scandinavian Meteorologists, Helsinki, Finland, May 27-30.

WULFF, M., MØLLER, H. BJERRUM and MACKINTOSH, A.R.. Excitations and magnetic ordering in Pr-Nd alloys. Danish Physical Society, Topical Meeting on Magnetism, Risø National Laboratory, Denmark, December 9.

6.4 Lectures

ALS-NIELSEN, J.. Kernefysik. (Lecture series on nuclear physics). Technical University of Denmark, Lyngby, Denmark.

ALS-NIELSEN, J.. Phase transitions and scattering spectroscopy. (Lecture series). University of California, Los Angeles, California, U.S.A. (January to March).

ALS-NIELSEN, J.. Critical phenomena at upper marginal dimensionality. An experiment on the dipole-coupled Ising ferromagnet. Bedford College, London, U.K. (September).

ALS-NIELSEN, J.. Flydende krystallers faser (The phases in liquid crystals). Selskabet for Naturlærens Udbredelse, Copenhagen (November).

BURAS, B.. European synchrotron radiation facility and x-ray energy-dispersive diffraction. Stanford Synchrotron Radiation Laboratory, Stanford, California, U.S.A. (May).

BURAS, B.. Status of the european synchrotron source - applications to energy-dispersive diffraction. Brookhaven National Laboratory, New York, U.S.A. (May).

BURAS, B.. European synchrotron radiation facility and x-ray energy-dispersive diffraction as an analogue to TOF neutron diffraction. Argonne National Laboratory, Argonne, Illinois, U.S.A. (May).

BURAS, B.. Resolution problems in x-ray scattering using synchrotron radiation. University of Vienna, Vienna, Austria (November).

BURAS, B.. Application of synchrotron radiation to condensed matter physics. Chemisch-Physikalische Gesellschaft, Vienna, Austria (November).

BURAS, B. and CARNEIRO, K.. Spektroskopiske metoder anvendt ved studiet af kondenserede stoffers fysik. (Lecture series on the use of spectroscopic methods in the study of condensed matter physics.) University of Copenhagen, Copenhagen. Denmark (Winter Semester).

BUSCH, N.E. (and GRYNING, S.E.). The use of on-site meteorological measurements in dispersion calculations. Contribution to a workshop held as part of the course "Problems connected with the evaluation of dispersion of air pollutants from major sources", held by "Nordforsk" (Nordic co-operation organization for applied research), Helsingfors, Finland (September).

BUSCH, N.E. (and JENSEN, N.O.). Scales of atmospheric turbulence. Contribution to workshop held as part of the course "Problems connected with the evaluation of dispersion of air pollutants

from major sources", held by "Nordforsk" (Nordic co-operation organization for applied research), Helsingfors, Finland (September).

BUSCH, N.E. (and GRYNING, S.E.). Meteorological measurement programmes for air pollution studies. Contribution to workshop held as part of the course "Problems connected with the evaluation of dispersion of air pollutants from major sources", held by "Nordforsk" (Nordic co-operation organization for applied research), Helsingfors, Finland (September).

GRYNING, S.E.. Elevated source SF_6-tracer dispersion experiments in the Copenhagen area. S.C.K./C.E.N., Mol, Belgium (March).

GRYNING, S.E.. Relation between dispersion characteristics and surfaces with dissimilar roughness and atmospheric stability. Contribution to workshop held as part of the course "Problems connected with the evaluation of dispersion of air pollutants from major sources", held by "Nordforsk" (Nordic co-operation organization for applied research), Helsingfors, Finland (September).

HØJSTRUP, J.. Measurements of velocity spectra with hotwires and cup anemometers. Oregon State University, Corvallis, Oregon, U.S.A. (April).

HØJSTRUP, J.. A simple model for the adjustment of velocity spectra in inhomogeneous terrain. University of Washington, Seattle, Washington, U.S.A. (July).

HØJSTRUP, J.. Velocity spectra in the unstable planetary boundary layer. Pennsylvania State University, State College, Pennsylvania, U.S.A. (December).

JENSEN, N.O.. Experimental capabilities of the Risø meteorology section. First planning meeting for an international experiment to study local wind flow at a potential WECS hill site. Ayr, Scotland, U.K. (February).

JENSEN, N.O.. Saltningens fysik (The physics of chemical thawing). Vejsektorens Efteruddannelseskurser, Middelfart, Denmark (October).

JENSEN, N.O.. Meteorologi - varsling (Meteorology - Forecasting). Vejsektorens Efteruddannelseskurser, Middelfart, Denmark (October).

JENSEN, P. HJULER. On the private and social economy of small wind turbines in large scale and in local energy plans.
1) Wind Meeting, Gerlev High School, Gerlev, Denmark (October).
2) Borvig High School, Denmark (March).
3) The Credit Union "Denmark", Hindsgaul, Denmark (April).

JENSEN, P. HJULER, KROGSGAARD, J., PEDERSEN, T. FRIIS and RASMUSSEN, F.. Status and development, technology, production and experience of small Danish wind turbines. (Four lectures.) Energy Exhibition, The Bella Centre, Copenhagen, Denmark, (November).

JENSEN, P. HJULER and PEDERSEN, T. FRIIS. Status for and development of small Danish wind turbines.
1) Nordic Energy Exhibition, Brønderslev, Denmark (March).
2) Aalborg University Centre, Aalborg, Denmark (March).
3) Tune Agricultural School, Roskilde, Denmark (March).
4) Næstved Local Energy Group, Næstved, Denmark (March).
5) Union of Danish Electricians, Copenhagen, Denmark (November).

JENSEN, V.O.. Fusion. Seminars on Energy Economy. University of Copenhagen, Copenhagen, Denmark (January).

JENSEN, V.O.. Plasma physics I and II. (Two lecture series on plasma physics and fusion research.) Technical University of Denmark, Lyngby, Denmark.

JENSEN, V.O.. Fusionsforskning (Fusion Research). Parentesen. University of Copenhagen, Copenhagen, Denmark (March).

KJÆR, K.. The critical behaviour of $LiTbF_4$ upon dilution with yttrium. Technical University of Denmark, Lyngby, Denmark (November).

KRISTENSEN, L.. Longitudinal and lateral coherence in the atmosphere.
1) Naval Postgraduate School, Monterey, California, U.S.A. (March).
2) National Centre of Atmospheric Research, Boulder, California, U.S.A. (March).
3) Pennsylvania State University, State College, Pennsylvania, U.S.A. (March).
4) Centre National d'Etudes des Telecommunications, Issy les Moulineaux, France (May).

LARSEN, S.E.. Analysis and results from the surface layer experiment in connection with JONSWAP 1975. The Energy Transfer Group, University of Washington, Seattle, Washington, U.S.A. (February).

LARSEN, S.E.. Dispersion modelling by means of puff-models.
1) University of Washington, Seattle, Washington, U.S.A. (February).
2) Naval Postgraduate School, Monterey, California, U.S.A. (February).

LEBECH, B.. The magnetic structure of Nd, a difficult problem to solve.
1) Oak Ridge National Laboratory, Oak Ride, Tennessee, U.S.A. (February).
2) National Bureau of Standards, Washington D.C., U.S.A. (February).
3) University of West Virginia, Morgantown, West Virginia, U.S.A. (February).
4) Brookhaven National Laboratory, New York, U.S.A. (February).
5) Institute Max von Laue - Paul Langevin, Grenoble, France (March).
6) ETHZ, Würenlingen, Switzerland (March).

LINDGÅRD, P.A.. Correlation theory of static and dynamic properties of multi-level systems.
1) Hannover University, Hannover, F.R.G. (February).
2) Aarhus University, Aarhus, Denmark (February).
3) Oxford University, Oxford, U.K. (April).
4) Southampton University, Southampton, U.K. (April).
5) Edinburgh University, Edinburgh, Scotland (May).
6) Frankfurt University, Frankfurt, F.R.G. (December).

LINDGÅRD, P.A.. Series of lectures on critical phenomena. Rutherford Laboratory, Oxfordshire, U.K. (April to May).

LUNDSAGER, P.. Status of and needs for research in and development of small wind turbines in Denmark. Hearing by the Government Advisory Committee for Energy Research, Copenhagen, Denmark (September).

LYNOV, J.P.. Mutual interaction between solitary electron holes. University of Kyoto, Kyoto, Japan (April).

LYNOV, J.P.. Recurrence and modification of solitons. Tohoku University, Sendai, Japan (April).

LYNOV, J.P.. Ikke-lineære elektronpulser i en magnetiseret, plasmafyldt bølgeleder (Nonlinear electron pulses in a magnetized, plasma-loaded wave-guide). Technical University of Denmark, Lyngby, Denmark (November).

MICHELSEN, P.. Observations of solitons in a magnetized plasma. University of Kyoto, Kyoto, Japan (April).

MICHELSEN, P.. Fusionsenergi (Fusion energy). Ungdommens Naturvidenskabelige Forening (Youth Society of Natural Sciences). University of Copenhagen, Copenhagen, Denmark (December).

MIKKELSEN, T.. Some puff modelling principles. Contribution to workshop held as part of the course "Problems connected with the evaluation of dispersion of air pollutants from major sources", held by "Nordforsk" (Nordic co-operation organization for applied research), Helsingfors, Finland (September).

NIELSEN, M.. Neutron and x-ray diffraction from physisorbed monolayers on graphite. University of Washington, Seattle, Washington, U.S.A. (May).

NIELSEN, M.. Phase transitions in physisorbed monolayers adsorbed on graphite studied by neutron and x-ray diffraction. Danish-Russian-United States Meeting at the Niels Bohr Institute, Copenhagen, Denmark (August).

PÉCSELI, H.L.. Experimental observation of phase space vortices in plasmas. M.I.T., Boston, Massachusetts, U.S.A. (January).

PÉCSELI, H.L.. Advanced Plasma Physics. (Lecture series.) University of Iowa, Iowa City, U.S.A. (Spring Semester).

PÉCSELI, H.L.. Nonlinear electron plasma waves. University of Iowa, Iowa City, U.S.A. (April).

PÉCSELI, H.L.. Field aligned irregularities in ionospheric heating experiments. University of Iowa, Iowa City, U.S.A. (September).

PÉCSELI, H.L.. Strong turbulence in partially ionized plasmas. University of Iowa, Iowa City, U.S.A. (October).

RASMUSSEN, J. JUUL. Limit cycle behaviour of the bump-on-tail and ion-acoustic instability. Innsbruck University, Innsbruck, Austria (January).

RASMUSSEN, J. JUUL. Amplitude oscillation due to particle trapping and detrapping. Tohoku University, Sendai, Japan (April).

RASMUSSEN, J. JUUL. Properties of the Korteweg-de Vries equation: recurrence, deformation of solitons in dissipative media. Royal Netherlands Meteorologigical Institute, de Bilt, The Netherlands (September).

RASMUSSEN, J. JUUL. Nonlinear electron plasma waves: particle trapping effects. University of Tromsø, Tromsø, Norway (November).

RASMUSSEN, J. JUUL. Observations of strong stationary double layers in laboratory plasmas. University of Tromsø, Tromsø, Norway (November).

RASMUSSEN, F.. The future of the renewable energy soucos, wind turbines. Energy Exhibition, The Bella Centre, Copenhagen, Denmark (November).

TROEN, I.. Vindatlas for Danmark (Windatlas for Denmark). Wind Meeting, Gerlev High School, Gerlev, Denmark (September).

6.5 Degrees, students, etc.

The following acquired the degree of lic. techn. or lic. scient. (Ph.D) for work carried out in the department:

Knud Møllenbach	(Solid State Physics)
Jens-Peter Lynov	(Plasma Physics)
Karen Schou Pedersen*	(Solid State Physics)

The following postgraduates carried out research which will lead to the degree of lic. techn. or lic. scient. at the department:

Henrik Bejder	(Plasma Physics)
Jakob Bohr	(Solid State Physics)
Peter Børgesen	(Plasma Physics)
Finn E. Christensen	(Solid State Physics)
Kurt Clausen	(Solid State Physics)
Mogens Gadeberg	(Plasma Physics)

* From the Technical University of Denmark

Sven-Erik Gryning	(Meteorology)
Palle Buus Jensen	(Plasma Physics)
Dorte Justesen**	(Solid State Physics)
Kristian Kjær	(Solid State Physics)
Torben Mikkelsen	(Meteorology)
Knud Thomsen	(Plasma Physics)

The following students from the Technical University of Denmark and the University of Copenhagen worked on Masters' thesis projects:

Henrik Bejder	(Plasma Physics)
Jakob Bohr	(Solid State Physics)
Preben Hansen	(Solid State Physics)
Dorte Justesen	(Solid State Physics)
Kristian Kjær	(Solid State Physics)
Knud Thomsen	(Plasma Physics)
Helge Rørdam Olesen	(Meteorology)
Michael Wulff	(Solid State Physics)

During February and September, students from the Universities of Aarhus and Copenhagen participated in the following laboratory courses:

1) Neutron Scattering, organized by
   N. Hessel Andersen, K. Carneiro,
   F.E. Christensen and K. Clausen.

2) Plasma Physics, organized by
   J.P. Lynov, P. Michelsen and
   J. Juul Rasmussen.

Two foreign students sponsored by the IAESTE carried out practical work at the department as part of their general training.

** Also at the Metallurgy Department, Risø

7. STAFF OF THE PHYSICS DEPARTMENT

Head:	Hans Bjerrum Møller
Office staff:	Lone Astradsson, Anne Carlsen, Kæth Kjøller, Gerda Stauning, Alice Thomson, and temporary assistants.
The sections:	7.1 Solid State Physics 7.1.1 Liquid N_2 and He plant 7.2 Plasma Physics 7.3 Meteorology 7.3.1 Test plant for small wind turbines.

7.1 Solid State Physics

Scientific staff	Technical staff
Jens Als-Nielsen	Bjarne Breiting
Niels Hessel Andersen[+]	Kaj Christensen
Ian Heilmann[**]	Bent Heiden
Jørgen Kjems	John Z. Jensen
Bente Lebech	Louis C. Jensen
Per-Anker Lindgård	Steen Jørgensen
Gordon A. MacKenzie[*]	Werner Kofoed
Hans Bjerrum Møller	Jens Linderholm
Mourits Nielsen	Morits Lund
	Paul Mackintosh[++]
	Jørgen Munck
	Jørgen Olsen[++]
	Allan Thuesen

---

[*] Until February 15

[**] Until July 31

[+] Also at the Metallurgy Department, Risø

[++] Temporary assistants

Collaborators	Postgraduates
Bronislav Buras[§]	Jakob Bohr
Kim Carneiro[§]	Finn Christensen
Hans L. Skriver[§§]	Kurt Clausen[*]
	Dorte Justesen[+]
	Kristian Kjær

Consultant

Allan R. Mackintosh[§]

Short-term visitors (two to twelve weeks)

M. Almeida	Instituto Superior Technico, Lisbon, Portugal
M. Bretz	University of Sussex, U.K.
G. Chevrier	CEN-Saclay, Gif-sur-Yvette, France
D. Cox	Brookhaven National Laboratory, New York, U.S.A.
P. Dutta	Argonne National Laboratory, Illinois, U.S.A.
R. Feile	Joh. Gutenberg University, Mainz, F.R.G.
T. Giebultowicz	University of Warsaw, Poland
W. Hayes	Clarendon Laboratory, Oxford University, U.K.
M.T. Hutchings	AERE, Harwell, U.K.
I. Imry	Tel Aviv University, Israel
M. de Jong	University of Amsterdam, The Netherlands
K. Kakurai	Hahn-Meitner Institute, Berlin
H. Kepa	University of Warsaw, Poland
G.P. Knudsen	Technical University of Copenhagen, Denmark
J. Kurittu	University of Helsinki, Finland
M. Loewenhaupt	KFA JÜlich, F.R.G.
A. Loidl	Johs. Gutenberg University, Mainz, F.R.G.
W.D. Lukas	Freie University Berlin, Berlin

---

[*] Until April 30

[§] From the University of Copenhagen

[§§] Also at NORDITA, Copenhagen

[+] Also at the Metallurgy Department, Risø

K.A. McEwen	University of Salford, U.K.
J. McTague	University of California, Los Angeles, California, U.S.A.
D. Moncton	Bell Laboratories, New York, U.S.A.
R. Nevald	Technical University of Copenhagen, Denmark
L. Nielsen	Technical University of Copenhagen, Denmark
L. Nilsson	Chalmers Institute of Technology, Göteborg, Sweden
R. Osborne	University of Southampton, U.K.
H.R. Ott	ETH, Zürich, Switzerland
S. Overell	University of Edinburgh, Scotland, U.K.
S. Pawley	University of Edinburgh, Scotland, U.K.
G. Pepy	CEN-Saclay, Gif-sur-Yvette, France
P. Pershan	Harvard University, Massachusetts, U.S.A.
I. Peschel	Freie University Berlin, Berlin
B.D. Rainford	University of Southampton, U.K.
E.K. Riedel	University of Washington, Seattle, Washington, U.S.A.
P. Schnabel	Oxford University, U.K.
I. Schuller	Argonne National Laboratory, Illinois, U.S.A.
S. Sinha	Argonne National Laboratory, Illinois, U.S.A.
T. Stebler	University of Bern, Switzerland
M. Steiner	Hahn-Meitner Institute, Berlin
W. Stirling	Institute Max von Laue - Paul Langevin, Grenoble, France
F.W. Voss	Technical University of Copenhagen, Denmark
D. Yang	University of West Virginia, Morgantown, West Virginia, U.S.A.

7.1.1 Liquid N_2 and He Plant

Technical staff

Bent Heiden

John Z. Jensen

7.2 Plasma Physics

Scientific staff

Stig A. Andersen[++]
Verner Andersen
Che-Tyan Chang
Vagn O. Jensen
Otto Kofoed-Hansen[†]
Jens-Peter Lynov
Poul Michelsen
Per Nielsen
Hans L. Pécseli[+]
Jens Juul Rasmussen
Jørgen Schou[*]
Hans Sørensen

Technical staff

Paul Andersen
Bengt Hurup Hansen
Jens A. Knudsen[§§]
Mogens Nielsen
Arne Nordskov
Jørgen Olsen[§]
John Petersen
Børge Reher
Hans Skovgård[*]
Bjarne Sass[**]

Consultant

Chan Mou Tchen[††]

Postgraduates

Henrik Bejder
Palle B. Jensen
Peter Børgesen
Mogens Gadeberg
Knud Thomsen

Long-term visitors

A. Balmashnov	People's Friendship University, Moscow, USSR
D. Jovanović	Institute of Physics, Beograd, Yugoslavia
Chen Hao-Ming	Tsing Hua University, Peking, China

---

[*] Until February 28
[**] From May 1
[§] From October 1
[§§] From November 1
[+] From November 15
[++] From December 1
[†] Also at the Niels Bohr Institute, Copenhagen
[††] From City University of New York, New York, U.S.A.

Short-term visitors (two to twelve weeks)

S. Iizuka	Tohoku University, Sendai, Japan
R. Schrittwieser	Innsbruck University, Austria

7.3 Meteorology

Scientific staff	Technical staff
Carl Jørgen Christensen	Jørgen Christensen
Ole Christensen	Gunner Dalsgård
Sten Frandsen	Morten Frederiksen
Sven-Erik Gryning[§]	Arent Hansen
Svend Ole Hansen	Per Ekelund Hansen[††]
Jørgen Højstrup[*]	Finn Hansen
Niels Otto Jensen	Gunnar Jensen
Leif Kristensen	Knud Sørensen
Søren E. Larsen	
Per Lundsager[†]	
Erik Lundtang Petersen	
Ib Troen	

Collaborators

Søren A. Jensen	Danish Ship Research Laboratory, Technical University of Denmark
Poul Nielsen	DEFU, Technical University of Denmark
Peter Dorph-Petersen	Danish Meteorological Institute, Copenhagen

Consultant	Postgraduates
Chan Mou Tchen[**]	Sven-Erik Gryning
	Torben Mikkelsen

[§] From September 1

[*] At Pennsylvania State University, Pennsylvania, U.S.A.

[**] From City University of New York, New York, U.S.A.

[†] From June 1 at the test plant (7.3.1)

[††] Temporary assistant

Long-term visitors

E. Donev	University of Sofia, Bulgaria
W.K. George	State University of New York at Buffalo, New York, U.S.A.
L. Mahrt	Oregon State University, Corvallis, Oregon, U.S.A.

Short-term visitors (two to twelve weeks)

K. Katsaros	University of Washington, Seattle, Washington, U.S.A.
D.H. Lenschow	National Center for Atmospheric Research, Boulder, Colorado, U.S.A.
H.A. Panofsky	Pennsylvania State University, Pennsylvania, U.S.A.
E. Peterson	Oregon State University, Corvallis, Oregon, U.S.A.

7.3.1 Test plant for small wind turbines

Scientific staff	Technical staff
Peter Hjuler Jensen	Joel Ethelfeld
Jørgen Krogsgård	Flemming Hagensen
Per Lundsager	
Troels Friis Pedersen	
Helge Petersen	
Flemming Rasmussen	Secretary
Peter Rasmussen	Anne Carlsen

Sales distributors:
Jul. Gjellerup, Sølvgade 87,
DK-1307 Copenhagen K, Denmark

Available on exchange from:
Risø Library, Risø National Laboratory,
P. O. Box 49, DK-4000 Roskilde, Denmark

ISBN 87-550-0761-9
ISSN 0106-2840